Mucosal neutrophil activation predisposes to respiratory viral infection

Running title: Roles of neutrophils & IL-17 in RSV infection

One sentence summary: Mucosal neutrophil activation at the time of respiratory virus exposure enhances infection and opposes early prodromal mucosal inflammatory responses that prevent disease.

Authors: Maximillian S Habibi[1*], Ryan S Thwaites[1*], Meiping Chang[2], Agnieszka Jozwik[1], Allan Paras[1], Freja Kirsebom[1], Augusto Varese[1], Amber Owen[1], Leah Cuthbertson[1], Phillip James[1], Tanushree Tunstall[1], David Nickle[3], Trevor T Hansel[1], Miriam F Moffatt[1], Cecilia Johansson[1], Christopher Chiu[4‡] and Peter J. M. Openshaw[1‡]

Affiliations:

[1]National Heart and Lung Institute, Imperial College London, London, United Kingdom

[2]Merck &Co., Inc., Kenilworth, NJ, USA

[3]Genetics & Pharmacogenomics, Department of Translational Medicine, Merck &Co., Inc., Boston, Massachusetts, USA

[4]Department of Infectious Diseases, Imperial College London, London, United Kingdom

*, ‡ these authors contributed equally

Correspondence should be addressed to: Peter J. M. Openshaw FRCP PhD, National Heart and Lung Institute, Imperial College London, London W2 1PG, UK. E-mail: p.openshaw@imperial.ac.uk;

or Christopher Chiu MRCP FRCPath Ph.D, Department of Infectious Disease, Imperial College London, London W12 0NN, UK. E-mail: c.chiu@imperial.ac.uk;

or Cecilia Johansson PhD, National Heart and Lung Institute, Imperial College London, London W2 1PG, UK. E-mail: c.johansson@imperial.ac.uk

Abstract:

The variable outcome of viral exposure is only partially explained by known factors. We administered respiratory syncytial virus (RSV) to 58 volunteers, of whom 57% became infected. Mucosal neutrophil activation prior to exposure was highly predictive of symptomatic RSV disease. This was associated with rapid pre-symptomatic decline in mucosal IL-17A and other mediators. Conversely, those who resisted infection showed pre-symptomatic activation of IL-17 and TNF-related pathways. Vulnerability to infection was not associated with baseline microbiome but was reproduced in mice by pre-infection chemokine-driven airway recruitment of neutrophils, which caused enhanced disease mediated by pulmonary $CD8^+$ T cell infiltration. Thus, mucosal neutrophilic inflammation at respiratory virus exposure enhances susceptibility, revealing dynamic time-dependent local immune responses before symptom onset and explaining hitherto unpredictable outcomes of pathogen exposure.

Main Text:

The respiratory tract is by necessity an open portal, highly vulnerable to invasion by many pathogens. A complex system of defenses counters this vulnerability, but current knowledge of what governs susceptibility fails to fully explain the erratic transmission of infectious agents (*1, 2*). For some infections, antibodies in the respiratory mucosa are clearly protective (*3*). Furthermore, infectious agents can also be blocked by antimicrobial peptides (*4*), entrapment in mucus (*5*), the downstream effects of pattern recognition receptor activation (*1, 2, 6*), as well as direct inactivation by immune cells (*6*). The SARS-CoV-2 pandemic has brought into sharp focus the need for greater understanding of the role of mucosal innate immunity in protection against respiratory infection. Better understanding of such defenses may offer ways to prevent or modulate viral disease, even against novel and emerging pathogens. Among innate immune cells, neutrophils are classically ascribed roles in defense against bacteria and fungi, but their role in antiviral responses is less clear. Although they are sometimes found in the lungs of patients with severe viral infections and have a demonstrable antiviral role in animal models, information concerning how they contribute to defense and disease in human respiratory viral infections is largely lacking (*7*).

Respiratory syncytial virus (RSV) is the leading cause of infant hospitalization worldwide, infecting around 34 million children each year (*8*) and contributing prominently to morbidity and mortality in elderly and immunosuppressed adults (*9, 10*). Though RSV infection is essentially confined to the respiratory epithelium, resultant neutrophilic lung inflammation can be life-threatening, particularly in at-risk children (*11, 12*). Although prophylaxis with palivizumab (a monoclonal anti-RSV antibody) can prevent hospitalization of premature infants (*13*), no specific therapeutic intervention is currently available and no vaccine has yet been licensed that protects against RSV (*14*). This is despite the existence of several promising candidates (*15*), including enhancement of placental anti-RSV IgG transfer by maternal immunization. There is therefore a pressing need to further identify interventions that prevent RSV and other respiratory viral diseases.

Animal models of respiratory viral infection provide useful mechanistic insights but do not fully recapitulate human disease (*6*). Conversely, observational studies of hospitalized children and high-risk adults are limited by heterogeneity of populations and disease severity, an inability to dynamically assess the status of host immunity and, specifically, the mucosa before and immediately after viral exposure. Experimental infection of human volunteers therefore provides a unique opportunity to identify pre-existing immune factors and pre-symptomatic responses in a controlled setting that correlate with protection and disease (*16, 17*).

All adults have RSV-specific antibodies, reflecting multiple rounds of infection throughout the course of their lives. Nevertheless, symptomatic re-infection occurs repeatedly even in healthy people and is associated with unusually short-lived humoral and cellular memory responses (*3*). Such defective defense against reinfection is also observed following some other respiratory viral infections, including coronaviruses (*18*). Furthermore, variations in antibody levels do not accurately predict susceptibility to RSV infection in experimental studies of volunteers, those with the lowest antibody levels being only modestly more susceptible to viral challenge (*3, 19*). Although mucosal IgA, circulating IgG (*3*), and resident memory $CD8^+$ T cells (*20*) show some association with resistance to infection and reduced disease severity, these factors do not completely explain who resists or succumbs. Additionally, although RSV viral burden approximately correlates with symptoms in experimentally infected adults (*16*) and moderately ill infants (*21, 22*), viral load may be paradoxically reduced in the most severely affected children (*23*).

How the very early events following viral exposure influence clinical outcomes has not been studied in either adults or children. Studying the respiratory mucosa before, during, and after human RSV challenge, we found that prior neutrophil activation in the upper respiratory tract predisposes to symptomatic viral infection. The neutrophilic mucosal environment was strongly associated with a reduction in antiviral mucosal inflammatory responses immediately after viral exposure that was followed by the onset of disease. By contrast, a protective response characterized by rapid activation of type-17 inflammation was observed in those resisting infection. Moreover, studies in mice showed that

recruitment of airway neutrophils prior to viral administration enhanced the cytotoxic $CD8^+$ T cell response and disease severity.

Results

Characterization of time-course of responses to human RSV challenge

Fifty-eight healthy adult volunteers were inoculated with RSV Memphis 37. Nasal sampling was performed at baseline (7-14 days pre-inoculation) and then repeatedly up to 14 days after inoculation (Fig. 1A). Symptoms were quantified using a previously validated self-reported symptom scale (*24*). Twenty-three participants developed PCR-positive RSV infection with symptoms of upper respiratory tract disease ("Cold"), whereas 25 had no evidence of RSV infection and did not develop symptoms ("No Cold"). Ten participants had PCR evidence of RSV infection, but had self-reported symptom scores that did not reach the threshold required for the "Cold" group. This indeterminate group was excluded from subsequent analyses, which focused on identifying factors associated with the most distinct outcomes. No significant demographic differences were observed between the Cold and No Cold groups (table S1).

In infected volunteers, viral load (determined by qPCR from daily nasal washes) broadly indicated three phases: (1) a pre-symptomatic incubation phase during the first 3 days post-inoculation when virus was undetectable; (2) a viral replication phase from days 3-7; and (3) a viral clearance phase from day 8 (previously shown to be associated with the rise in virus-specific $CD8^+$ T cells in both blood and lower airway (*20*)) (Fig. 1B). Low level detection of virus on day 1 probably represented residual viral inoculum. Severity of the resultant upper respiratory tract disease (measured by a self-reported symptom score) peaked at day 7, around the same time as viral load (Fig. 1C). In agreement with previous reports (*16*), total symptom scores positively correlated with total viral shedding throughout the study duration ($P<0.001$, fig. S1), despite the known shortcomings of viral load measurement and variability of symptom quantification.

Susceptibility to RSV infection is associated with airway neutrophil activation

Human challenge studies are exceptional in allowing the investigation of events prior to symptom onset, enabling us to examine the influence of immune activation in the airway at baseline and during the early pre-symptomatic period on the course of infection. In agreement with our previous report (*3*), anti-RSV

IgA titers in the nose at baseline were higher in the No Cold group (fig. S2A and S2B). However, titers showed a substantial overlap with the Cold group, suggesting that nasal IgA alone did not adequately explain susceptibility unless at extremely low or high levels. Additionally, the frequency of RSV-specific $CD8^+$ T cells in the lung at baseline did not distinguish between infection (Cold) or protection (No Cold) (fig. S2C), as we have previously reported (*20*). Thus, correlates of protection against RSV are likely multifactorial with no single dominant protective mechanism yet defined.

To enable discovery of previously unanticipated factors associated with susceptibility to infection, RNA-Seq of nasal tissue collected from Cold and No Cold group volunteers pre-inoculation was performed, identifying 80 differentially expressed genes (DEGs) that distinguished the two divergent outcomes (Padj<0.05; Fig. 2A, table S2). Seventy-three (91%) DEGs were significantly higher in the Cold group, whereas a smaller cluster (7/80, 9%) was elevated in the No Cold group. For pathway enrichment analyses, a looser cut-off (Padj<0.1) was applied, resulting in inclusion of a further 155 DEGs (table S2). Strikingly, biological processes associated with neutrophil activation made up the most significantly enriched pathways at baseline in those susceptible to infection (Fig. 2B, table S3), with many DEGs also associated with hydrolase and peptidase activity (Fig. 2C, table S4). Furthermore, weighted gene co-expression network analysis (WGCNA) identified a cluster of highly correlated genes that was enriched for genes associated with neutrophil activity, including *CDA, IGF2R, ITGAX, UNC13D, SIGLEC14, SIRPA, PREX1,* and *MMP9* (Fig. 2D). In agreement with these transcriptomic data, nasal protein levels of the neutrophil-associated mediators myeloperoxidase (MPO), lipocalin-2/neutrophil gelatinase-associated lipocalin (LCN-2), and IL-17A were significantly higher in the Cold group, relative to No Cold at day 0 (P=0.010, P=0.017 and P=0.039, respectively, Fig. 2E and table S5). There was no difference in other cytokines or chemokines (table S5), but with IL-17 known to induce neutrophil activation and chemotaxis, these data supported the hypothesis that greater airway neutrophil activity at the time of virus exposure increases susceptibility to symptomatic RSV infection (*25, 26*). No correlation was observed between baseline nasal antibody titers and neutrophil mediator levels (data not shown), suggesting that these were independent correlates of susceptibility.

Early immune activation prevents symptomatic RSV infection

To investigate the relationship between airway neutrophil activity and subsequent mucosal inflammatory responses, nasal tissue samples collected at day 3 post-inoculation (prior to the phase of concerted net viral replication) were analyzed by RNA-Seq and compared to matched pre-inoculation samples. Sixteen volunteers from each of the Cold and No Cold groups yielded RNA suitable for sequencing and were included in the analysis. This identified 87 DEGs ($P<0.01$, $\log^2$ fold-change>0.5) in the No Cold group (Fig. 3A, table S6) and 77 DEGs in the Cold group (Fig. 3B, table S7). In both Cold and No Cold groups, the majority of DEGs were upregulated post-inoculation (as shown by mean expression values for each gene and K-means clustering). However, only two genes (*ITLN1* and *JUN*) overlapped between both groups, emphasizing the divergence of local responses associated with these two polar outcomes (Fig. 3C).

Next, the functional pathways to which DEGs associated with No Cold at day 3 significantly contributed were tested by enrichment analysis using gene ontology (GO) and Kyoto encyclopedia of genes and genomes (KEGG) pathways. GO biological processes analysis for the Cold group showed significant enrichment of several processes, but none specifically related to immune responses (table S8). By contrast, in the No Cold group, GO biological processes analysis yielded several immune-related pathways that were significantly enriched. These could be categorized into three areas: (1) epidermis/skin development and bacterial defense; (2) humoral immunity, including the *JCHAIN* required for secretory IgA formation; and (3) leukocyte/granulocyte migration and chemotaxis (table S9). Additionally, the DEGs in the No Cold group showed the enrichment of molecular functions for protease, cytokine and chemokine activities (Fig. 3D and table S10). KEGG analysis also revealed a number of pathways related to cytokine and chemokine signaling. Of these the "IL-17 signaling pathway" was the most significantly enriched (Fig. 3E and table S11), comprising chemokines *CXCL1/2/3/6*, the transcription factor *JUN*, the major gel-forming mucin *MUC5B*, and the antimicrobial protein *S100A7*, which is induced by IL-17 and important in protection against Gram negative bacteria (*27*). Other closely related KEGG terms were also enriched, including "Cytokine–cytokine receptor interaction" and "TNF signaling pathway". No KEGG pathways were significantly enriched in the Cold group.

Thus, the activation of an early inflammatory response is associated with protection from symptomatic RSV infection. This early protective inflammatory response is characterized by signatures of leukocyte migration and cytokine and chemokine signaling. By contrast, such inflammatory responses are not observed in volunteers who went on to develop RSV disease.

Early RSV clearance is associated with type-17 immunity

To define the core transcriptional signatures of co-expressed genes without biasing by predetermined or putative biological function knowledge, we next applied WGCNA to establish interrelated DEG networks associated with protection in No Cold individuals. Three gene clusters (depicted and named "brown", "turquoise" and "blue") were identified at day 3 post-inoculation, relative to baseline (Fig. 4A). The brown module mainly contained genes encoding peptidase and hydrolase activity (Figs. 4B, 4C and table S12). This was also true of the turquoise module, which clustered closely with the brown module, (Figs. 4D, 4E and table S13). However, the blue module was highly enriched in IL-17 pathway components and closely corresponded to the DEGs featured in the KEGG "IL-17 signaling pathway" (Fig. 3E), namely *CXCL1/2/3/6 and JUN* (Fig. 4F). Indeed, GO molecular function analysis of the blue module identified enrichment of cytokine and chemokine activity and signaling (Fig. 4G and table S14). Thus, the blue module represents a signature of type-17 inflammatory gene expression induced on RSV exposure, which is associated with the prevention of infection.

To validate these findings, cytokines and chemokines in nasal lining fluid were quantified over time. In the Cold group, a limited response was detected until day 3 after which the expression of antiviral mediators (IFN-α, IFN-γ, CXCL10, and IL-15) substantially increased with maximal detection on day 7 (Fig. 5A), in line with the peak of symptoms and viral load (Figs. 1B and 1C). The chemokines CCL3 (MIP-1α) and CCL5 (RANTES), the anti-inflammatory cytokine IL-10, and TNF-α all followed similar kinetics (Fig. 5B). The levels of all mediators in the Cold group declined during the phase of viral clearance (days 7-14). Cytokines and chemokines are well recognized to be closely associated with symptoms in a variety of inflammatory conditions, including the response to infection (*28, 29*). Indeed, within the Cold group, cumulative viral load and inflammatory mediator levels over the study duration

were closely correlated (fig. S3), emphasizing their role in pro-inflammatory responses and disease triggered by infection (*16*). However, in the No Cold group, despite the absence of symptoms prior to day 4 post-inoculation, several cytokines (including IL-1β, IL-6, IL-17A, and TNF-α) underwent a rapid burst of expression during the incubation phase shortly after virus inoculation (Figs. 5B and 5C). Logistic regression analysis showed statistically significant associations between induction of IL-1β, IL-6, and IL-17A (P=0.04, 0.05 and 0.03, respectively, Fig. 5D) in the first 3 days following RSV exposure and protection from developing symptoms. After day 3, mediators returned to baseline levels in No Cold volunteers, who did not develop the later response seen in the Cold group. Conversely, in the Cold group, almost all mediators declined relative to day 0 levels during the incubation phase, despite the presence of virus (Figs. 5A-C). Thus, a local type-17 inflammatory response early after pathogen exposure prevents the development of a symptomatic infection. Failure to mount a protective inflammatory response rapidly post-inoculation is itself associated with airway neutrophil activity at the time of exposure, suggesting that neutrophilic inflammation may disrupt this early protective response.

The airway microbiome is not associated with susceptibility to infection

Neutrophils are classically ascribed antibacterial and antifungal functions, and recent studies have shown perturbations of the airway bacterial microbiome in children hospitalized with RSV (*30*). To test for associations between the pre-infection airway microbiome and susceptibility to RSV infection, 16S ribosomal RNA from nasopharyngeal bacteria was quantified and sequenced. Despite differential neutrophil activation in the nasal mucosa by multiple measures, no significant differences in bacterial load were observed between Cold and No Cold groups at baseline (fig. S4A). Moreover, 16S sequencing demonstrated similar baseline diversity and community composition in these groups (fig. S4B; Richness, P=0.948; Shannon–Weiner, P=0.263; Simpsons, P=0.166, Bray–Curtis dissimilarity, R^2=0.055, P=0.087). Thus, there are no significant associations between the baseline airway microbiome and nasal neutrophilic inflammation prior to viral exposure, and thus susceptibility to RSV infection.

Elevated airway neutrophils in the murine lung at the time of exposure enhance RSV disease via pulmonary cytotoxic T cells

To investigate the role of neutrophilic inflammation on early and late outcomes in respiratory viral infection, we modeled the impact of increased pulmonary neutrophils at the time of RSV challenge in mice. C57BL/6 mice were treated intranasally (i.n.) with recombinant (r)CXCL1 or PBS. Administration of rCXCL1 caused short-lived recruitment of neutrophils to the bronchoalveolar lavage (BAL) and lung parenchyma within 12 hours (Fig. 6A, gating strategies are shown in Fig. S5) resulting in elevated levels of the neutrophil mediators MMP-9, MPO, and neutrophil elastase in BAL (Fig. 6B) analogous to human volunteers in the Cold group. The effect of rCXCL1 treatment was restricted to neutrophils and had no impact on either alveolar macrophage (AM) numbers in the airway or monocyte abundance in the lung (Fig. S6A). Furthermore, no differences were observed in cytokine (Fig. S6B) or chemokine (Fig. S6C) levels in the lung prior to virus challenge following rCXCL1.

As in human challenge, increased neutrophilic inflammation prior to (but not shortly after (*31*)) RSV infection led to significant enhancement of disease (measured by weight loss), with a nadir at day 6-7 post-infection (p.i.) (Fig. 6C). RSV infection resulted in rapid upregulation of pro-inflammatory cytokines including IFN-α and IL-6 at 18 hours p.i. (Fig. 6D). Production of these cytokines were not significantly altered by rCXCL1 pretreatment. Furthermore, rCXCL1 conditioning did not change the gene expression of *Tnfa* but did coincide with reduced gene expression of *Il1b, Cxcl2, Cxcl10,* and *Ccl2* in the lung tissue after RSV infection (Figs. 6E-G). The infiltration of antiviral monocytes (*32*) did not change after rCXCL1 conditioning (Fig. 6H) but neutrophils and neutrophil mediators were increased in the rCXCL1 treated mice compared to mice with RSV alone (fig. S7). Nevertheless, rCXCL1 conditioning was associated with a modestly but significantly higher viral load at 18 hours p.i., which was not sustained to days 4 (the peak of viral replication) or 8 p.i. (clearance of the virus) (Fig. 6I). Thus, neutrophil infiltration at the time of respiratory viral challenge transiently alters the inflammatory environment and is associated with a subtle early impairment in control of virus replication during the asymptomatic period only.

Immunopathology in the murine RSV model causes enhanced disease, which has been shown to be partially mediated by over-exuberant T cell activity (*6, 33, 34*). In human challenge, $CD8^+$ T cell numbers in bronchial biopsies at day 7 post-inoculation showed a non-significant positive association with disease severity (P=0.088, Fig. 7A), suggesting that this may be a contributory mechanism (*20*). To further examine this issue, T cell responses were analyzed in mice pretreated with rCXCL1. At day 8 p.i., there was significantly higher total lung cellularity in RSV-infected rCXCL1 pretreated mice (Fig. 7B), despite the decreasing viral load (Fig. 6I) and resolution of the pulmonary neutrophil response (fig. S8A). Although $CD4^+$ T cell numbers were somewhat increased (P<0.05, Fig. 7C), the most marked elevation in rCXCL1 pretreated mice was of $CD8^+$ T cell numbers (P<0.0001, Fig. 7D), suggesting that these might be the predominant mediators of immunopathology.

Tetramer staining revealed no significant difference in the frequencies of RSV-specific $CD8^+$ T cells in the lung at day 8 p.i. following rCXCL1 pretreatment (Fig. 7E), but the greater total influx of $CD8^+$ T cells in rCXCL1 pretreated mice resulted in significantly increased numbers of virus-specific $CD8^+$ T cells in the lung around the peak of disease severity (Fig. 7F). Functional markers of these RSV-specific $CD8^+$ T cells were assessed by short-term in vitro restimulation and intracellular cytokine staining (Fig. 7G). Neither granzyme B nor IFN-γ production were enhanced by rCXCL1 pretreatment (Fig. 7H). Depletion of neutrophils by anti-Ly6G antibody treatment in rCXCL1 pretreated mice prior to RSV inoculation partially abrogated weight loss at days 6 and 7 p.i. (Fig. 7I). Thus, rCXCL1-driven airway neutrophils at the time of RSV exposure are at least in part responsible for $CD8^+$ T cell recruitment and enhanced disease. Antibody-mediated depletion of $CD8^+$ T cells during the course of infection abrogated weight loss in rCXCL1 pretreated RSV-infected mice at days 6-8 p.i. (Figs. 7J and S8B). This strongly suggests that $CD8^+$ T cells are the predominant effectors causing enhanced disease. These findings agreed with previous murine studies showing the role of $CD8^+$ T cells in mediating RSV-induced weight loss (*33*).

Thus, pre-existing neutrophilic inflammation alters the tissue environment so that the recruitment but not cytotoxic function of $CD8^+$ T cells to the lung is increased later in the disease course. This is associated with transient early changes in soluble mediators and viral load during the asymptomatic

period, while peak disease is mediated by immunopathology despite the absence of elevated pulmonary neutrophils or viral load at that later time.

Discussion

Using experimental RSV infection of human volunteers and mice, we identified a mechanism of susceptibility and resistance to infection. Prior to exposure, airway neutrophil activation was associated with enhanced subsequent RSV disease in both mice and in volunteers. This pre-existing neutrophilic inflammation was linked to a failure to induce the transient early mucosal inflammatory response to viral exposure, dominated by IL-17 and related pathways, which was upregulated in individuals who resisted infection. Our findings highlight the complex role of the mucosal microenvironment in early responses to respiratory viral infection and demonstrate that the prior state of the mucosa alters the subsequent negotiation between virus and host, which determines the outcome of viral exposure.

Associations between RSV disease and neutrophil or IL-17 related inflammatory responses during infection have been observed in other settings. For example, IL-17 has been detected in the airway both at the height of severe symptoms and/or during convalescence in infants with RSV (*35*). However, little is known about its protective role early in the course of infection. IL-17A blockade in clinical trials of secukinumab, an anti-IL-17A monoclonal antibody, caused increased susceptibility to upper respiratory tract infections (*36-38*). Furthermore, in a BALB/c murine RSV model, BPZE1 (an attenuated *Bordetella pertussis* vaccine candidate) induces IL-17 and protects against RSV infection *(39, 40).* Moreover, the intranasal administration of IL-17A 2 hours post-RSV challenge decreases disease severity (*41*). These studies support our finding that an IL-17 dominated response during the early phase of infection may be critical for protection before viral replication is established.

The pleiotropic functions of IL-17 are integral to mucosal immunity, and include maintenance of barrier integrity, induction of antimicrobial proteins by epithelial cells and recruitment of inflammatory myeloid cells (*27*). However, here in our controlled studies of adults during the earliest stages after virus exposure, IL-17 signaling is associated with abortive infection. The apparently "silent" incubation phase is therefore immunologically dynamic, representing a critical interval during which clinical outcome is determined. Although an early inflammatory response prevents the establishment of viral infection, subjects destined for symptomatic colds show generalized downregulation of mucosal

defense as the virus gains control. In our studies, pre-existing neutrophilic inflammation appears to prevent this early protective response and is instead associated with enhanced susceptibility to infection and disease. Although we were unable to show an association between the nasal microbiome and susceptibility to RSV infection in our volunteers our studies do not preclude subtle influences of fungal or viral commensals that may alter the state of the mucosa or the effects of recent or subclinical bacterial or viral infections.

Our study has limitations. To avoid traumatic injury to nasal tissue prior to RSV inoculation, sampling for cytometric analysis (e.g., nasal biopsy) was not performed. The transcriptional and proteomic analyses that we report do not distinguish between elevated neutrophil abundance and greater activity of a static number of neutrophils, nor could we identify the cellular sources of cytokines such as IL-17A that we found elevated at baseline and during the pre-symptomatic viral incubation period. In future studies, we hope to resolve these questions by single-cell analysis of airway cells in early stages of viral infection. Although our murine studies were unable to replicate all aspects of human respiratory viral infection, they permitted the examination of possible mechanisms by detailed cytometric analysis of the airway and selective recruitment of airway neutrophils via CXCL1 instillation. Enhancement of viral load at 18 hours in mice pretreated with CXCL1 showed that induction of neutrophilic inflammation in the airway did indeed enhance RSV susceptibility, with an early impairment of antiviral immune responses translating into enhanced disease driven by $CD8^+$ T cells.

Previous studies have demonstrated that activation of one arm of the immune response may simultaneously suppress or disable another. For example, the activation of the T helper (Th)1 transcription factor T-bet limits Th2 responses by inhibiting GATA3 (*42*). Patients with chronic neutrophilic lung inflammation (such as bronchiectasis, chronic obstructive pulmonary disease, and some types of asthma) are known to have enhanced susceptibility to respiratory virus-induced disease (*43*). Similarly, in naturally acquired human influenza infection, we recently showed inflammatory signatures characteristic of antibacterial immunity correlate with severe disease, whereas antiviral responses were associated with milder illness (*44*). In murine models of colitis, RIG-I mediated IL-15 secretion induced by commensal viruses supports the survival of intraepithelial lymphocytes, which can

in turn inhibit aberrant inflammation (*45*). Additionally, viral bacteriophages within *Pseudomonas aeruginosa* have been shown to induce TLR3- and TRIF-mediated type I IFN production with associated suppression of phagocytic responses (*46*). These studies thus show that antiviral immunity can suppress responses typically associated with antibacterial and inflammatory mechanisms at multiple levels. Together with our present findings, they suggest that there may be opposing mechanisms whereby neutrophilic inflammation prior to viral exposure antagonizes optimal antiviral defense and results in failure to control viral infection.

We postulate that this apparent competition between alternative types of immune response may be relevant in a number of infections with protracted incubation periods, including coronaviruses (*47*). The prolonged presymptomatic period that we observe during RSV infection is also evident in SARS-CoV-2 infection, the interval between exposure and symptom development typically being ~5.2 days (*48*) compared to 4-5 days for RSV shown here. By contrast, during infections such as influenza A in which there is a very short incubation period (typically ~2 days (*47*)), intrinsic and innate responses may be rapidly overtaken by viral replication. Again, antibody response to SARS-CoV-2 (*49*) and other human coronaviruses (*50*) are apparently short-lived, a feature shared with RSV infection (*3*).

The distinct separation of pulmonary neutrophil and $CD8^+$ T cell infiltration (which show no temporal overlap) implies an indirect relationship between these immune effectors. The early production of IL-17 may be by a variety of cell types including $CD4^+$ Th17 and $CD8^+$ T cytotoxic (Tc)17 T cells, γδ T cells, neutrophils and type 3 innate lymphoid cells (ILC3), which are abundant at mucosal surfaces (*51-53*). A number of mechanisms may link neutrophilic inflammation with enhanced $CD8^+$ T cell recruitment. The pre-infection pattern of neutrophil activation was associated with the upregulation of peptidases and hydrolases, which have been shown to modulate cytokine activity (*54*) in other systems, potentially altering the immediate antiviral response and signaling to natural killer (NK) and T cells (*55*). This is supported by the observation that *Il1b, Cxcl2, Cxcl10,* and *Ccl2* expression, all of which have been implicated in antiviral defense, were perturbed, either directly or through negative feedback. Enhanced $CD8^+$ T cell migration may also result from neutrophil-derived CXCL12-containing trails, as shown in the influenza-infected mouse trachea (*56*). Furthermore, TLR4 antagonists reduce influenza-

induced mortality in mice (*57*) so neutrophil-derived oxidized phospholipids (which are TLR4 agonists) may enhance susceptibility. Neutrophil proteases may also degrade antiviral peptides, such as cathelicidin (LL-37) (*4*), which would influence immediate susceptibility and might contribute to the early transient difference seen in viral load. The direct enhancement of antigen processing or presentation of antigen by neutrophils to T cells (*58*) is less likely due to the low number of T cells present early post-infection when neutrophils are high and vice versa later. However, it is possible that neutrophils influence antigen presentation by dendritic cells, synergizing with the early increase in viral load and promoting $CD8^+$ T cell activation, differentiation and proliferation to enhance viral clearance. The large number of potential contributors means that the precise mechanism(s) through which neutrophils enhance $CD8^+$ T cell recruitment and therefore exacerbated RSV disease remains a major topic of future studies.

Together, our results reveal an integrated time-dependent mucosal response that critically determines the outcome of pathogen exposure. The susceptibility to infection associated with neutrophilic inflammation prior to viral exposure reflects a multi-layered protective network that reacts rapidly to viral encounter, determining outcome prior to the presentation of disease. These findings not only increase our capacity to predict hitherto inexplicable variations in the outcome of exposure to viral pathogens, but also suggest that manipulation of neutrophil, peptidase, and IL-17-related pathways may affect antiviral protection, offering additional strategies to prevent disease caused by existing and emerging viral pathogens.

Materials and Methods

Human volunteer infection study design

Healthy non-smoking adults aged 18-55 were eligible as previously described except no pre-screening for serum neutralizing antibodies was performed (*16*). As an exploratory study, no power calculations were performed to determine sample size before the study began. Participants provided written informed consent and the study was approved by the UK National Research Ethics Service (study reference numbers 10/H0711/94 and 11/LO/1826). The study was registered on clinicaltrials.gov under ID NCT01349543. Volunteers provided a full clinical history, underwent a physical examination, and a panel of screening blood tests to exclude underlying hematological, biochemical or immune abnormalities. All participants were screened for HIV, hepatitis B virus and hepatitis C virus. Participants were excluded if they developed common cold symptoms or any acute illness within 6 weeks prior to inoculation. On the day before inoculation, a nasal lavage specimen was tested using multiplex PCR for a panel of 13 respiratory viruses and bacteria to exclude concurrent upper respiratory tract infection. Volunteers entered quarantine on study day –1, were inoculated by intra-nasal drops with 10^4 plaque forming units of RSV strain M37 (Meridian Lifesciences, Memphis, USA, GenBank Sequence Accession KM360090) the next day, and remained in quarantine as described (*3*). Volunteers provided daily assessment of their clinical symptoms in the following categories: nasal discharge, nasal obstruction, sneezing, sore throat, headache, fever, and malaise. Each category was scored by volunteers as either 0 (absent), 2 (moderate), or 3 (severe). A symptomatic cold was defined as fulfilment of two of the three following conditions: (1) a cumulative symptom score ≥14, (2) nasal discharge lasting ≥3 days, (3) subjective assessment of having a cold.

Samples of nasal mucosal lining fluid (MLF) were collected daily using pre-cut strips of Leukosorb (Pall Life Sciences, Portsmouth, UK), eluted in 300 µl of phosphate buffered saline (+ 1% bovine serum albumin w/v, + 0.5 % Triton-X v/v, and + 0.05% sodium azide w/v) (Sigma, UK) and stored at –80°C for later analysis, as previously described (*59*). Nasal washes were performed as previously described (*3*). Nasal tissue samples were collected on days 0 and 3 using ASI-Rhinopro nasal curettage devices

(Arlington Scientific, Springville, Utah, USA), immediately placed in 800 µl TRIZol (Life technologies, Paisley, UK) buffer, vortexed thoroughly, and stored at –80°C for later analysis.

Quantification of viral load

RSV load in humans was determined from daily nasal wash samples by quantitative PCR as previously described (*20*).

Immunoassays

Levels of CCL3 (MIP-1α), CCL5 (RANTES), CXCL8 (IL-8), CXCL10 (IP-10), IFN-α, IFN-β, IFN-γ, IL-1β, IL-6, IL-10, IL-15, IL-17A, and TNF-α were assayed using MSD multiplex immunoassays (Mesoscale Diagnostics, Rockville, Maryland, USA).

RNA sequencing of nasal curettage tissue samples

Nasal curettage samples were collected as previously described (*60*), preserved in Trizol. After collection, 0.2× chloroform was added to the samples for every 1× of Trizol, mixed by inverting the tube 10 times, incubated for 5 min, and centrifuged for 10 min at 3500*g*. The supernatant was then transferred into a new tube and total RNA was extracted with an SV96 kit, as per the manufacturer's protocol (Promega, Madison, USA).

cDNA libraries were prepared with TruSeq Stranded Total RNA Library Prep Kit with Ribo-Zero Human Sample Prep Kit (Illumina, San Diego, USA). Final cDNA libraries were analyzed for size distribution using the Tapestation 2200 (Agilent), quantitated by qPCR (KAPA Library Quant Kit, KAPA Biosystems, Wilmington, USA), normalized to 2 nM, and sequenced with 2×50-bp paired-end reads on a HiSeq 2500 (Illumina) with a minimum of 3 GB of raw RNA sequencing data.

RNAseq reads were mapped to human B38 genome with Omicsoft OSA, and read counts mapped to the ensemble genes (Release 75) were calculated with RSEM. Gene count data were normalized by DESeq2 (R package, version 1.18.1). An arbitrary filter to remove genes with low counts was applied to the normalized count data (only protein-coding genes and normalized count >35 in at least six

samples was kept, which resulted in 14670 ensembl genes). DESeq2 was then used to identify differential expression of these genes. Differentially expressed genes (DEGs) were determined as those with an *P*-value <0.01 and a >0.5 $\log^2$ fold-change, relative to baseline for the Cold or No-cold group; and adjusted *P*-value < 0.05 for Cold vs No-cold at baseline. Log^2 normalized count data was used in the heatmap. Gene set over-representation analysis of GO and KEGG pathways was done with clusterProfiler (R package, version 3.6.0). Co-expression gene network was built with WGCNA (R package, version 1.63), and visualized with Cytoscape (*61*).

Bronchial biopsy immunohistochemistry

Endobronchial biopsies were fixed immediately in 4% paraformaldehyde and paraffin embedded. RSV was stained using polyvalent mouse anti-RSV antibody (NCL-RSV3, Leica Biosystems, UK) at 1:50 dilution. $CD8^+$ T cells were identified by staining with mouse anti-CD8 (M0707, Dako) at 1:100 dilution using the EnVision peroxidase staining method (Dako, Denmark) as previously described (*62*). Briefly, 5μm sections were stained according to the manufacturer's instructions and an irrelevant mouse IgG1 kappa antibody (MOPC21) was used as negative control for staining specificity of mouse monoclonal antibodies. RSV-infected A549 cells were used as positive staining controls. Quantification was achieved as previously described with operators blinded to sample timing and infection status (*62*). Briefly, slides were coded to avoid observer bias and areas of epithelium and subepithelium assessed using a Leitz Dialux 20 light microscope, Apple Macintosh computer and Image 1.5 software. Total epithelial and subepithelial areas of two to three bronchial biopsies were counted for each bronchoscopy. Cell counts were expressed as the number of cut cell profiles with visible nucleus per mm^2 of subepithelium and per 0.1 mm^2 of epithelium. The coefficient of variation for repeat counts of positive cells by a single observer ranged from 5-6%.

Respiratory bacterial load and 16S sequencing

DNA extraction was performed on throat swabs using the MPBio FastDNA™ spin kit for soil as per the manufacturer's instructions. Blank swabs were extracted and sequenced to control for

contamination. Bacterial loads were quantified in triplicate by SYBR green qPCR as previously described (*63*).

Sequencing of the 16S rRNA gene was performed on the Illumina MiSeq platform using dual barcode fusion primers targeting the V4 region of the 16S rRNA gene as previously decided (*63*). Extraction controls, PCR-negative, and mock communities were included on sequencing runs. Sequence processing was carried out using QIIME and UCLUST was used to assign taxonomic identification to operational taxonomic units (OTU) using the Silva 115 NR database, as previously described (*63*). OTU and tree files were output into R version 3.3.2.

Mouse infection studies

Female wild-type (wt) C57BL/6 mice (8 weeks of age) were purchased from Charles River. All mice were housed in specific pathogen-free conditions. All animal experiments were reviewed and approved by the Animal Welfare and Ethical Review Board (AWERB) within Imperial College London and approved by the UK Home Office in accordance with the Animals (Scientific Procedures) Act 1986 and the ARRIVE guidelines.

Plaque-purified human RSV (originally A2 strain from ATCC, USA) was grown in HEp2 cells (from ATCC, CCL-23) (*64*). Mice were lightly anaesthetized before intranasal (i.n.) administration of 100 µl containing 7.5-10×10^5 focus forming units (FFU) RSV or PBS control. In some instances, this was preceded by i.n. instillation of 5-10 µg recombinant murine CXCL1 (Biolegend, San Diego, USA) 12 hours before infection, 500µg anti-Ly6G (1A8) or isotype control (2A3) intraperitonially (i.p.) on day -1, day 1 and day 3 post-infection (p.i.), or 250µg anti-CD8 (YTS169.4) or isotype control (LTF-2) i.p. on day -1, day 2 and day 5 p.i. (all antibodies from BioXCell, West Lebanon, USA). Mice were sacrificed by a fatal dose of pentobarbital injected i.p..

To enumerate neutrophils in the bronchoalveolar lavage (BAL), 1 ml of PBS supplemented with 0.5 mM EDTA was used to flush the lungs three times. The BAL was centrifuged and red blood cells were

removed by lysis with ACK buffer (0.15 M NH_4Cl, 1.0 mM $KHCO_3$, 0.1 mM Na_2EDTA). The cell number was determined by Trypan Blue (Thermo Scientific) exclusion of dead cells. The cellular composition was determined by spinning 1-2×10^5 cells onto a microscope slide (Thermo Scientific) at 1000*g* for 5 min using Cytospin 4 Cytocentrifuge (Thermo Scientific). Slides were H&E stained using Reastain Quick-Diff kit (Gentaur, Kampenhout, Belgium), according to the manufacturer's instructions. Cells were classified as neutrophils using a microscope and ≥300 cells were counted.

Mediators in the BAL was measured using ELISA. Murine IFN-α and IL-6 were detected as previously described (*32*). Murine MMP-9, MPO, and NE were detected using DuoSet ELISA kits (R&D systems). Data were acquired on a FLUOstar Omega plate reader (BMG LABTECH) and analyzed using MARS data analysis (BMG LABTECH).

Lung tissue was homogenized using a TissueLyser LT (Qiagen) and total RNA was extracted from homogenized lung tissue supernatant using RNeasy Mini kit including DNA removal (Qiagen). RNA concentration was determined by NanoDrop (Thermo Scientific) and RNA was converted to cDNA using High Capacity RNA-to-cDNA kit (Applied Biosystems). All primers and probes used are listed in the supplementary materials and all assays used QuantiTect Probe PCR Master Mix (Qiagen). To quantify RSV L gene and *Tnfa* levels in lung tissue (*64, 65*), the exact number of copies was calculated using a plasmid standard, and the results were normalized to the housekeeping gene *Gapdh* (Applied Biosystems). For relative quantification, the expression of *Ccl2*, *Cxcl2*, *Cxcl10,* and *Il1b* (all from Applied Biosystems) were expressed relatively to the expression of *Gapdh*. First, the ΔCT (Ct=cycle threshold) between the target gene and the *Gapdh* for each sample was calculated. Then the expression was calculated as $2^{-\Delta CT}$. Analysis was performed using 7500 Fast System SDS Software (Applied Biosystems).

Flow cytometry and restimulation experiments

For flow cytometry staining, 2.5×10^6 lung cells were incubated for 20 min at 4°C with purified rat IgG2b anti-mouse CD16/CD32 receptor antibody in PBS containing 1% BSA and 5 mM EDTA and

then stained with fluorochrome-conjugated antibodies (see supplementary materials in PBS for 30 min at 4°C. Cells were fixed with fixation buffer (Biolegend, Cambridge, UK). For RSV M Tetramer staining, Alexa Fluor 647-conjugated $M_{187\text{-}195}$ tetramers (H-2D^b/NAITNAKII) were obtained from the NIH Tetramer Core Facility (Emory University, Atlanta, GA, USA). Tetramer staining was performed following Fc-block and prior to surface staining for 30 min at RT in PBS containing 1% BSA and 5 mM EDTA. For intracellular staining, the cells were re-stimulated with 5 μg/ml RSV $M_{187\text{-}195}$-peptide (A&A labs LLC) for 1 hour at 37°C. After addition of Golgi Plug (BD Biosciences) the samples were incubated for another 3 hours, stained for surface marker expression as described above and fixed in fixation buffer (Biolegend). Cells were stained with fluorochrome-conjugated antibodies against granzyme B and IFN-γ in the presence of purified rat IgG2b anti-mouse CD16/CD32 receptor antibody in permeabilization buffer (Biolegend) for 1 hour. Analysis was performed on a BD LSR Fortessa. Acquisition was set to 250,000 single, live, CD45$^+$ cells. The gating strategies are shown in fig. S5. Monocyte and neutrophil enumeration in Fig. 6G and fig. S7A was performed using gating strategies described previously (*32*). Data were analyzed with FlowJo software (Tree Star Inc, Ashland, Oregon, USA). Total cell populations were quantified as the whole lung count × (% population of CD45$^+$ cells) × (% CD45$^+$ cell of live cells) × (proportion of lung tissue sampled).

Data Availability

RNAseq data have been deposited in the NCBI Gene Expression Omnibus with the accession code [TBC]. Sequences from 16S rRNA sequencing have been deposited in the European Nucleotide Archive with the accession codes PRJEB28323 (ERP110514). Other data that support the findings of this study are available from the corresponding authors upon reasonable request.

Statistical Analyses

Statistical analyses used GraphPad Prism v7 (GraphPad, La Jolla, California, USA) and R version 3.3.2. Mediator concentrations were determined from a standard curve with a four-parameter logistic model fit as per product literature. Limits of detection for each mediator were calculated as twice the standard deviation of the assay blank well (background signal) duplicates and samples yielding a signal below

this value were assigned a value of this limit. Daily mediator concentrations were expressed as $\log_2$ fold-change over the baseline (day 0) value for each subject and a least-squares LOESS model was applied using a polynomial degree of 1 and a span of 0.75. A grid of 100 points across the span of day 1 to 10 was used to produce the prediction curves. Point-wise 95% confidence intervals were derived using a bootstrap percentile method as previously described (*3*) except the derived LOESS fit was used to calculate the predicted response values. One property of this LOESS fitting is that the graphical representation of the line at each time point is influenced by preceding and subsequent data. As such, any apparent differences between groups at baseline results from the difference between groups at day 1 (the next time point). Univariate logistic regression was performed with disease status ("Cold" or "No Cold") as the dependent variable to identify mediator response(s) associated with inoculation outcome. For the mouse studies, statistical analysis was performed using Prism (GraphPad software) version 7. Data are presented as the mean ± SEM. As indicated, Student's *t* test was used to compare two groups, one-way ANOVA followed by Tukey's post hoc was used to compare multiple groups. The weight curves were analyzed using a two-way ANOVA followed by Bonferroni's post hoc test. *P* values <0.05 were considered statistically significant for all tests. * $P< 0.05$; ** $P< 0.01$; *** $P< 0.001$.

Funding/Acknowledgements: The authors gratefully acknowledge support from the Wellcome Trust (087805/Z/08/Z and 109058/Z/15/Z); The Medical Research Council HIC-Vac network (MR/R005982/1); RSV Consortium in Europe (RESCEU) Horizon 2020 Framework Grant 116019; the UK National Institute for Health Research (NIHR) Comprehensive Local Research Networks (CLRNs); European Respiratory Society and the Asociación Latinoamericana de Tórax joint long-term Research Fellowship 2019 (Number: LTRF 201901-00546); an NIHR Senior Investigator award; the Biomedical Research Centre (NIHR Imperial BRC) and the Health Protection Research Unit in Respiratory Infections at Imperial College London (NIHR HPRU RI). We also thank the NIH Tetramer Core Facility at Emory University for providing tetramers and the St Mary's flow cytometry and animal facilities.

Author Contributions: P.J.M.O. and C.C. conceived the study. M.S.H., A.P. and C.C. performed infections and collected volunteer samples. M.S.H., R.S.T., A.J., L.C., P.J. and C.C. collected human data. Murine experiments were designed, performed and analyzed by F.K. A.V., A.O. and C.J. Human data were analyzed by M.S.H., R.S.T., M.C., L.C., T.T., D.N., T.T.H., M.F.M., C.C. and P.J.M.O. The paper was written by M.S.H., R.S.T., C.J., C.C. and P.J.M.O with input from all authors.

Reference List

1. J. A. Whitsett, T. Alenghat, Respiratory epithelial cells orchestrate pulmonary innate immunity. *Nat Immunol* **16**, 27-35 (2015).
2. T. T. Hansel, S. L. Johnston, P. J. Openshaw, Microbes and mucosal immune responses in asthma. *Lancet* **381**, 861-873 (2013).
3. M. S. Habibi *et al.*, Impaired Antibody-mediated Protection and Defective IgA B-Cell Memory in Experimental Infection of Adults with Respiratory Syncytial Virus. *Am J Respir Crit Care Med* **191**, 1040-1049 (2015).
4. S. M. Currie *et al.*, Cathelicidins Have Direct Antiviral Activity against Respiratory Syncytial Virus In Vitro and Protective Function In Vivo in Mice and Humans. *J Immunol* **196**, 2699-2710 (2016).
5. M. Zanin, P. Baviskar, R. Webster, R. Webby, The Interaction between Respiratory Pathogens and Mucus. *Cell Host Microbe* **19**, 159-168 (2016).
6. P. J. Openshaw, C. Chiu, F. J. Culley, C. Johansson, Protective and Harmful Immunity to Respiratory Syncytial Virus Infection. *Annual Review of Immunology* **35**, 501-532 (2017).
7. R. J. Geerdink, J. Pillay, L. Meyaard, L. Bont, Neutrophils in respiratory syncytial virus infection: A target for asthma prevention. *J Allergy Clin Immunol* **136**, 838-847 (2015).
8. T. Shi *et al.*, Global, regional, and national disease burden estimates of acute lower respiratory infections due to respiratory syncytial virus in young children in 2015: a systematic review and modelling study. *Lancet* **390**, 946-958 (2017).
9. A. R. Falsey, P. A. Hennessey, M. A. Formica, C. Cox, E. E. Walsh, Respiratory syncytial virus infection in elderly and high-risk adults. *N Engl J Med* **352**, 1749-1759 (2005).
10. T. Shi *et al.*, Global Disease Burden Estimates of Respiratory Syncytial Virus-Associated Acute Respiratory Infection in Older Adults in 2015: A Systematic Review and Meta-Analysis. *J Infect Dis*, (2019).
11. L. Zhang, M. E. Peeples, R. C. Boucher, P. L. Collins, R. J. Pickles, Respiratory syncytial virus infection of human airway epithelial cells is polarized, specific to ciliated cells, and without obvious cytopathology. *J Virol* **76**, 5654-5666 (2002).
12. W. Aherne, T. Bird, S. D. Court, P. S. Gardner, J. McQuillin, Pathological changes in virus infections of the lower respiratory tract in children. *J Clin Pathol* **23**, 7-18 (1970).
13. D. Committee on Infectious, From the American Academy of Pediatrics: Policy statements--Modified recommendations for use of palivizumab for prevention of respiratory syncytial virus infections. *Pediatrics* **124**, 1694-1701 (2009).
14. J. Vekemans *et al.*, Respiratory syncytial virus vaccine research and development: World Health Organization technological roadmap and preferred product characteristics. *Vaccine* **37**, 7394-7395 (2019).
15. M. C. Crank *et al.*, A proof of concept for structure-based vaccine design targeting RSV in humans. *Science* **365**, 505-509 (2019).
16. J. P. DeVincenzo *et al.*, Viral load drives disease in humans experimentally infected with respiratory syncytial virus. *Am J Respir Crit Care Med* **182**, 1305-1314 (2010).
17. A. J. Pollard *et al.*, Human microbial challenge: the ultimate animal model. *Lancet Infect Dis* **12**, 903-905 (2012).
18. P. K. Kiyuka *et al.*, Human Coronavirus NL63 Molecular Epidemiology and Evolutionary Patterns in Rural Coastal Kenya. *J Infect Dis* **217**, 1728-1739 (2018).
19. B. Bagga *et al.*, Effect of Preexisting Serum and Mucosal Antibody on Experimental Respiratory Syncytial Virus (RSV) Challenge and Infection of Adults. *J Infect Dis* **212**, 1719-1725 (2015).
20. A. Jozwik *et al.*, RSV-specific airway resident memory CD8+ T cells and differential disease severity after experimental human infection. *Nat Commun* **6**, 10224 (2015).
21. J. P. Devincenzo, Natural infection of infants with respiratory syncytial virus subgroups A and B: a study of frequency, disease severity, and viral load. *Pediatr Res* **56**, 914-917 (2004).

22. C. M. El Saleeby, A. J. Bush, L. M. Harrison, J. A. Aitken, J. P. Devincenzo, Respiratory syncytial virus load, viral dynamics, and disease severity in previously healthy naturally infected children. *J Infect Dis* **204**, 996-1002 (2011).
23. R. S. Thwaites *et al.*, Reduced Nasal Viral Load and IFN Responses in Infants with Respiratory Syncytial Virus Bronchiolitis and Respiratory Failure. *Am J Respir Crit Care Med* **198**, 1074-1084 (2018).
24. G. G. Jackson, H. F. Dowling, I. G. Spiesman, A. V. Boand, Transmission of the common cold to volunteers under controlled conditions. I. The common cold as a clinical entity. *AMA Arch Intern Med* **101**, 267-278 (1958).
25. A. J. Stoppelenburg *et al.*, Local IL-17A potentiates early neutrophil recruitment to the respiratory tract during severe RSV infection. *PLoS One* **8**, e78461 (2013).
26. N. Amatya, A. V. Garg, S. L. Gaffen, IL-17 Signaling: The Yin and the Yang. *Trends Immunol* **38**, 310-322 (2017).
27. S. J. Aujla *et al.*, IL-22 mediates mucosal host defense against Gram-negative bacterial pneumonia. *Nat Med* **14**, 275-281 (2008).
28. F. G. Hayden *et al.*, Local and systemic cytokine responses during experimental human influenza A virus infection. Relation to symptom formation and host defense. *J Clin Invest* **101**, 643-649 (1998).
29. E. G. Nicholson *et al.*, Robust Cytokine and Chemokine Response in Nasopharyngeal Secretions: Association With Decreased Severity in Children With Physician Diagnosed Bronchiolitis. *J Infect Dis* **214**, 649-655 (2016).
30. W. A. de Steenhuijsen Piters *et al.*, Nasopharyngeal Microbiota, Host Transcriptome, and Disease Severity in Children with Respiratory Syncytial Virus Infection. *Am J Respir Crit Care Med* **194**, 1104-1115 (2016).
31. F. Kirsebom, C. Michalaki, M. Agueda-Oyarzabal, C. Johansson, Neutrophils do not impact viral load or the peak of disease severity during RSV infection. *Sci Rep* **10**, 1110 (2020).
32. M. Goritzka *et al.*, Alveolar macrophage-derived type I interferons orchestrate innate immunity to RSV through recruitment of antiviral monocytes. *J Exp Med* **212**, 699-714 (2015).
33. M. J. Cannon, P. J. Openshaw, B. A. Askonas, Cytotoxic T cells clear virus but augment lung pathology in mice infected with respiratory syncytial virus. *J Exp Med* **168**, 1163-1168 (1988).
34. F. C. M. Kirsebom, F. Kausar, R. Nuriev, S. Makris, C. Johansson, Neutrophil recruitment and activation are differentially dependent on MyD88/TRIF and MAVS signaling during RSV infection. *Mucosal Immunol* **12**, 1244-1255 (2019).
35. T. E. Faber, H. Groen, M. Welfing, K. J. Jansen, L. J. Bont, Specific increase in local IL-17 production during recovery from primary RSV bronchiolitis. *J Med Virol* **84**, 1084-1088 (2012).
36. R. G. Langley *et al.*, Secukinumab in plaque psoriasis--results of two phase 3 trials. *N Engl J Med* **371**, 326-338 (2014).
37. P. J. Mease *et al.*, Secukinumab Inhibition of Interleukin-17A in Patients with Psoriatic Arthritis. *N Engl J Med* **373**, 1329-1339 (2015).
38. I. B. McInnes *et al.*, Secukinumab, a human anti-interleukin-17A monoclonal antibody, in patients with psoriatic arthritis (FUTURE 2): a randomised, double-blind, placebo-controlled, phase 3 trial. *Lancet* **386**, 1137-1146 (2015).
39. C. Schnoeller *et al.*, Attenuated Bordetella pertussis vaccine protects against respiratory syncytial virus disease via an IL-17-dependent mechanism. *Am J Respir Crit Care Med* **189**, 194-202 (2014).
40. G. Fedele, M. Bianco, A. S. Debrie, C. Locht, C. M. Ausiello, Attenuated Bordetella pertussis vaccine candidate BPZE1 promotes human dendritic cell CCL21-induced migration and drives a Th1/Th17 response. *J Immunol* **186**, 5388-5396 (2011).
41. H. Huang, J. Saravia, D. You, A. J. Shaw, S. A. Cormier, Impaired gamma delta T cell-derived IL-17A and inflammasome activation during early respiratory syncytial virus infection in infants. *Immunol Cell Biol* **93**, 126-135 (2015).
42. J. Zhu *et al.*, The transcription factor T-bet is induced by multiple pathways and prevents an endogenous Th2 cell program during Th1 cell responses. *Immunity* **37**, 660-673 (2012).

43. A. Jha *et al.*, Patterns of systemic and local inflammation in patients with asthma hospitalised with influenza. *Eur Respir J* **54**, (2019).
44. J. Dunning *et al.*, Progression of whole-blood transcriptional signatures from interferon-induced to neutrophil-associated patterns in severe influenza. *Nat Immunol* **19**, 625-635 (2018).
45. L. Liu *et al.*, Commensal viruses maintain intestinal intraepithelial lymphocytes via noncanonical RIG-I signaling. *Nat Immunol* **20**, 1681-1691 (2019).
46. J. M. Sweere *et al.*, Bacteriophage trigger antiviral immunity and prevent clearance of bacterial infection. *Science* **363**, eaat9691 (2019).
47. X. He *et al.*, Temporal dynamics in viral shedding and transmissibility of COVID-19. *Nat Med* **26**, 672-675 (2020).
48. Q. Li *et al.*, Early Transmission Dynamics in Wuhan, China, of Novel Coronavirus-Infected Pneumonia. *N Engl J Med* **382**, 1199-1207 (2020).
49. D. F. Robbiani *et al.*, Convergent Antibody Responses to SARS-CoV-2 Infection in Convalescent Individuals. *bioRxiv*, (2020).
50. K. A. Callow, H. F. Parry, M. Sergeant, D. A. Tyrrell, The time course of the immune response to experimental coronavirus infection of man. *Epidemiol Infect* **105**, 435-446 (1990).
51. C. E. Sutton, L. A. Mielke, K. H. Mills, IL-17-producing gammadelta T cells and innate lymphoid cells. *Eur J Immunol* **42**, 2221-2231 (2012).
52. H. Hamada *et al.*, Tc17, a unique subset of CD8 T cells that can protect against lethal influenza challenge. *J Immunol* **182**, 3469-3481 (2009).
53. K. C. De Grove *et al.*, Characterization and Quantification of Innate Lymphoid Cell Subsets in Human Lung. *PLoS One* **11**, e0145961 (2016).
54. D. M. Clancy *et al.*, Extracellular Neutrophil Proteases Are Efficient Regulators of IL-1, IL-33, and IL-36 Cytokine Activity but Poor Effectors of Microbial Killing. *Cell Rep* **22**, 2937-2950 (2018).
55. J. A. Nicolas-Avila, J. M. Adrover, A. Hidalgo, Neutrophils in Homeostasis, Immunity, and Cancer. *Immunity* **46**, 15-28 (2017).
56. K. Lim *et al.*, Neutrophil trails guide influenza-specific CD8(+) T cells in the airways. *Science* **349**, aaa4352 (2015).
57. K. A. Shirey *et al.*, The TLR4 antagonist Eritoran protects mice from lethal influenza infection. *Nature* **497**, 498-502 (2013).
58. M. M. Hufford *et al.*, Influenza-infected neutrophils within the infected lungs act as antigen presenting cells for anti-viral CD8(+) T cells. *PLoS One* **7**, e46581 (2012).
59. R. Thwaites *et al.*, Absorption of Nasal and Bronchial Fluids: Precision Sampling of the Human Respiratory Mucosa and Laboratory Processing of Samples. *J. Vis. Exp.* **131**, (2018).
60. J. Dhariwal *et al.*, Mucosal Type 2 Innate Lymphoid Cells Are a Key Component of the Allergic Response to Aeroallergens. *Am J Respir Crit Care Med* **195**, 1586-1596 (2017).
61. P. Shannon *et al.*, Cytoscape: a software environment for integrated models of biomolecular interaction networks. *Genome Res* **13**, 2498-2504 (2003).
62. J. Zhu *et al.*, Airway inflammation and illness severity in response to experimental rhinovirus infection in asthma. *Chest* **145**, 1219-1229 (2014).
63. L. Cuthbertson *et al.*, The impact of persistent bacterial bronchitis on the pulmonary microbiome of children. *PLoS One* **12**, e0190075 (2017).
64. D. C. Lee *et al.*, CD25+ natural regulatory T cells are critical in limiting innate and adaptive immunity and resolving disease following respiratory syncytial virus infection. *J Virol* **84**, 8790-8798 (2010).
65. M. Goritzka *et al.*, Alpha/beta interferon receptor signaling amplifies early proinflammatory cytokine production in the lung during respiratory syncytial virus infection. *J Virol* **88**, 6128-6136 (2014).

Figure legends

Fig. 1: The kinetics of viral replication and symptoms correlate closely, with no viral replication or symptoms evident until day 3 post-inoculation (A) Participants were inoculated with RSV at day 0. Nasal wash and nasosorption samples were taken daily during quarantine (up to day 10) and at day 14. Nasal curettage was performed at baseline (7-14 days pre-inoculation) and day 3. **(B)** Daily viral load, measured by qPCR of nasal wash, in volunteers who developed symptomatic RSV infections ("Cold", n=23). **(C)** Daily upper respiratory tract (URT) symptom scores in the Cold (red, n=23) and No Cold (blue, n=25) groups. Data in panels B and C are represented as median ± interquartile ranges.

Fig. 2: Pre-exposure airway neutrophil activation is associated with susceptibility to RSV infection (A) Differentially expressed genes (DEGs; adjusted *P*-value <0.05; n=80) were determined in baseline (7-14 days pre-inoculation) nasal curettage samples between Cold and No Cold groups by RNA-Seq. **(B)** Gene Ontology molecular functions enrichment analysis of DEGs (adjusted *P*-value < 0.1, n=235) **(C)** Gene Ontology biological processes enrichment analysis of DEGs (adjusted *P*-value < 0.1, n=235). **(D)** Weighted gene co-expression network analysis cluster of DEGs (adjusted *P*-value < 0.1, n=235), enriched for those with annotations of neutrophil association. **(E)** Day 0 levels of myeloperoxidase (MPO), lipocalin-2 (LCN-2) and IL-17A in nasosorption samples between No Cold (n=10-25) and Cold (n=9-23) groups. **P*<0.05. Data in panel E are represented as median and interquartiles with minimum and maximum values.

Fig. 3: Early pre-symptomatic viral clearance is associated with activation of IL-17 signaling Differentially expressed genes (DEGs) were determined by RNA-Sequencing of nasal curettage samples at day 3 post-inoculation relative to baseline (7-14 days pre-inoculation) in the No Cold (n=16) and Cold (n=16) groups; Heatmaps show **(A)** DEGs in the No Cold group (n=87); **(B)** DEGs in the Cold group (n=77). **(C)** Venn diagram of the number of overlapping DEGs in the Cold and No Cold groups. DEGs from the No Cold group were analyzed for enrichment of **(D)** GO molecular functions and **(E)** KEGG pathways. DEGs were defined as transcripts with adjusted *P*<0.01 and $\log^2$ fold-change >0.5.

Fig. 4: Network analysis reveals a module of correlated DEGs enriched for IL-17 signaling in pre-symptomatic individuals Weighted gene co-expression network analysis (WGCNA) of the differentially expressed genes (n=87) was performed in the No Cold group at day 3, relative to baseline. **(A)** Classification of WGCNA modules. Brown module: **(B)** network map and **(C)** molecular function enrichment. Turquoise module: **(D)** network map and **(E)** molecular function enrichment. Blue module: **(F)** network map and **(G)** molecular function enrichment. DEGs were defined as transcripts with *P*<0.01 and $\log^2$ fold-change >0.5.

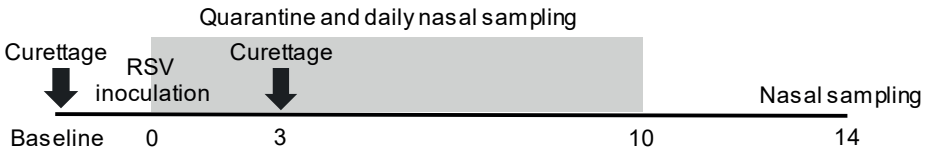
Fig. 5: Early pre-symptomatic secretion of intranasal IL-1β, IL-6 and IL-17A is associated with protection from RSV infection (A-C) Soluble protein cytokine and chemokine mediator levels from nasosorption samples were determined on each study day and expressed as LOESS plots between Cold (Red) and No Cold (Blue) groups of $\log^2$ fold-change levels normalized to day 0. The 95% confidence intervals of LOESS curves are denoted by shaded areas. **(D)** Logistic regression analysis of mediator responses during days 1-3 post-inoculation, measured at protein level from nasosorption samples.

Fig. 6: Mice treated with the neutrophil chemoattractant CXCL1 pre-RSV infection show an early increase in viral load and develop more severe disease Mice were treated with mock (PBS) or 10 μg CXCL1 intranasally (i.n.). **(A)** At 12 hours post treatment, BAL and lung neutrophils were quantified by flow cytometry and **(B)** MMP-9, MPO and NE levels in the BAL were quantified by ELISA. Mice were treated with mock (PBS) or 5-10 μg CXCL1 i.n. and after 9-12 hours infected with

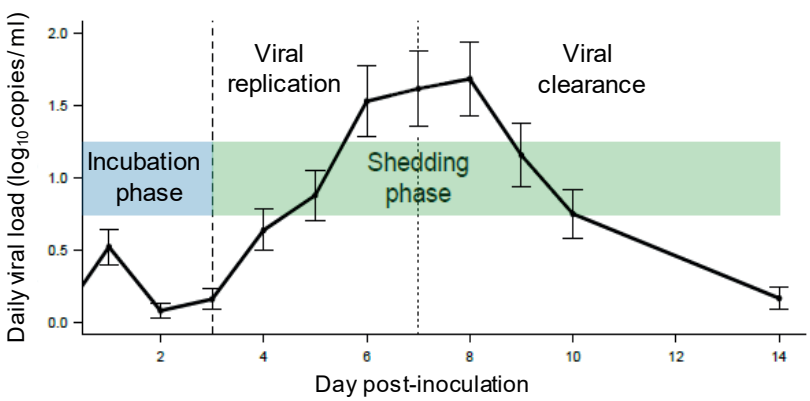
mock (PBS) or 7.5×10^5 FFU RSV i.n.. **(C)** Weight loss as a percentage of original weight. **(D)** IFN-α and IL-6 was quantified in BAL using ELISA. **(E)** Levels of *Il1b, Tnfa,* **(F)** *Cxcl2, Cxcl10,* and **(G)** *Ccl2* were determined in lung tissue using qPCR. **(H)** The total number of lung monocytes was quantified by flow cytometry as previously described (*32*). **(I)** RSV L gene copy numbers were quantified on days 0.75, 4, and 8 p.i. in lung tissue by qPCR. Data in (A) and (B) are presented as mean ± SEM of eight individual mice per group, pooled from two independent experiments. Data in (C) are presented as mean ± SEM of 10 (PBS/PBS) or 14-16 (RSV) individual mice, pooled from two (PBS/PBS) or three (RSV) independent experiments. Data in (D-H) are presented as mean ± SEM of 10 individual mice per group, pooled from two independent experiments. Data in (I) are presented as mean ± SEM of five individual mice per group, representative of at least two independent experiments, with the dotted line representing the limit of detection of the assay. Statistical significance of differences in; (A-B) was analyzed using unpaired, two-tailed Student's *t* test. The data in (C) and (I) were analyzed using two-way ANOVA with Bonferroni's post hoc test and only the statistically significant differences between RSV infected groups are shown. (D-H) were analyzed using one-way ANOVA with Tukey's post hoc test. **P*<0.05, ***P*<0.01, ****P*<0.001.

Fig. 7: Mice treated with the neutrophil chemoattractant CXCL1 pre-RSV infection develop CD8$^+$ T cell driven disease (A) Correlation between CD8$^+$ T cell numbers in the subepithelial layer of endobronchial biopsy samples from human participants infected with RSV at day 7 p.i. and cumulative symptom scores over the course of infection (n=11). **(B-H)** Mice were treated with mock (PBS) or 10 µg CXCL1 i.n. 12 hours pre RSV infection. Lungs were analyzed at day 8 p.i.. **(B)** Total number of lung cells, **(C)** lung CD4$^+$ T cells and **(D)** lung CD8$^+$ T cells assessed by flow cytometry. **(E)** Representative flow cytometry plots of lung RSV tetramer positive CD8$^+$ T cells and the mean percentage ± SEM is indicated in the upper right quadrant. **(F)** Total number of lung RSV tetramer positive CD8$^+$ T cells as quantified by flow cytometry. **(G)** Representative flow cytometry plots of lung Granzyme B (GzmB)$^+$ and IFN-γ$^+$ CD8$^+$ T cells. **(H)** Frequency of GzmB$^+$ and IFN-γ$^+$ CD8$^+$ T cells, as quantified by flow cytometry. **(I)** Anti-Ly6G or isotype control treated mice were administered PBS or 10 µg CXCL1 i.n. on day 0 and after 12 hours infected with mock (PBS) or 6-7.5×10^5 FFU RSV i.n.. Weight loss is shown as a percentage of original weight. **(J)** Mice treated with anti-CD8 or isotype control antibodies were administered PBS or 10 µg CXCL1 i.n. on day 0 and after 12 hours infected with mock (PBS) or 6-7.5×10^5 FFU RSV i.n.. Weight loss is shown as a percentage of original weight. Data in (B-D), (F), and (H) are presented as mean ± SEM of 10 (PBS/PBS, PBS/RSV) or 9 (CXCL1/RSV) mice, pooled from two independent experiments - repeat 1 (10 µg CXCL1; circles), repeat 2 (8 µg CXCL1; squares). Statistical significance of differences in; (A) was analyzed using Spearman's rank correlation test, where the R-score is given as R_S, (B-D), (F), and (H) were analyzed using one-way ANOVA with Tukey's post hoc test, and (I-J) were analyzed using two-way ANOVA with Bonferroni's post hoc test. Asterisks indicate statistically significant differences between RSV infected groups. Hash symbols indicate statistically significant differences between PBS/PBS and CXCL1/PBS groups. *#*P*<0.05, ***P*<0.01, ****P*<0.001.

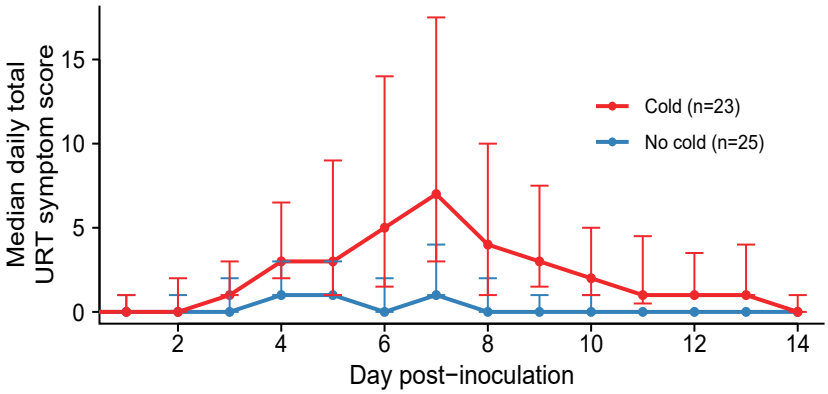
A

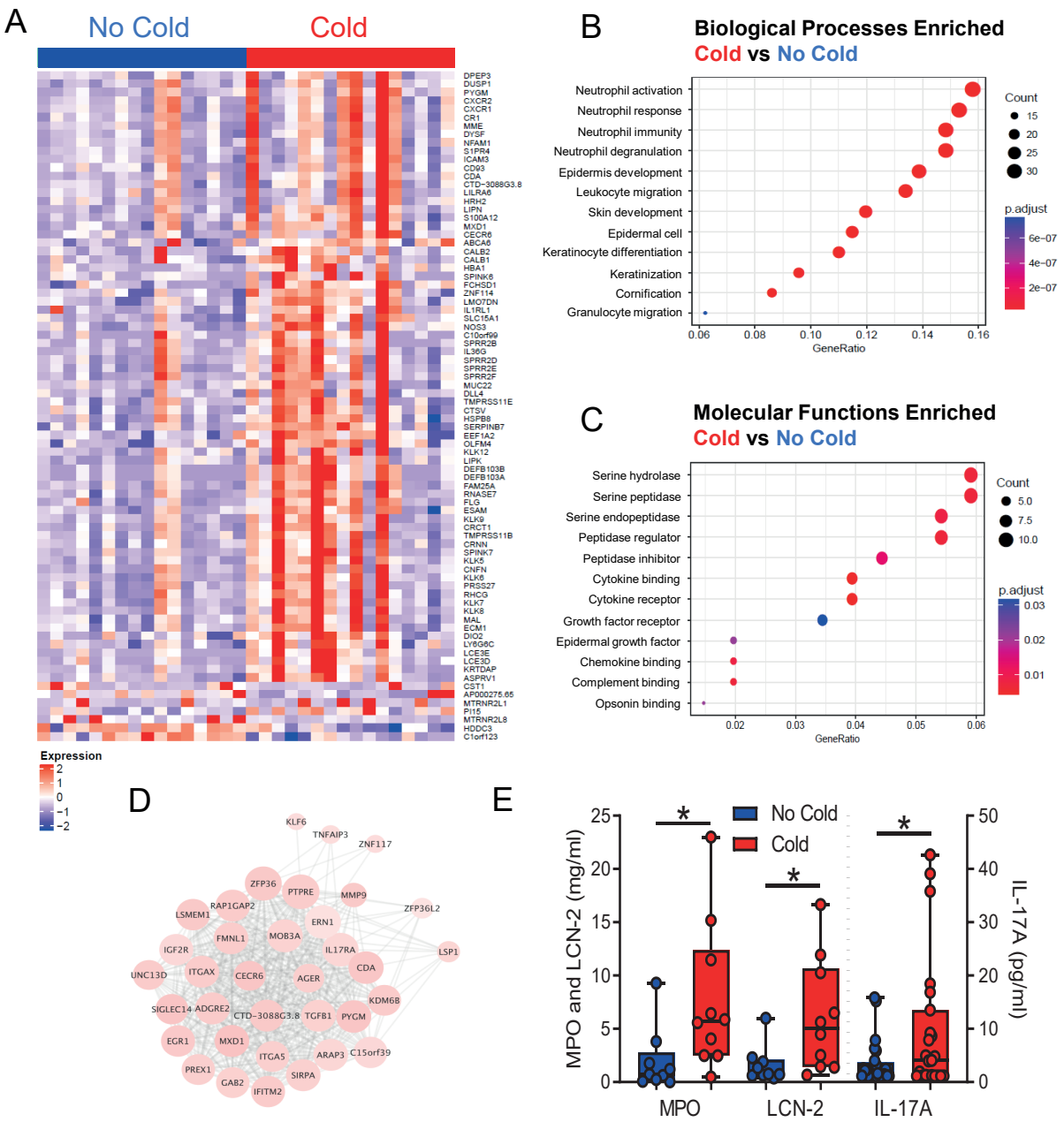

Quarantine and daily nasal sampling
Curettage
RSV inoculation
Curettage
Nasal sampling
Baseline
0
3
10
14

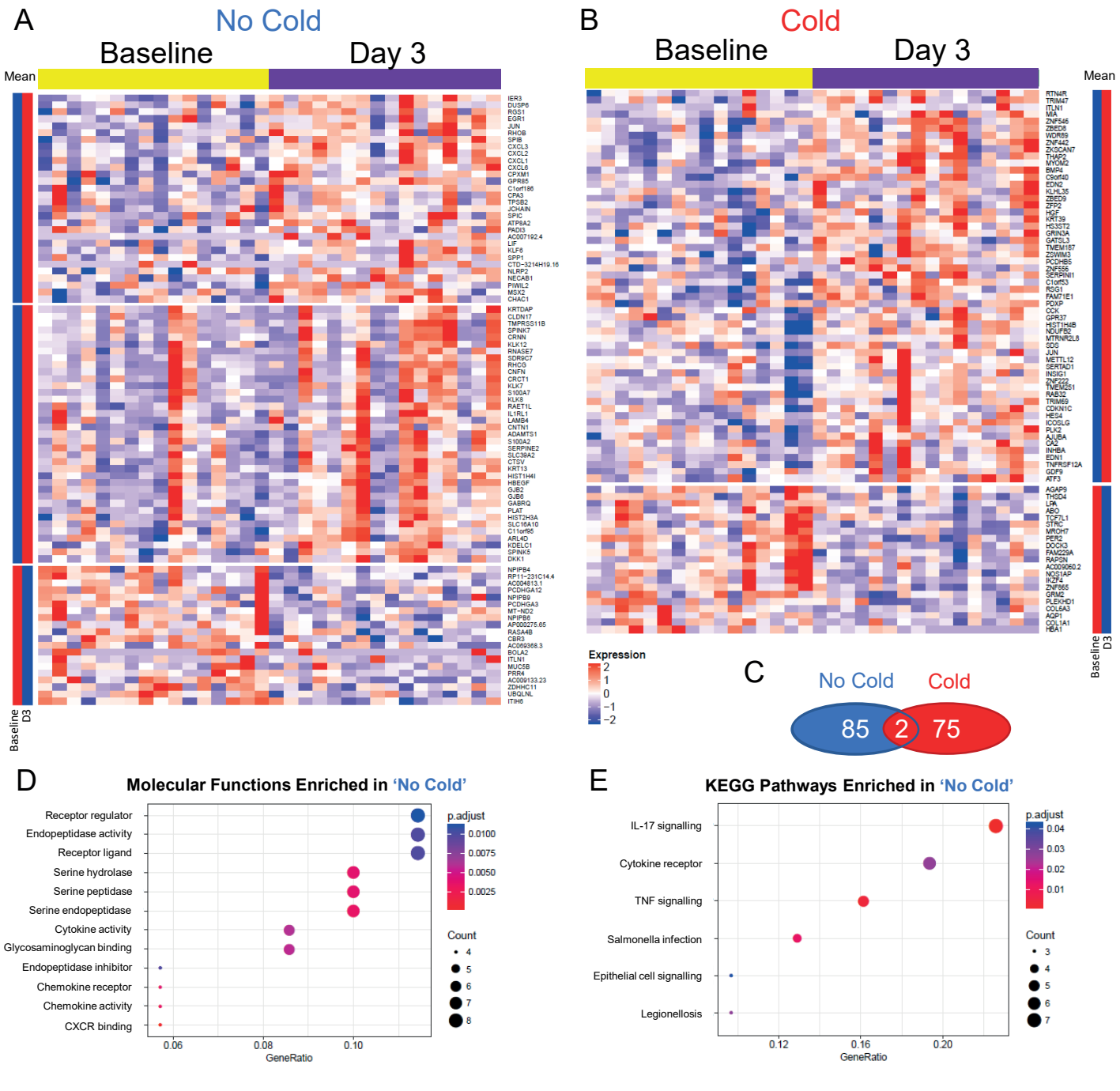
B


Daily viral load (log10copies/ml)
Viral replication
Viral clearance
Incubation phase
Shedding phase
Day post-inoculation

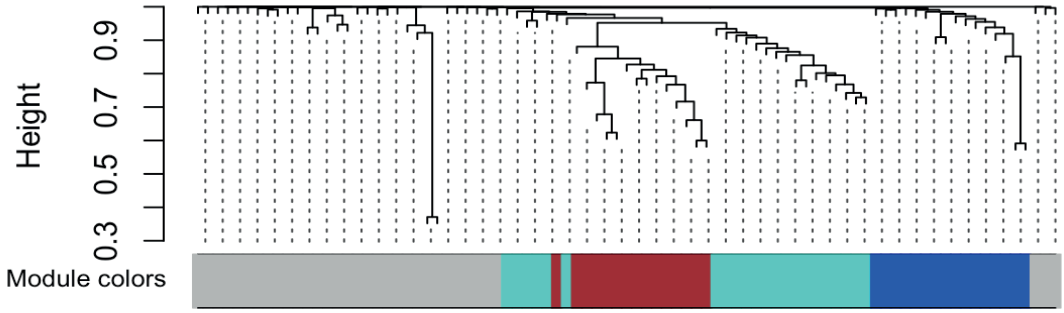
C


Median daily total URT symptom score
Cold (n=23)
No cold (n=25)
Day post−inoculation

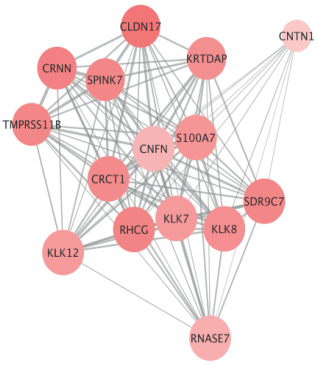

A
No Cold
Cold
Expression
2
1
0
−1
−2
B
Biological Processes Enriched
Cold vs No Cold
Neutrophil activation
Neutrophil response
Neutrophil immunity
Neutrophil degranulation
Epidermis development
Leukocyte migration
Skin development
Epidermal cell
Keratinocyte differentiation
Keratinization
Cornification
Granulocyte migration
0.06
0.08
0.10
0.12
0.14
0.16
GeneRatio
Count
15
20
25
30
p.adjust
6e-07
4e-07
2e-07
C
Molecular Functions Enriched
Cold vs No Cold
Serine hydrolase
Serine peptidase
Serine endopeptidase
Peptidase regulator
Peptidase inhibitor
Cytokine binding
Cytokine receptor
Growth factor receptor
Epidermal growth factor
Chemokine binding
Complement binding
Opsonin binding
0.02
0.03
0.04
0.05
0.06
GeneRatio
Count
5.0
7.5
10.0
p.adjust
0.03
0.02
0.01
D
KLF6
TNFAIP3
ZNF117
ZFP36
PTPRE
MMP9
ZFP36L2
RAP1GAP2
LSMEM1
ERN1
FMNL1
MOB3A
IGF2R
IL17RA
LSP1
UNC13D
ITGAX
CECR6
AGER
CDA
KDM6B
SIGLEC14
ADGRE2
CTD−3088G3.8
TGFB1
PYGM
EGR1
MXD1
ITGA5
ARAP3
C15orf39
PREX1
SIRPA
GAB2
IFITM2
E
No Cold
Cold
MPO and LCN-2 (mg/ml)
IL-17A (pg/ml)
0
5
10
15
20
25
0
10
20
30
40
50
*
*
*
MPO
LCN-2
IL-17A


A
No Cold
Baseline
Day 3
Mean
Baseline
D3
B
Cold
Baseline
Day 3
Mean
Baseline
D3
Expression
2
1
0
−1
−2
C
No Cold
Cold
85
2
75
D
Molecular Functions Enriched in 'No Cold'
Receptor regulator
Endopeptidase activity
Receptor ligand
Serine hydrolase
Serine peptidase
Serine endopeptidase
Cytokine activity
Glycosaminoglycan binding
Endopeptidase inhibitor
Chemokine receptor
Chemokine activity
CXCR binding
0.06
0.08
0.10
GeneRatio
p.adjust
0.0100
0.0075
0.0050
0.0025
Count
4
5
6
7
8
E
KEGG Pathways Enriched in 'No Cold'
IL-17 signalling
Cytokine receptor
TNF signalling
Salmonella infection
Epithelial cell signalling
Legionellosis
0.12
0.16
0.20
GeneRatio
p.adjust
0.04
0.03
0.02
0.01
Count
3
4
5
6
7

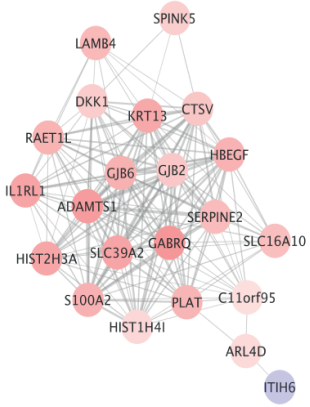
A



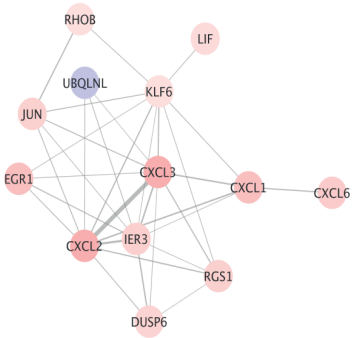
B Brown



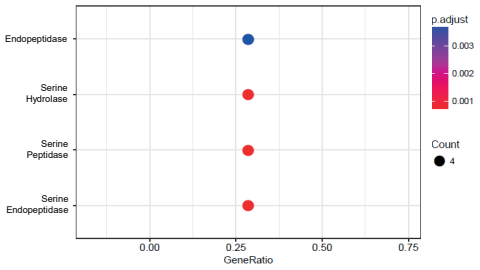
D Turquoise



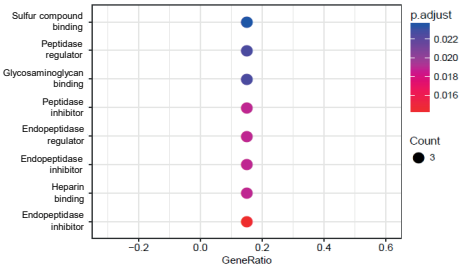
F Blue



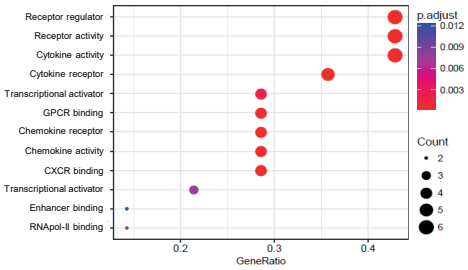
C Molecular Functions Enrichment
Brown Module



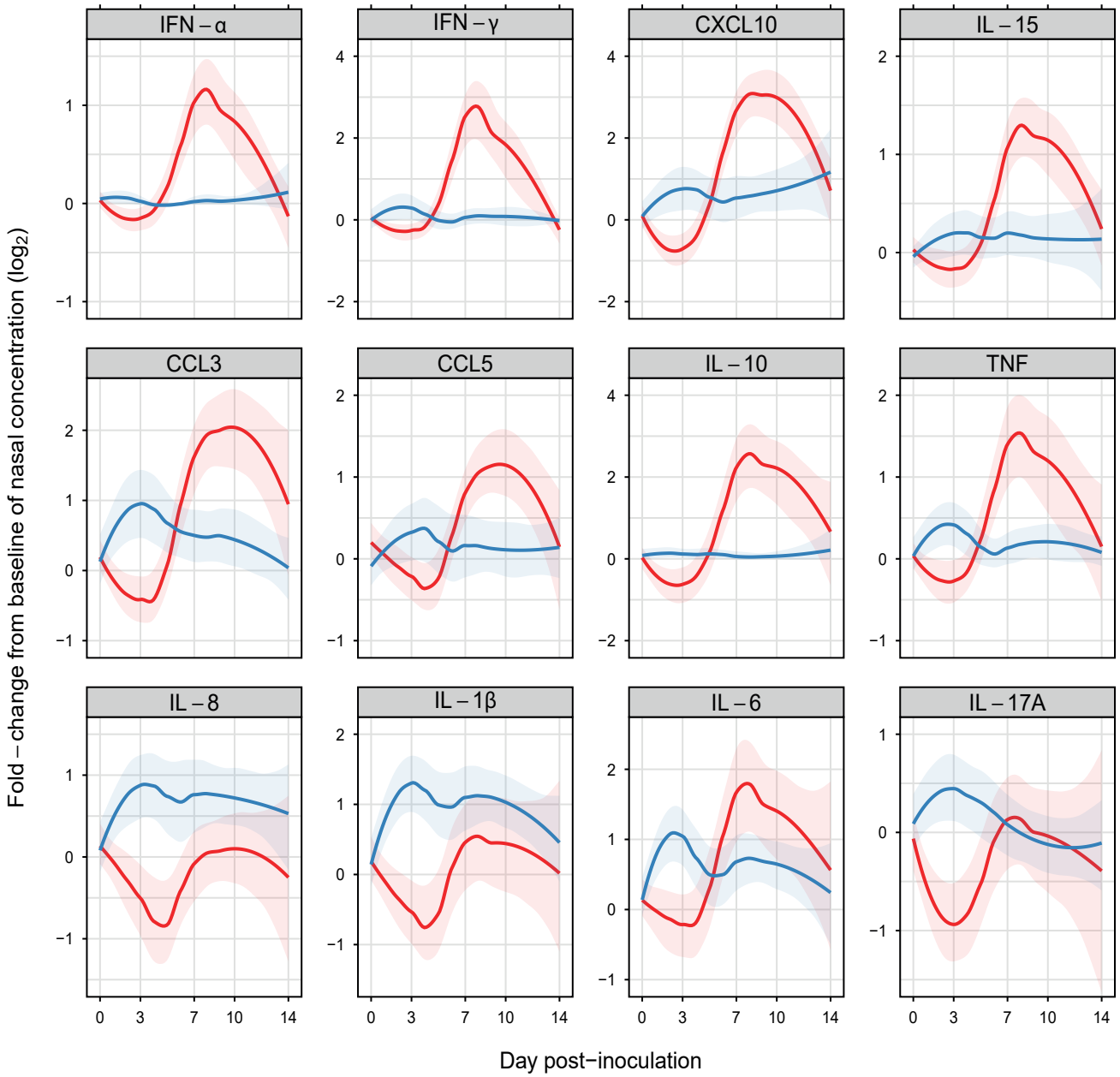
E Molecular Functions Enrichment
Turquoise Module



G Molecular Functions Enrichment
Blue Module

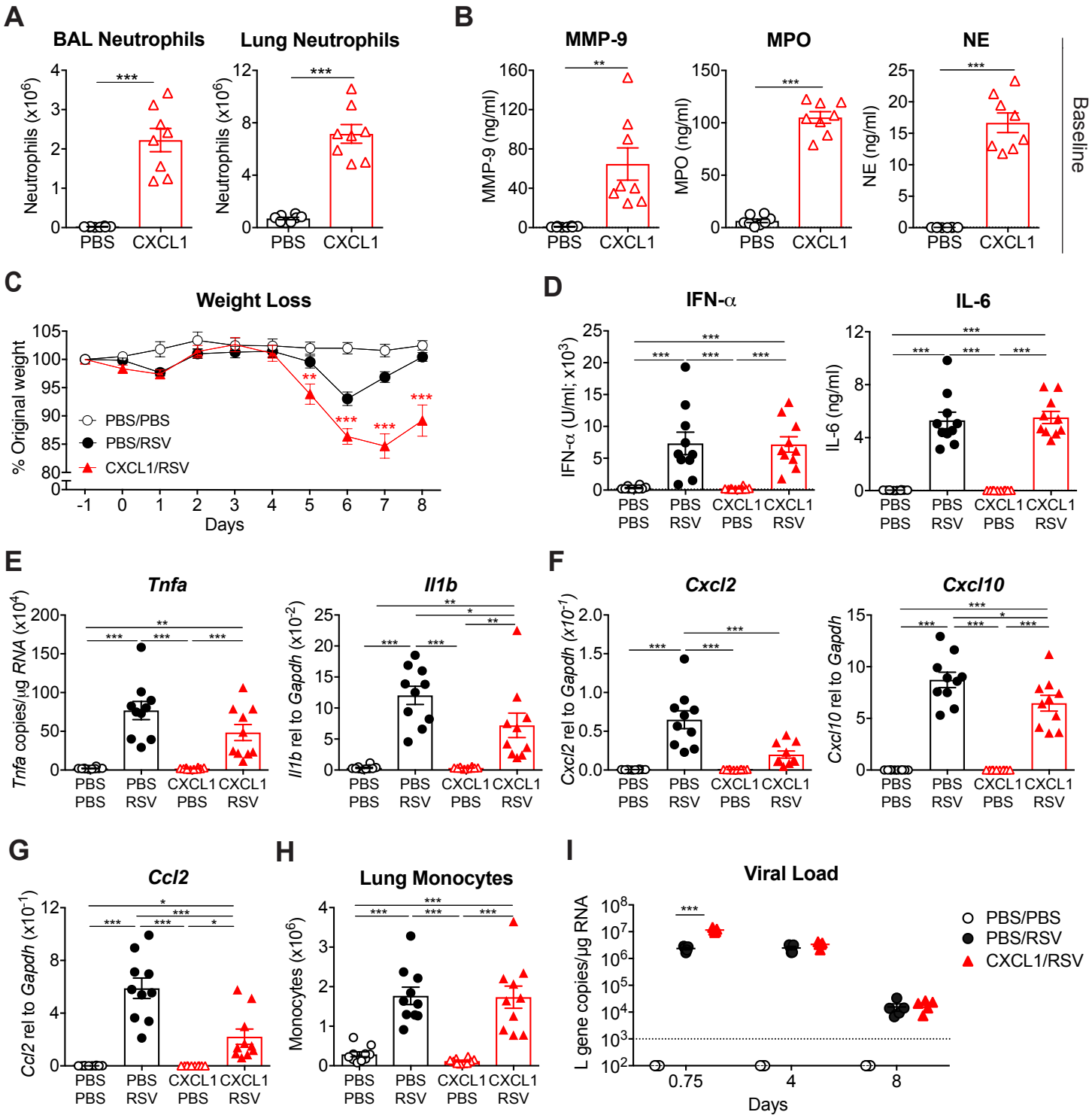


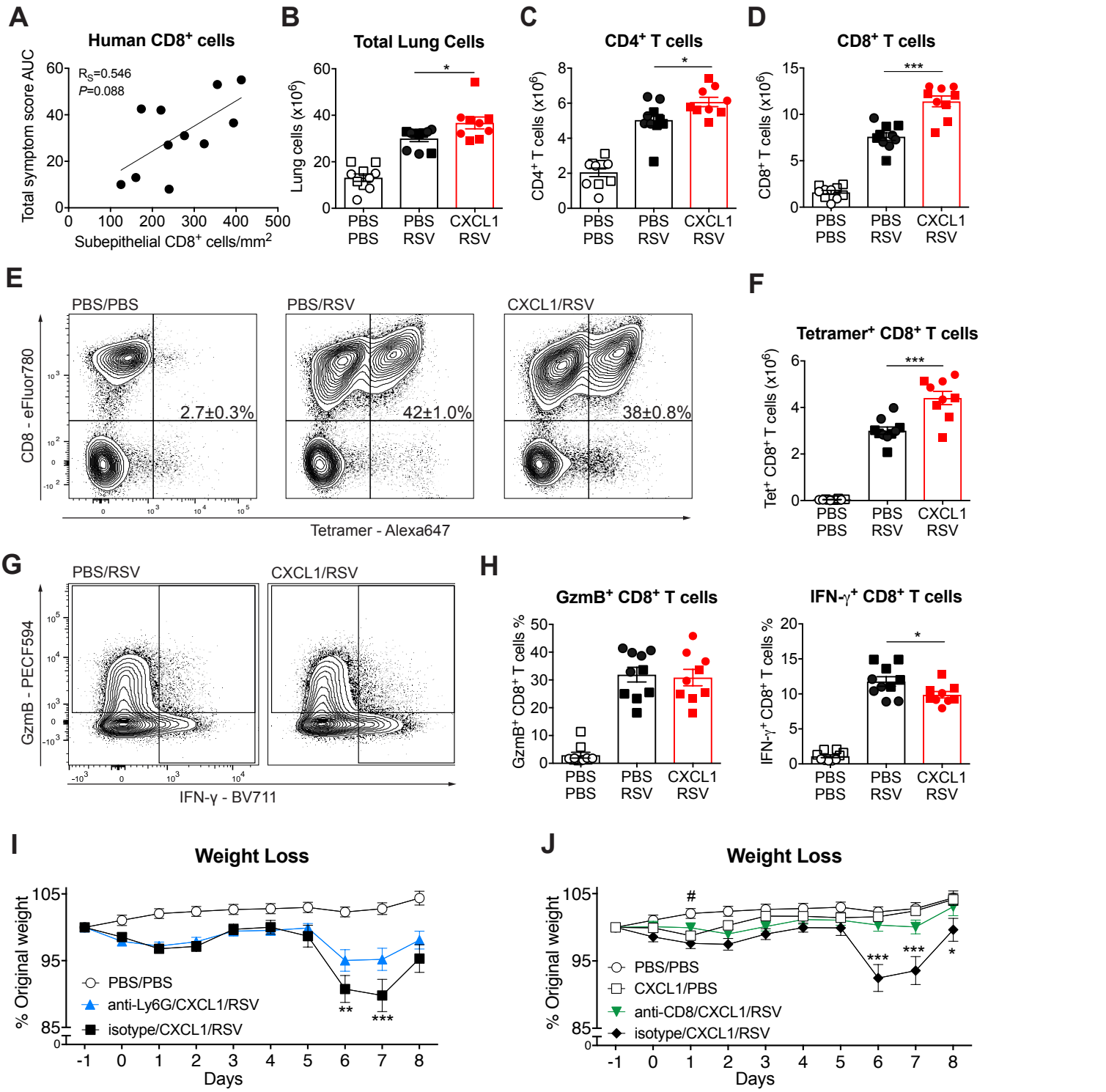
A



D

Mediator	IFN-α	IFN-γ	IP-10	IL-15	CCL3	CCL5	IL-10	TNF-α	IL-8	IL-1β	IL-6	IL-17A
***P*-value**	0.20	0.22	0.07	0.41	0.10	0.92	0.10	0.12	0.10	0.04*	0.05*	0.03*
Odds-ratio (95% CI)	0.49 (0.10, 1.06)	0.83 (0.57, 1.06)	0.88 (0.74, 1.00)	0.88 (0.63, 1.19)	0.87 (0.71, 1.01)	1.01 (0.83, 1.23)	0.78 (0.52, 0.99)	0.82 (0.61, 1.03)	0.85 (0.69, 1.01)	0.86 (0.73, 0.98)	0.82 (0.65, 0.97)	0.80 (0.63, 0.95)


A
BAL Neutrophils
Lung Neutrophils
Neutrophils (x10^6)
PBS
CXCL1
B
MMP-9
MPO
NE
MMP-9 (ng/ml)
MPO (ng/ml)
NE (ng/ml)
Baseline
C
Weight Loss
% Original weight
PBS/PBS
PBS/RSV
CXCL1/RSV
Days
D
IFN-α
IL-6
IFN-α (U/ml; x10^3)
IL-6 (ng/ml)
PBS PBS
PBS RSV
CXCL1 PBS
CXCL1 RSV
E
Tnfa
Il1b
Tnfa copies/µg RNA (x10^4)
Il1b rel to Gapdh (x10^-2)
F
Cxcl2
Cxcl10
Cxcl2 rel to Gapdh (x10^-1)
Cxcl10 rel to Gapdh
G
Ccl2
Ccl2 rel to Gapdh (x10^-1)
H
Lung Monocytes
Monocytes (x10^6)
I
Viral Load
L gene copies/µg RNA
Days


A
Human CD8+ cells
Total symptom score AUC
Subepithelial CD8+ cells/mm2
RS=0.546
P=0.088
B
Total Lung Cells
Lung cells (x10^6)
C
CD4+ T cells
CD4+ T cells (x10^6)
D
CD8+ T cells
CD8+ T cells (x10^6)
PBS PBS
PBS RSV
CXCL1 RSV
E
PBS/PBS
PBS/RSV
CXCL1/RSV
2.7±0.3%
42±1.0%
38±0.8%
CD8 - eFluor780
Tetramer - Alexa647
F
Tetramer+ CD8+ T cells
Tet+ CD8+ T cells (x10^6)
G
PBS/RSV
CXCL1/RSV
GzmB - PECF594
IFN-γ - BV711
H
GzmB+ CD8+ T cells
GzmB+ CD8+ T cells %
IFN-γ+ CD8+ T cells
IFN-γ+ CD8+ T cells %
I
Weight Loss
% Original weight
PBS/PBS
anti-Ly6G/CXCL1/RSV
isotype/CXCL1/RSV
Days
J
Weight Loss
% Original weight
PBS/PBS
CXCL1/PBS
anti-CD8/CXCL1/RSV
isotype/CXCL1/RSV
Days

Science
AAAS

Supplementary Materials for

Mucosal neutrophil activation predisposes to respiratory viral infection

Maximillian S Habibi[*], Ryan S Thwaites[*], Meiping Chang, Agnieszka Jozwik, Allan Paras, Freja Kirsebom, Augusto Varese, Amber Owen, Leah Cuthbertson, Phillip James, Tanushree Tunstall, David Nickle, Trevor T Hansel, Miriam F Moffatt, Cecilia Johansson, Christopher Chiu[‡] and Peter J. M. Openshaw[‡]

Correspondence to: p.openshaw@imperial.ac.uk, c.chiu@imperial.ac.uk or c.johansson@imperial.ac.uk

This PDF file includes:

Material and Methods
Figs. S1 to S8
Tables S1 to S14

Materials and Methods

Flow cytometry reagents for murine studies

Target	Clone or order number	Fluorochrome	Vendor	Final concentration and dilution
Live cells	L34957	Aqua	Invitrogen	1:500
CD3	17A2	AF700	eBioscience	2 mg/ml
CD3	145-2C11	FITC	Biolegend	2.5 mg/ml
CD4	GK1.5	PE	eBioscience	0.5 mg/ml
CD8	53-6.7	eFluor780	eBioscience	0.5 mg/ml
CD11b	M1/70	AF700	eBioscience	0.5 mg/ml
CD11c	HL3	PE-CF594	BD Horizon	1 mg/ml
CD19	6D5	FITC	Biolegend	5 mg/ml
CD44	IM7	PE-Cy7	Biolegend	2 mg/ml
CD45	30-F11	BV605	Biolegend	0.25 mg/ml
CD62L	MEL-14	BV421	Biolegend	1 mg/ml
CD64	X54-5/7	APC	Biolegend	1 mg/ml
CD69	H1.2F3	BUV737	BD Horizon	1 mg/ml
CD103	2E7	PerCP-Cy5.5	Biolegend	1 mg/ml
Fc block (CD16/32)	93		Biolegend	2.5 mg/ml
Granzyme B	GB11	PECF594	BD Horizon	1:200
IFN-γ	XMG1.2	BV711	BD Horizon	1 mg/ml
Ly6C	HK1.4	BV421	Biolegend	0.125 mg/ml
Ly6C	HK1.4	eFluor450	eBioscience	0.25 mg/ml
Ly6G	1A8	FITC	Biolegend	5 mg/ml
Ly6G	1A8	APC-Cy7	Biolegend	0.5 mg/ml
Ly6G	1A8	BV785	Biolegend	1 mg/ml
MHC-II	M5/114.15.2	APC-eF780	eBiosciences	1 mg/ml
Siglec-F	E50-2440	PE	BD Pharmingen	1 mg/ml
Tetramer	RSV $M_{187-195}$	Alexa647	NIH Tetramer facility	15 mg/ml

qPCR reagents for murine studies

Gene	Primer/Probe	Assay ID or order number	Vendor
Ccl2	TaqMan® Gene Expression Assay	Mm00441242_m1 FAM	Thermo Fisher (ABI)
Cxcl2	TaqMan® Gene Expression Assay	Mm00436450_m1 FAM	Thermo Fisher (ABI)
Cxcl10	TaqMan® Gene Expression Assay	Mm00445235_m1 FAM	Thermo Fisher (ABI)
Gapdh	TaqMan® Gene Expression Assay	4351309 VIC	Thermo Fisher (ABI)
Il1b	TaqMan® Gene Expression Assay	Mm00434228_m1 FAM	Thermo Fisher (ABI)
L gene	Fwd: 5'-gaactcagtgtaggtagaatgtttgca-3' Rev: 5'-ttcagctatcattttctctgccaat-3' Probe: 5'-(FAM)tttgaacctgtct gaacattcccggtt(TAM)-3'	Previously reported *(65)*	Invitrogen Invitrogen Eurofin
Tnfa	Fwd: 5'-catcttctcaaaattcgagtgacaa-3' Rev: 5'-tgggagtagacaaggtacaaccc-3' Probe:5'-(FAM)cacgtcgtagcaaac (TAM)-3'	Previously reported *(64)*	Invitrogen Invitrogen Eurofin

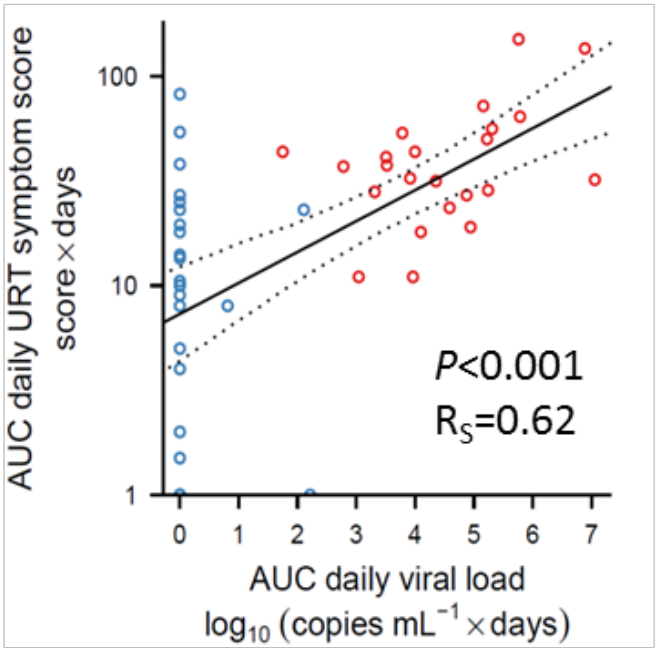


Fig. S1: Correlation between total upper respiratory tract symptom scores and viral load.

Correlation between area under the curve (AUC) of upper respiratory tract (URT) symptoms and AUC of daily viral load within the "Cold" (red, n=23) and "No Cold" (blue, n=25) groups was assessed using Spearman's test.

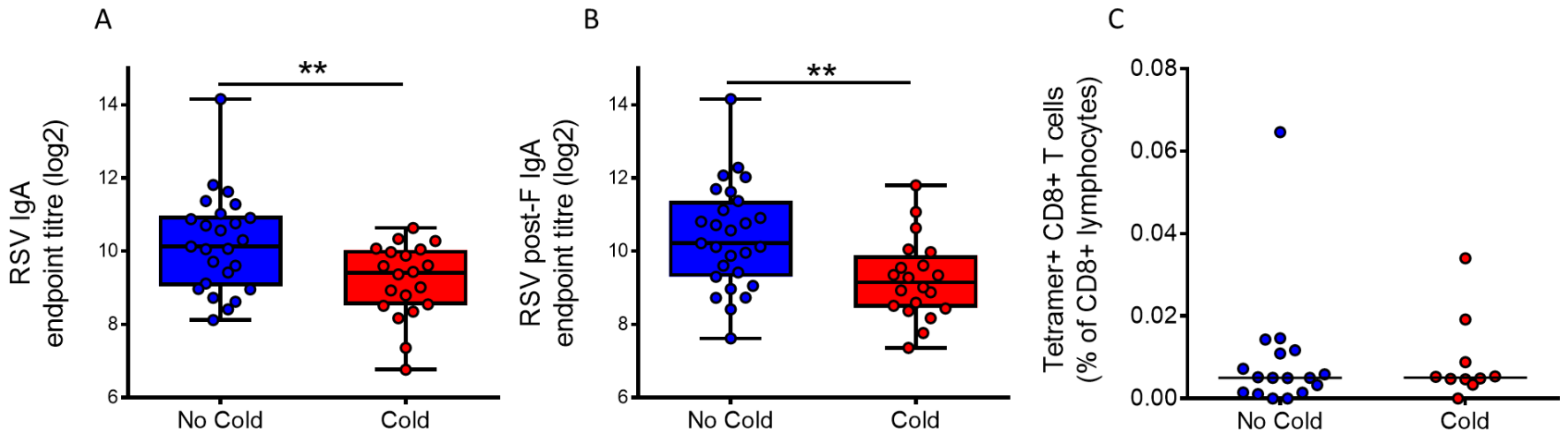


Fig. S2: Pre-inoculation nasal anti-RSV antibody levels, but not anti-RSV CD8$^+$ T cell proportions, are associated with protection from infection.

Baseline levels of **(A)** total anti-RSV IgA and **(B)** post-F specific IgA in nasal lavage from "No Cold" (n=25, blue) and "Cold" (n=20, red) groups were measured by ELISA. **(C)** Frequencies of RSV-specific tetramer positive CD8$^+$T cells in the lung from "No Cold" (n=17) and "Cold" (n=10) groups were quantified by flow cytometry. Significance was tested by Mann Whitney *U* test. ***P*<0.01.

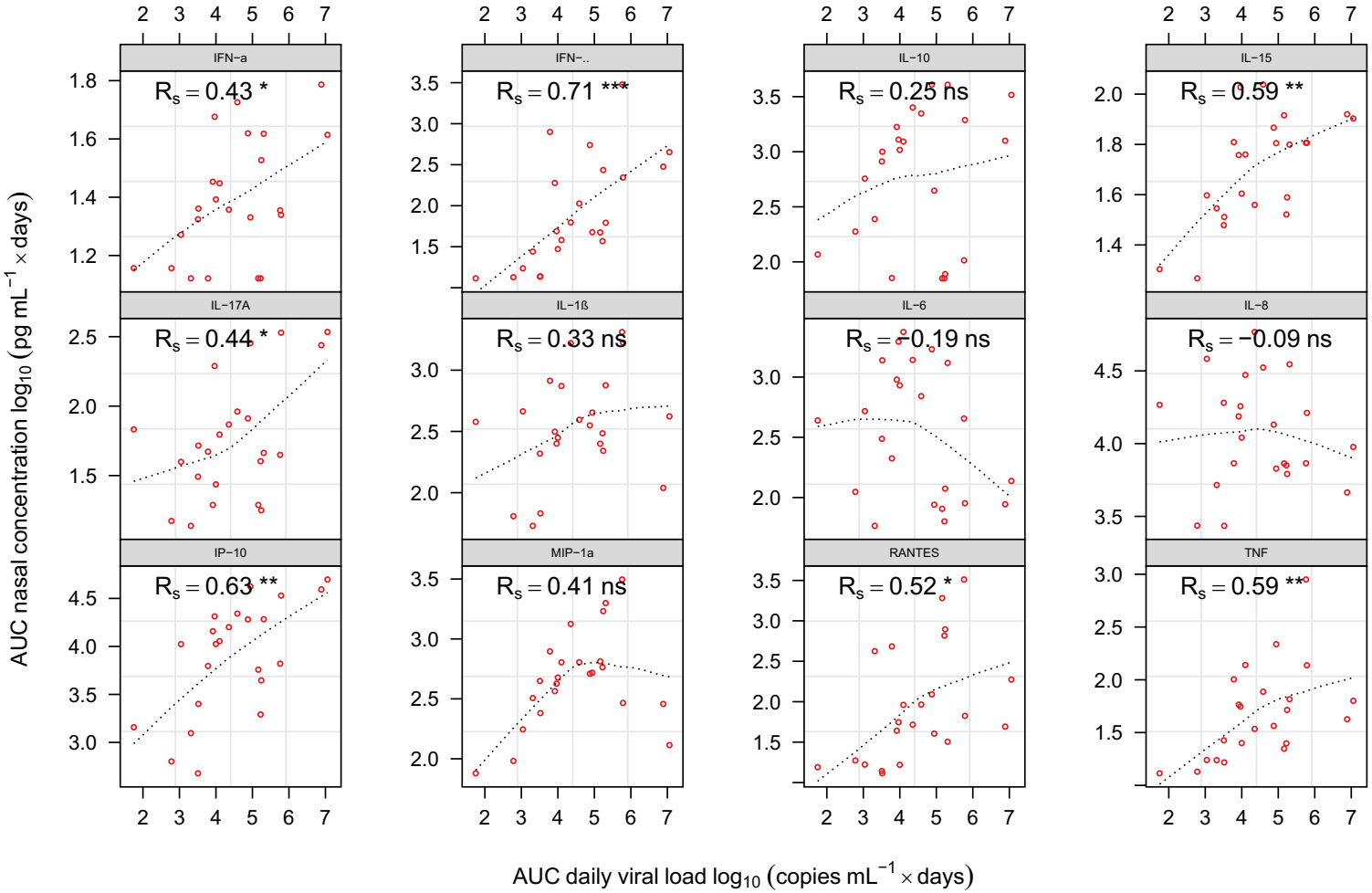


Fig. S3: Cumulative viral load correlates with the levels of several inflammatory mediators.

Within the Cold group (n=23), correlations between area under the curve (AUC) levels of daily viral load and cytokine/chemokine mediator levels for **(A)** IFN-α, **(B)** IL-17A, **(C)** CXCL10/IP-10, **(D)** IFN-γ, **(E)** IL-1β, **(F)** CCL3/MIP-1α, **(G)** IL-10, **(H)** IL-6, **(I)** CCL5/RANTES, **(J)** IL-15, **(K)** CXCL8/IL-8 and **(L)** TNF-α. Correlations were assessed using Spearman's test. **P*<0.05, ***P*<0.01, ****P*<0.001, ns=not significant.

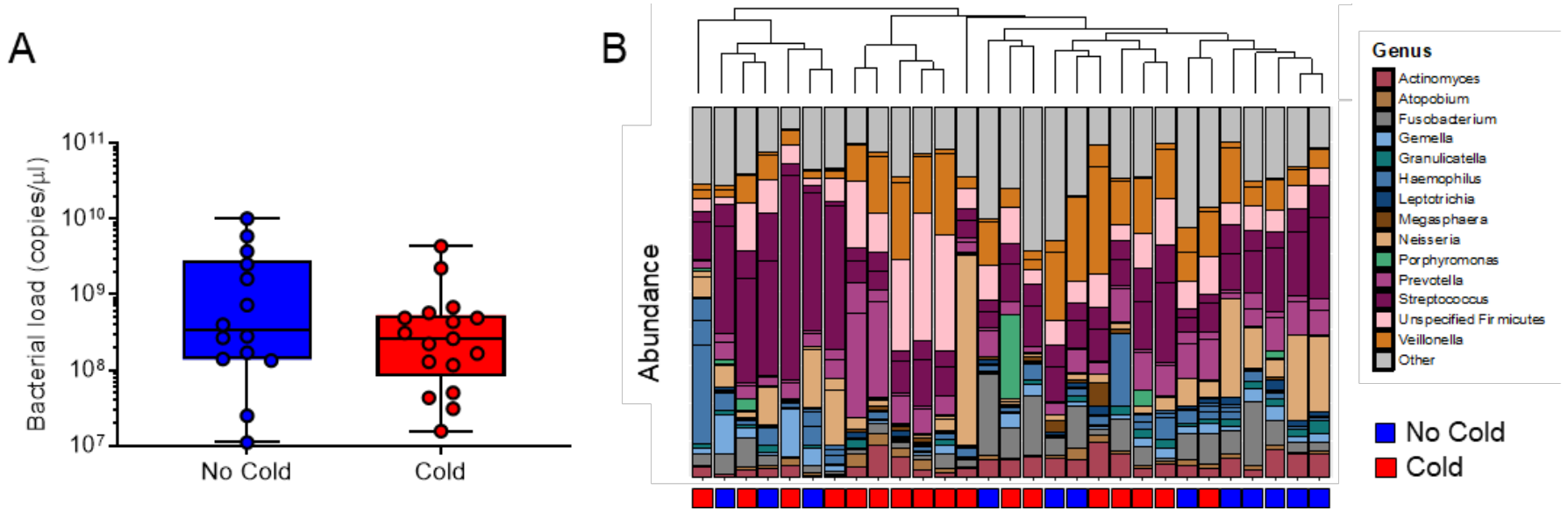
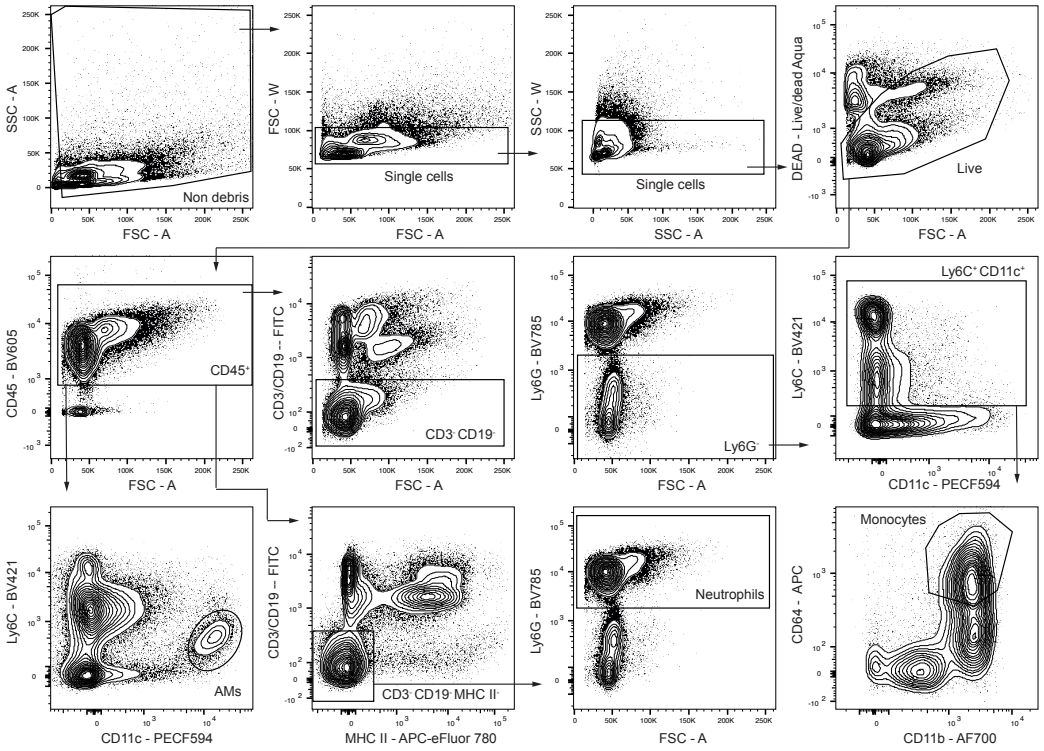


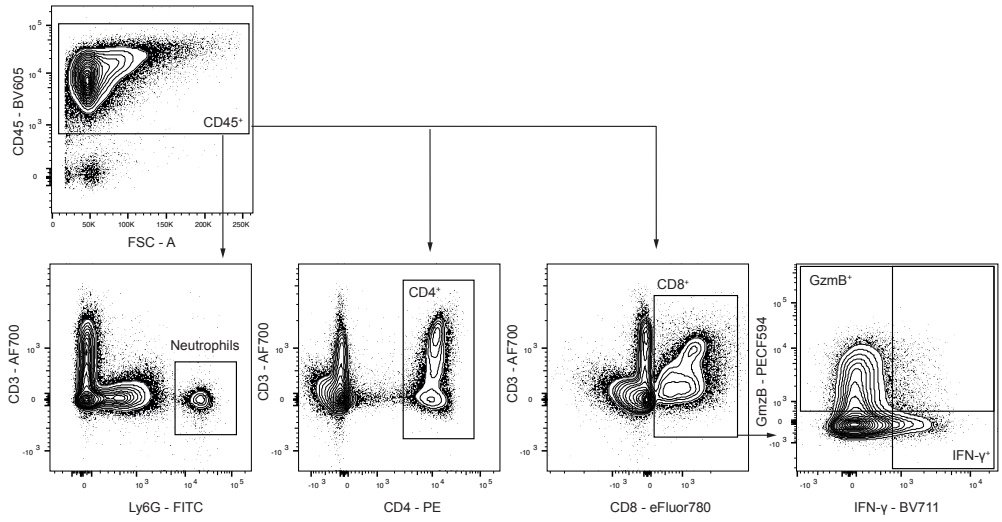
Fig. S4: The airway microbiome at point of virus exposure is not associated with susceptibility to infection.

(A) Bacterial load, measured by 16S qPCR, from baseline nasopharyngeal swabs of No Cold (n=12) and Cold (n=17) participants. **(B)** Baseline bacterial community ordered by Bray-Curtis hierarchical clustering where the top 20 OTUs are shown. **P*<0.05. Data in part A are represented as median and interquartiles with minimum and maximum values.

A Alveolar macrophages, monocytes and neutrophils



B T cell staining panel - Intracellular cytokine stain (gated to live cells as above)



C T cell staining panel - CD8⁺ tetramer stain (gated to live cells as above)

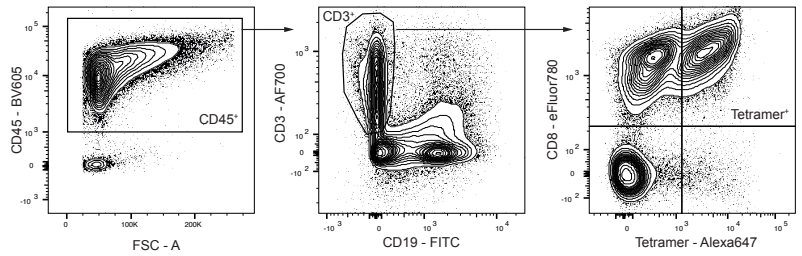


Fig. S5: Gating strategies for identifying murine lung cells.

(A) Mice were treated with mock (PBS) or 5-10 µg rCXCL1 i.n.. **(A)** At 12 hours or 18 hours post-RSV infection airway and lung innate immune cells were obtained by collagenase digestion and stained for the indicated cell surface molecules. After excluding debris and gating on single, live, $CD45^+$ cells, the depicted gates were used to identify AMs, monocytes, and neutrophils. **(B)** Mice were treated with mock (PBS) or 10 µg rCXCL1 i.n. and after 12 hours infected with mock (PBS) or 7.5×10^5 FFU RSV i.n.. After 8 days, lung cells were obtained by collagenase digestion and stained for the indicated cell surface molecules. After excluding debris and gating on single, live, $CD45^+$ cells, the depicted gates were used to identify neutrophils, $CD4^+$ and $CD8^+$ T cells as well as $GzmB^+$ and IFN-γ^+ $CD8^+$ T cells. **(C)** After excluding debris and gating on single, live, $CD45^+$ cells, the depicted gates were used to identify RSV $tetramer^+$ $CD8^+$ T cells.

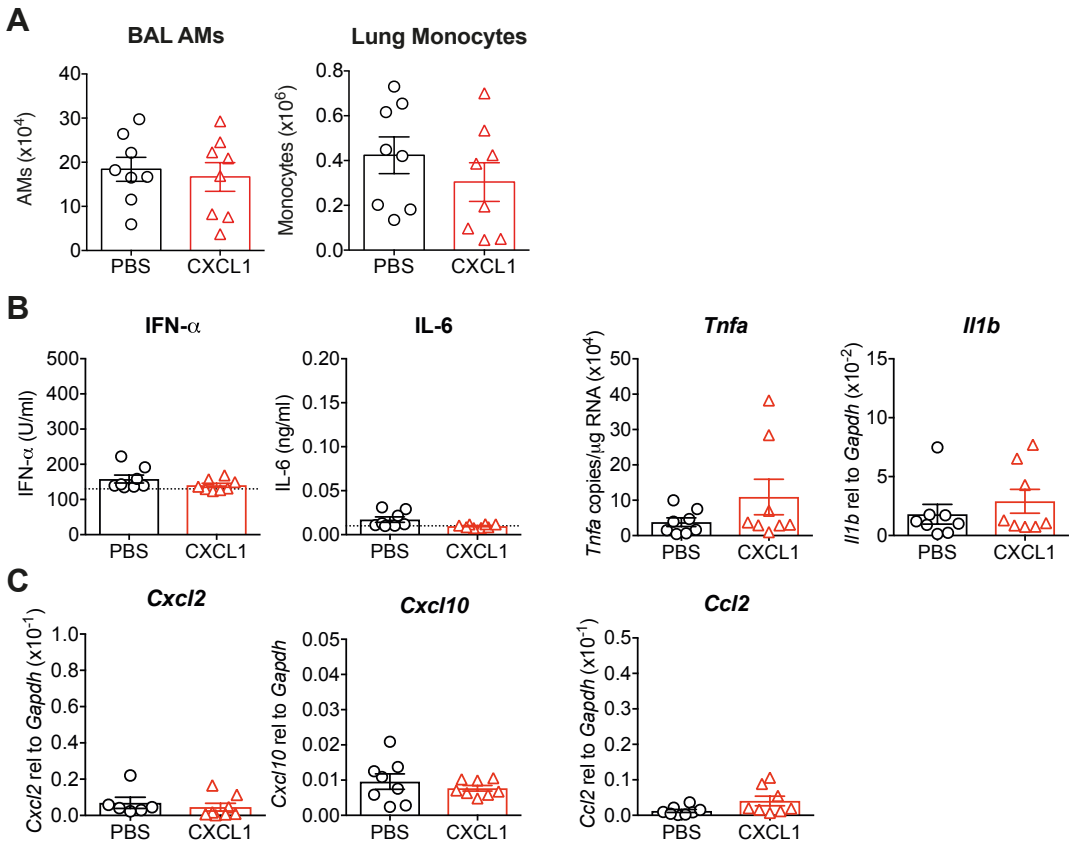


Fig. S6: Treatment with rCXCL1 alone causes no change in alveolar macrophages, monocytes or inflammatory mediators in the lung.

Mice were treated with mock (PBS) or 10 µg rCXCL1 i.n. and after 12 hours, cells and mediators were quantified in the lung. **(A)** BAL AMs and lung monocytes were quantified 12 hours post CXCL1 treatment by flow cytometry. **(B)** IFN-α and IL-6 was quantified in BAL using ELISA and levels of *Il1b* and *Tnfa* were determined in lung tissue using qPCR. **(C)** *Cxcl2, Cxcl10,* and *Ccl2* were determined in lung tissue using qPCR. Data are presented as mean±SEM of eight individual mice per group, pooled from two independent experiments. The dotted line represents the limit of detection of the assay. Statistical significance was analyzed using unpaired, two-tailed Student's *t* test.

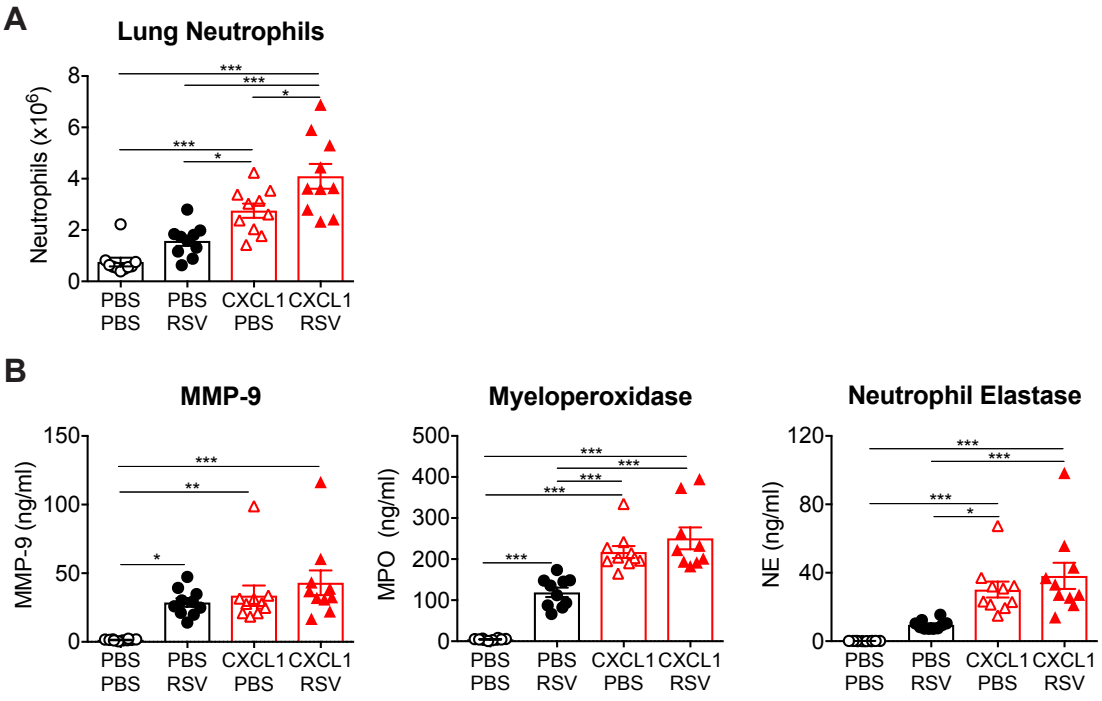


Fig. S7: RSV infection of rCXCL1 pre-treated mice enhances the early production of neutrophil markers.

Mice were treated with mock (PBS) or 5 µg rCXCL1 i.n. and after 9 hours infected with mock (PBS) or 7.5×10^5 FFU RSV i.n. for 18 hours. **(A)** The total number of lung neutrophils was quantified by flow cytometry as previously described in *(65)*. **(B)** MMP-9, MPO and NE was quantified in BAL using ELISA. The data are presented as mean±SEM of 10 individual mice per group, pooled from two independent experiments. Statistical significance of differences was analyzed by one-way ANOVA with Tukey's post hoc test.*P<0.05, **P<0.01, ***P<0.001.

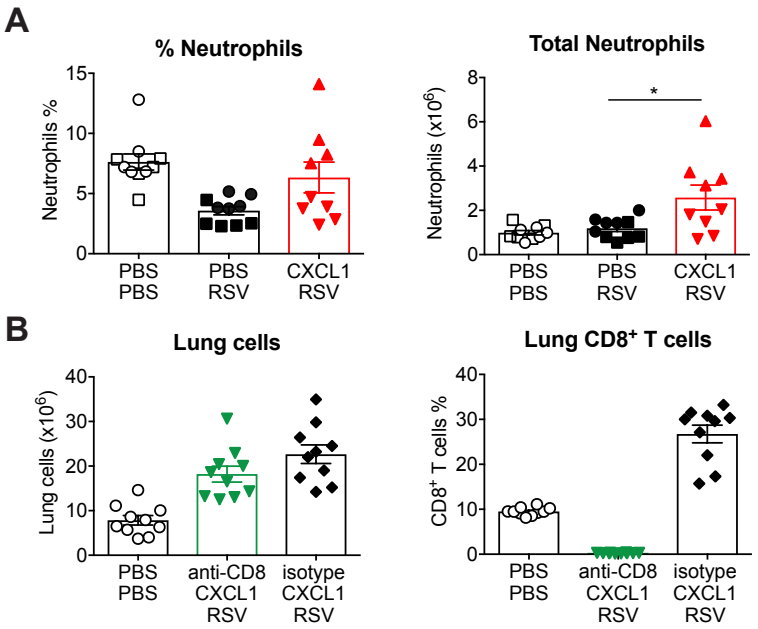


Fig. S8: Treatment with rCXCL1 pre-RSV infection does not result in an increase in neutrophil frequency on day 8 p.i. and treatment with anti-CD8 antibodies is sufficient to remove CD8$^+$ T cells during RSV infection.

Mice were treated with mock (PBS) or 8 µg or 10 µg rCXCL1 i.n. and after 12 hours infected with mock (PBS) or 7.5×10^5 FFU RSV i.n.. **(A)** The frequency and total number of lung neutrophils was quantified by flow cytometry. **(B)** To deplete CD8$^+$ T cells, mice were treated with 250 µg anti-CD8 or isotype control i.p. on day -1, day 2 and day 5 p.i. and lung were analyzed on day 8 p.i.. Total number of lung cells and frequency of CD8$^+$ T cells as quantified by flow cytometry. Data from (A) are presented as mean±SEM of 10 (PBS/PBS, PBS/RSV) or 9 (CXCL1/RSV) mice, pooled from two independent experiments - repeat 1 (10 µg CXCL1; circles) and repeat 2 (8 µg CXCL1; squares). Data from (B) are presented as mean±SEM of 10 mice, pooled from two independent experiments. Data in (A and B) were analyzed using one-way ANOVA with Tukey's post hoc test. *P<0.05

Table S1

	Cold (n=23)	No Cold (n=25)	*P*-value
Age in years, mean (range)	23.3 (18-50)	23.6 (18-39)	0.84
Sex (M:F)	12:11	15:10	0.77
Ethnicity (n=)			
White	17 (74%)	19 (76%)	>0.99
Black	1 (4%)	4 (16%)	0.37
Asian	2 (9%)	0	0.22
Mixed	1 (4%)	2 (8%)	>0.99
Other	2 (9%)	0	0.22

Table S1: Demographics

Volunteer demographics were collected at study enrolment and categorized on subsequent development of a symptomatic infection following RSV inoculation (Cold, n=23) or not (No Cold, n=25). A two-tailed *t*-test was used to assess significance in volunteer age. Fisher's exact tests were used to assess significance in sex and ethnicity data.

Table S2: Baseline DEGs between 'Cold' and 'No Cold' groups (*P*adj<0.1, LFC>0.5)

	GeneName	baseMean	log^2FoldChange	lfcSE	stat	*P*value	*P*adj
ENSG00000129455	*KLK8*	64.04073471	4.50463631	0.725538	6.208681	0.0000000005	0.0000078
ENSG00000140519	*RHCG*	327.2661994	3.899687376	0.687333	5.673651	0.0000000140	0.0001025
ENSG00000143536	*CRNN*	717.7315072	3.961919136	0.710893	5.573155	0.0000000250	0.0001124
ENSG00000136688	*IL36G*	119.3575404	3.485458598	0.629406	5.537698	0.0000000306	0.0001124
ENSG00000203785	*SPRR2E*	549.5597617	3.759191643	0.694542	5.412479	0.0000000622	0.0001823
ENSG00000244617	*ASPRV1*	201.6683348	2.541982486	0.473897	5.363995	0.0000000814	0.0001990
ENSG00000163216	*SPRR2D*	493.240127	3.489918519	0.673736	5.179946	0.0000002219	0.0004651
ENSG00000172137	*CALB2*	7.432513115	3.827424619	0.744758	5.139154	0.0000002760	0.0005060
ENSG00000102837	*OLFM4*	9.018542922	2.379694573	0.485505	4.901481	0.0000009512	0.0015502
ENSG00000164867	*NOS3*	39.06236907	2.172068356	0.455328	4.770338	0.0000018392	0.0024524
ENSG00000104327	*CALB1*	97.2215325	3.213472664	0.672135	4.780991	0.0000017443	0.0024524
ENSG00000145879	*SPINK7*	214.5721968	3.777459369	0.795095	4.750953	0.0000020246	0.0024747
ENSG00000167755	*KLK6*	219.7775905	3.749018528	0.793685	4.723561	0.0000023175	0.0026149
ENSG00000143369	*ECM1*	368.3426926	2.548748229	0.543078	4.693155	0.0000026902	0.0028186
ENSG00000088386	*SLC15A1*	58.06521529	1.444700757	0.309249	4.671646	0.0000029880	0.0029218
ENSG00000167754	*KLK5*	58.04069283	4.183165833	0.901151	4.642025	0.0000034501	0.0031629
ENSG00000244094	*SPRR2F*	174.9314565	3.559094351	0.769266	4.62661	0.0000037170	0.0032071
ENSG00000197948	*FCHSD1*	433.0477186	0.555918016	0.122298	4.545597	0.0000054780	0.0044639
ENSG00000188508	*KRTDAP*	56.82226766	4.12052942	0.913535	4.510532	0.0000064665	0.0049922
ENSG00000165799	*RNASE7*	76.05592952	2.591086011	0.578846	4.476294	0.0000075950	0.0055702
ENSG00000158825	*CDA*	31.30464651	3.126427907	0.70532	4.432636	0.0000093088	0.0060990
ENSG00000172005	*MAL*	315.8263003	2.780102998	0.629321	4.417623	0.0000099792	0.0060990
ENSG00000188100	*FAM25A*	52.79654449	3.385115694	0.766093	4.418675	0.0000099308	0.0060990
ENSG00000178734	*LMO7DN*	7.032824408	2.363797695	0.534435	4.422982	0.0000097348	0.0060990
ENSG00000256618	*MTRNR2L1*	31.19207611	4.405844562	1.017059	4.331946	0.0000147797	0.0078477
ENSG00000166396	*SERPINB7*	133.8826024	1.568727074	0.362378	4.328974	0.0000149805	0.0078477
ENSG00000105427	*CNFN*	357.4556348	2.628314998	0.606082	4.336567	0.0000144726	0.0078477
ENSG00000169035	*KLK7*	460.4004676	3.236932356	0.746379	4.336849	0.0000144540	0.0078477
ENSG00000177243	*DEFB103B*	12.86752713	4.068667323	0.94596	4.301099	0.0000169953	0.0083096
ENSG00000176797	*DEFB103A*	12.86752713	4.068667323	0.94596	4.301099	0.0000169953	0.0083096
ENSG00000196805	*SPRR2B*	12.46642556	4.007415528	0.94584	4.236884	0.0000226643	0.0105675
ENSG00000255823	*MTRNR2L8*	99.96331934	-2.063829514	0.487551	-4.23305	0.0000230542	0.0105675
ENSG00000185966	*LCE3E*	18.55284064	4.403689631	1.044843	4.214692	0.0000250120	0.0111174
ENSG00000269741	*KLK9*	38.39528424	3.634649191	0.869249	4.181368	0.0000289761	0.0125006
ENSG00000163202	*LCE3D*	21.85709696	3.766259743	0.907597	4.149703	0.0000332906	0.0136037
ENSG00000172382	*PRSS27*	235.5149533	2.146835495	0.51743	4.149036	0.0000333878	0.0136037
ENSG00000265590	*AP000275.65*	13.45435781	-2.313482025	0.565829	-4.08866	0.0000433880	0.0172004
ENSG00000163221	*S100A12*	117.0760162	2.42404596	0.595909	4.067813	0.0000474564	0.0183182
ENSG00000115602	*IL1RL1*	44.99164745	2.186332063	0.544735	4.01357	0.0000598072	0.0224936
ENSG00000185873	*TMPRSS11B*	162.1426424	2.930935532	0.738498	3.968781	0.0000722414	0.0264909
ENSG00000183307	*CECR6*	16.55877878	1.882385854	0.478856	3.93101	0.0000845897	0.0302625
ENSG00000178172	*SPINK6*	11.19634078	3.736066016	0.960846	3.88831	0.0001009446	0.0352537

ENSG00000169509	*CRCT1*	124.6713786	3.255307448	0.839868	3.875975	0.0001061984	0.0353209
ENSG00000087128	*TMPRSS11E*	856.279728	2.335954629	0.603236	3.872373	0.0001077807	0.0353209
ENSG00000235568	*NFAM1*	385.2546016	2.109095274	0.544836	3.871064	0.0001083611	0.0353209
ENSG00000143631	*FLG*	60.85365689	2.707724203	0.703833	3.847112	0.0001195184	0.0381108
ENSG00000059728	*MXD1*	3049.682399	1.568764572	0.411317	3.814	0.0001367357	0.0407370
ENSG00000204421	*LY6G6C*	11.23753312	2.015579995	0.530386	3.800212	0.0001445722	0.0407370
ENSG00000137558	*PI15*	7.292990874	2.650754443	0.696318	3.806818	0.0001407663	0.0407370
ENSG00000188373	*C10orf99*	11.24888949	3.740112396	0.980735	3.813582	0.0001369669	0.0407370
ENSG00000125910	*S1PR4*	174.6183595	2.16060284	0.569216	3.795754	0.0001471953	0.0407370
ENSG00000186474	*KLK12*	66.90156166	2.810027115	0.739856	3.798075	0.0001458243	0.0407370
ENSG00000101210	*EEF1A2*	8.860473621	1.927591183	0.50611	3.808641	0.0001397326	0.0407370
ENSG00000261272	*MUC22*	53.13744678	2.376412656	0.628685	3.779973	0.0001568455	0.0418293
ENSG00000154262	*ABCA6*	91.04472433	0.918131079	0.242831	3.780947	0.0001562332	0.0418293
ENSG00000162384	*C1orf123*	400.5115764	-0.274660048	0.072946	-3.76525	0.0001663849	0.0435810
ENSG00000180871	*CXCR2*	559.0871712	2.296300313	0.613115	3.745302	0.0001801766	0.0447868
ENSG00000196549	*MME*	223.9783358	2.350426949	0.628268	3.74112	0.0001832022	0.0447868
ENSG00000136943	*CTSV*	169.9791044	1.651903131	0.441093	3.745024	0.0001803766	0.0447868
ENSG00000204020	*LIPN*	40.67847121	2.99211748	0.797534	3.751711	0.0001756320	0.0447868
ENSG00000135636	*DYSF*	374.8411619	2.317309474	0.621536	3.728362	0.0001927284	0.0462954
ENSG00000113749	*HRH2*	69.49149917	2.193258848	0.588972	3.723878	0.0001961854	0.0462954
ENSG00000204021	*LIPK*	6.857510391	2.959242988	0.798168	3.707544	0.0002092793	0.0462954
ENSG00000068976	*PYGM*	17.33765035	2.050543859	0.552144	3.713782	0.0002041850	0.0462954
ENSG00000211448	*DIO2*	155.321791	1.510686245	0.406436	3.716914	0.0002016710	0.0462954
ENSG00000128917	*DLL4*	11.45535912	2.447852976	0.660082	3.708409	0.0002085653	0.0462954
ENSG00000188897	*CTD-3088G3.8*	323.1906061	1.78061636	0.480706	3.70417	0.0002120839	0.0462954
ENSG00000125810	*CD93*	601.1405142	1.759188231	0.475308	3.701152	0.0002146229	0.0462954
ENSG00000178150	*ZNF114*	7.989085047	2.029484872	0.549584	3.692762	0.0002218314	0.0471569
ENSG00000149564	*ESAM*	18.14827649	1.523369052	0.41299	3.688637	0.0002254587	0.0472433
ENSG00000203710	*CR1*	411.1933018	2.299624216	0.627107	3.667037	0.0002453771	0.0481389
ENSG00000163464	*CXCR1*	453.8760438	2.616490966	0.712521	3.672159	0.0002405100	0.0481389
ENSG00000120129	*DUSP1*	6115.128063	1.732263316	0.473872	3.655551	0.0002566297	0.0481389
ENSG00000152137	*HSPB8*	900.9324017	1.778499688	0.487281	3.649845	0.0002623991	0.0481389
ENSG00000184508	*HDDC3*	101.6802136	-0.391065227	0.106941	-3.65684	0.0002553462	0.0481389
ENSG00000206172	*HBA1*	9.437796303	3.255644841	0.885269	3.677576	0.0002354608	0.0481389
ENSG00000141096	*DPEP3*	8.922090167	2.600257498	0.709629	3.66425	0.0002480641	0.0481389
ENSG00000076662	*ICAM3*	139.9038075	2.270536264	0.620081	3.661675	0.0002505716	0.0481389
ENSG00000244482	*LILRA6*	189.3604241	2.418416833	0.662635	3.649695	0.0002625518	0.0481389
ENSG00000170373	*CST1*	131.6759055	-3.542321735	0.97027	-3.65086	0.0002613632	0.0481389
ENSG00000171476	*HOPX*	495.7867843	1.529493784	0.420797	3.634752	0.0002782483	0.0503870
ENSG00000254415	*SIGLEC14*	45.14160974	1.877309137	0.517712	3.626168	0.0002876585	0.0514558
ENSG00000081237	*PTPRC*	4546.785921	1.738982361	0.480872	3.616312	0.0002988305	0.0519840
ENSG00000107736	*CDH23*	109.6230575	0.860731249	0.238059	3.615619	0.0002996305	0.0519840
ENSG00000142347	*MYO1F*	1440.496128	1.976436605	0.546849	3.614228	0.0003012436	0.0519840
ENSG00000188404	*SELL*	592.631915	1.4423354	0.40133	3.593889	0.0003257790	0.0523150

ENSG00000163219	*ARHGAP25*	554.8197482	1.597820813	0.44492	3.591254	0.0003290910	0.0523150
ENSG00000132965	*ALOX5AP*	361.1835711	1.581896625	0.440738	3.5892	0.0003316943	0.0523150
ENSG00000132359	*RAP1GAP2*	213.009783	1.296496824	0.360265	3.598735	0.0003197694	0.0523150
ENSG00000185862	*EVI2B*	461.495179	1.699127547	0.472435	3.596531	0.0003224895	0.0523150
ENSG00000276070	*CCL4L2*	68.6673633	1.767519198	0.491474	3.596362	0.0003226984	0.0523150
ENSG00000239998	*LILRA2*	156.1708969	2.41359626	0.67145	3.594603	0.0003248862	0.0523150
ENSG00000156282	*CLDN17*	49.71152413	3.337239908	0.926759	3.600977	0.0003170233	0.0523150
ENSG00000163563	*MNDA*	868.6380366	2.092578113	0.58443	3.580547	0.0003428759	0.0523886
ENSG00000100908	*EMC9*	129.5613142	-0.518890144	0.14484	-3.5825	0.0003403253	0.0523886
ENSG00000124126	*PREX1*	1676.142545	1.370895286	0.382525	3.583807	0.0003386230	0.0523886
ENSG00000116741	*RGS2*	2515.481448	2.068800406	0.579639	3.569118	0.0003581852	0.0525386
ENSG00000159884	*CCDC107*	36.05187668	-0.506034534	0.141596	-3.57379	0.0003518523	0.0525386
ENSG00000077420	*APBB1IP*	243.778356	1.64456222	0.460633	3.570225	0.0003566752	0.0525386
ENSG00000185201	*IFITM2*	1123.511188	1.573639347	0.440251	3.574411	0.0003510174	0.0525386
ENSG00000198576	*ARC*	12.59565389	1.921251953	0.54003	3.557676	0.0003741507	0.0543370
ENSG00000012779	*ALOX5*	542.1569197	1.341197064	0.3777	3.55096	0.0003838295	0.0551962
ENSG00000147408	*CSGALNACT1*	47.32334612	1.736073692	0.489823	3.544287	0.0003936766	0.0552874
ENSG00000127084	*FGD3*	488.0688261	1.329285081	0.375463	3.540387	0.0003995406	0.0552874
ENSG00000160593	*AMICA1*	1529.369162	1.427087059	0.402968	3.541442	0.0003979461	0.0552874
ENSG00000184922	*FMNL1*	417.2457271	1.543935634	0.435267	3.547097	0.0003895014	0.0552874
ENSG00000203786	*KPRP*	5.488623737	3.534762474	1.000553	3.532808	0.0004111703	0.0563649
ENSG00000115008	*IL1A*	41.13563665	2.044716665	0.579827	3.526423	0.0004212131	0.0572070
ENSG00000085514	*PILRA*	213.260431	1.839828677	0.522145	3.523597	0.0004257310	0.0572901
ENSG00000015285	*WAS*	196.6610082	1.566856851	0.445876	3.514111	0.0004412283	0.0588358
ENSG00000204305	*AGER*	31.35634892	1.115269179	0.317594	3.511616	0.0004453905	0.0588557
ENSG00000081041	*CXCL2*	121.8368299	1.121447805	0.320025	3.504247	0.0004578998	0.0599685
ENSG00000117115	*PADI2*	311.0156325	1.595711216	0.455678	3.501843	0.0004620517	0.0599768
ENSG00000186806	*VSIG10L*	112.6784624	1.836473622	0.524908	3.498656	0.0004676100	0.0601658
ENSG00000123329	*ARHGAP9*	479.2259745	1.504954786	0.430779	3.493566	0.0004766144	0.0607911
ENSG00000197405	*C5AR1*	1048.994493	2.117769646	0.606742	3.490394	0.0004823089	0.0609871
ENSG00000111181	*SLC6A12*	40.50839526	1.247431148	0.357807	3.486322	0.0004897108	0.0612578
ENSG00000169715	*MT1E*	513.315856	-0.685757788	0.196795	-3.48464	0.0004928019	0.0612578
ENSG00000132510	*KDM6B*	579.8129011	1.305400127	0.375133	3.479832	0.0005017278	0.0618432
ENSG00000189051	*RNF222*	48.81576384	2.238886942	0.643902	3.477063	0.0005069389	0.0619648
ENSG00000130775	*THEMIS2*	767.653598	1.653998209	0.477286	3.465427	0.0005293899	0.0625580
ENSG00000016602	*CLCA4*	2436.442163	1.817346604	0.523652	3.470523	0.0005194464	0.0625580
ENSG00000151702	*FLI1*	244.7806654	1.307265921	0.377325	3.464563	0.0005310932	0.0625580
ENSG00000126860	*EVI2A*	228.3966342	1.699506437	0.489786	3.469899	0.0005206545	0.0625580
ENSG00000127507	*ADGRE2*	416.7557519	1.753547713	0.506288	3.463541	0.0005331160	0.0625580
ENSG00000059804	*SLC2A3*	905.4839017	2.010343885	0.581013	3.460064	0.0005400461	0.0628682
ENSG00000114268	*PFKFB4*	165.0457522	1.460312211	0.422942	3.452745	0.0005549131	0.0635896
ENSG00000155926	*SLA*	742.9187908	1.459286381	0.422635	3.452832	0.0005547350	0.0635896
ENSG00000159337	*PLA2G4D*	13.88198456	1.569829037	0.455069	3.44965	0.0005613144	0.0638245
ENSG00000171608	*PIK3CD*	776.2463976	1.270669369	0.368994	3.443601	0.0005740223	0.0647674

ENSG00000132334	*PTPRE*	1056.794435	1.364429099	0.396935	3.437411	0.0005873037	0.0657601
ENSG00000148841	*ITPRIP*	553.3588369	1.316881276	0.383757	3.431554	0.0006001332	0.0659737
ENSG00000129353	*SLC44A2*	3678.47438	0.488097138	0.142286	3.430394	0.0006027045	0.0659737
ENSG00000101187	*SLCO4A1*	160.6016704	1.311705529	0.382227	3.431743	0.0005997159	0.0659737
ENSG00000124216	*SNAI1*	7.696103487	1.970326867	0.574818	3.427739	0.0006086298	0.0661288
ENSG00000152518	*ZFP36L2*	658.0270618	0.533612565	0.155805	3.424877	0.0006150775	0.0663379
ENSG00000140678	*ITGAX*	1565.747602	1.594065917	0.465752	3.42256	0.0006203438	0.0664175
ENSG00000082074	*FYB*	991.9259765	1.340812758	0.392852	3.413019	0.0006424741	0.0665579
ENSG00000197081	*IGF2R*	4115.112231	0.870500071	0.254689	3.41789	0.0006310867	0.0665579
ENSG00000106780	*MEGF9*	783.34156	1.002450648	0.293299	3.417844	0.0006311927	0.0665579
ENSG00000178372	*CALML5*	227.8365785	1.723079938	0.505537	3.408413	0.0006534185	0.0665579
ENSG00000033327	*GAB2*	587.0589028	1.009740964	0.2958	3.413589	0.0006411326	0.0665579
ENSG00000091592	*NLRP1*	904.1310348	0.92872128	0.272274	3.410982	0.0006472944	0.0665579
ENSG00000092929	*UNC13D*	348.5835282	1.30726178	0.383488	3.40887	0.0006523250	0.0665579
ENSG00000183091	*NEB*	147.948048	1.165209102	0.342494	3.402126	0.0006686381	0.0676385
ENSG00000095370	*SH2D3C*	124.8445678	1.396717987	0.410791	3.40007	0.0006736854	0.0676823
ENSG00000105329	*TGFB1*	135.7183389	1.026453687	0.30292	3.388533	0.0007026760	0.0701146
ENSG00000151726	*ACSL1*	3497.092379	1.115803771	0.329795	3.383326	0.0007161359	0.0709749
ENSG00000213190	*MLLT11*	34.96655406	0.991937175	0.293853	3.375624	0.0007364847	0.0720184
ENSG00000128016	*ZFP36*	2290.304626	1.418453692	0.420154	3.376035	0.0007353859	0.0720184
ENSG00000183625	*CCR3*	42.86315786	2.443863244	0.726592	3.363461	0.0007697164	0.0728125
ENSG00000120738	*EGR1*	617.768747	2.058619948	0.613673	3.354587	0.0007948363	0.0728125
ENSG00000057657	*PRDM1*	535.5767203	1.000608405	0.298692	3.349963	0.0008082233	0.0728125
ENSG00000181016	*LSMEM1*	44.37615442	1.542909674	0.460244	3.35237	0.0008012297	0.0728125
ENSG00000120156	*TEK*	12.27850013	2.088865477	0.62069	3.365391	0.0007643512	0.0728125
ENSG00000107796	*ACTA2*	21.98390633	-1.229083585	0.36527	-3.36486	0.0007658134	0.0728125
ENSG00000066336	*SPI1*	474.2143771	1.539695642	0.4568	3.370612	0.0007500137	0.0728125
ENSG00000168010	*ATG16L2*	754.9539635	1.226851569	0.366626	3.346334	0.0008188782	0.0728125
ENSG00000161638	*ITGA5*	427.2568365	1.294966403	0.385826	3.356348	0.0007897905	0.0728125
ENSG00000166501	*PRKCB*	420.2501617	1.554013311	0.462873	3.357318	0.0007870255	0.0728125
ENSG00000167916	*KRT24*	2397.09258	2.331361408	0.692022	3.368913	0.0007546513	0.0728125
ENSG00000172081	*MOB3A*	500.967832	1.077518538	0.322239	3.343849	0.0008262464	0.0728125
ENSG00000099308	*MAST3*	289.4385807	1.096338807	0.327958	3.342928	0.0008289942	0.0728125
ENSG00000175489	*LRRC25*	220.170772	1.705010136	0.508146	3.355353	0.0007926364	0.0728125
ENSG00000171777	*RASGRP4*	169.2813114	2.401692932	0.718349	3.343353	0.0008277259	0.0728125
ENSG00000105501	*SIGLEC5*	68.90107457	2.374748837	0.709128	3.348828	0.0008115406	0.0728125
ENSG00000177663	*IL17RA*	892.8199897	0.919762481	0.273986	3.356964	0.0007880339	0.0728125
ENSG00000166535	*A2ML1*	1002.086654	1.450167898	0.434398	3.33834	0.0008428066	0.0730048
ENSG00000110876	*SELPLG*	498.0963179	1.383877919	0.414676	3.337251	0.0008461152	0.0730048
ENSG00000128383	*APOBEC3A*	456.5435759	1.968695343	0.589511	3.339542	0.0008391660	0.0730048
ENSG00000091106	*NLRC4*	63.59447992	1.595926681	0.479431	3.32879	0.0008722405	0.0732848
ENSG00000115165	*CYTIP*	605.0026885	1.549162056	0.465529	3.327745	0.0008755193	0.0732848
ENSG00000173559	*NABP1*	3508.644402	1.454169197	0.437143	3.326532	0.0008793378	0.0732848
ENSG00000175315	*CST6*	43.40935031	1.437118927	0.431248	3.332468	0.0008607948	0.0732848

ENSG00000133246	*PRAM1*	42.79085834	1.154190513	0.346598	3.330052	0.0008682973	0.0732848
ENSG00000198053	*SIRPA*	520.3180461	1.149634662	0.345046	3.331828	0.0008627758	0.0732848
ENSG00000163209	*SPRR3*	9398.66207	1.892942748	0.569654	3.32297	0.0008906446	0.0733931
ENSG00000188305	*C19orf35*	14.74118642	2.027840744	0.610195	3.323266	0.0008897002	0.0733931
ENSG00000115590	*IL1R2*	359.8218257	2.191449718	0.661145	3.31463	0.0009176438	0.0747778
ENSG00000124882	*EREG*	227.0051715	1.760952973	0.531171	3.315229	0.0009156795	0.0747778
ENSG00000113070	*HBEGF*	280.9775264	1.604054578	0.484422	3.311273	0.0009287250	0.0752626
ENSG00000178726	*THBD*	569.6998692	2.072148166	0.626151	3.30934	0.0009351605	0.0753678
ENSG00000197943	*PLCG2*	550.1524259	0.988242075	0.299196	3.302994	0.0009565855	0.0766732
ENSG00000162572	*SCNN1D*	52.00949878	0.779800895	0.236387	3.298826	0.0009709006	0.0768620
ENSG00000158887	*MPZ*	43.30825426	1.239879961	0.376097	3.296706	0.0009782593	0.0768620
ENSG00000214113	*LYRM4*	209.8049346	-0.386119827	0.117153	-3.29586	0.0009811975	0.0768620
ENSG00000151948	*GLT1D1*	194.0027529	2.453177853	0.744772	3.293865	0.0009882004	0.0768620
ENSG00000141527	*CARD14*	189.6181425	0.664607081	0.201809	3.293245	0.0009903816	0.0768620
ENSG00000198342	*ZNF442*	55.29332415	-0.633468395	0.191935	-3.30043	0.0009653628	0.0768620
ENSG00000163218	*PGLYRP4*	35.40514359	1.507393971	0.45914	3.283079	0.0010267976	0.0792688
ENSG00000130475	*FCHO1*	85.17477418	1.396035122	0.426313	3.274673	0.0010578446	0.0812380
ENSG00000167759	*KLK13*	432.5007784	2.177708944	0.667258	3.263671	0.0010997881	0.0840192
ENSG00000143546	*S100A8*	10686.37567	2.151083123	0.659681	3.260795	0.0011110021	0.0843267
ENSG00000213347	*MXD3*	159.4639724	1.254876515	0.385071	3.25882	0.0011187671	0.0843267
ENSG00000101336	*HCK*	871.1965188	1.616043212	0.495987	3.258239	0.0011210598	0.0843267
ENSG00000204542	*C6orf15*	6.203863346	3.043601347	0.935576	3.253185	0.0011411927	0.0853732
ENSG00000110203	*FOLR3*	10.09684646	2.947475316	0.906403	3.251838	0.0011466131	0.0853732
ENSG00000062282	*DGAT2*	385.1136643	1.889009237	0.582431	3.243316	0.0011814721	0.0875244
ENSG00000133710	*SPINK5*	1396.236797	1.523517868	0.47005	3.241184	0.0011903453	0.0877386
ENSG00000119535	*CSF3R*	3574.954552	2.277942108	0.706229	3.225502	0.0012575197	0.0899771
ENSG00000159516	*SPRR2G*	8.900936315	2.970580876	0.920519	3.22707	0.0012506472	0.0899771
ENSG00000154429	*CCSAP*	160.9765066	0.524627084	0.162647	3.225554	0.0012572927	0.0899771
ENSG00000188549	*C15orf52*	151.2467778	0.785723445	0.243249	3.23012	0.0012373831	0.0899771
ENSG00000160255	*ITGB2*	1285.404679	1.207525803	0.373976	3.22889	0.0012427170	0.0899771
ENSG00000173638	*SLC19A1*	147.9920447	1.589686916	0.492758	3.2261	0.0012548962	0.0899771
ENSG00000155307	*SAMSN1*	447.0759092	1.459101124	0.453116	3.220151	0.0012812317	0.0912287
ENSG00000162747	*FCGR3B*	1127.66368	2.265580387	0.706557	3.206507	0.0013435703	0.0915786
ENSG00000168918	*INPP5D*	539.7586028	0.759423223	0.236774	3.207374	0.0013395295	0.0915786
ENSG00000188001	*TPRG1*	146.6351541	0.982323984	0.305399	3.216525	0.0012975312	0.0915786
ENSG00000120318	*ARAP3*	312.6943691	0.880062277	0.274794	3.202629	0.0013617921	0.0915786
ENSG00000152926	*ZNF117*	700.4702591	0.667203224	0.208406	3.201464	0.0013673106	0.0915786
ENSG00000059377	*TBXAS1*	356.7962638	1.33421913	0.415333	3.212407	0.0013162757	0.0915786
ENSG00000187479	*C11orf96*	14.69699214	1.958308711	0.611243	3.203816	0.0013561901	0.0915786
ENSG00000171310	*CHST11*	408.7728418	1.186643045	0.370603	3.201929	0.0013651076	0.0915786
ENSG00000131471	*AOC3*	22.77300856	1.226591369	0.381778	3.212835	0.0013143161	0.0915786
ENSG00000173868	*PHOSPHO1*	209.3184166	2.627190768	0.818348	3.21036	0.0013256865	0.0915786
ENSG00000160229	*ZNF66*	56.13988521	0.87651468	0.273497	3.204843	0.0013513616	0.0915786
ENSG00000188505	*NCCRP1*	649.3820155	1.424720362	0.443692	3.211057	0.0013224755	0.0915786

ENSG00000100985	*MMP9*	105.0085456	1.801939784	0.560903	3.212569	0.0013155353	0.0915786
ENSG00000189056	*RELN*	20.41484416	1.821826465	0.570354	3.194201	0.0014021827	0.0934873
ENSG00000130592	*LSP1*	1872.970387	0.886506466	0.277959	3.189347	0.0014259475	0.0946416
ENSG00000106541	*AGR2*	41664.02551	-0.714062434	0.224157	-3.18555	0.0014447875	0.0954601
ENSG00000104894	*CD37*	157.4882807	1.249881462	0.393085	3.179671	0.0014744245	0.0969814
ENSG00000146112	*PPP1R18*	570.9228967	1.216818205	0.382862	3.178213	0.0014818607	0.0970354
ENSG00000112137	*PHACTR1*	270.347717	1.480915393	0.466756	3.17278	0.0015098686	0.0970487
ENSG00000112195	*TREML2*	177.9198685	2.368986837	0.747134	3.170764	0.0015203883	0.0970487
ENSG00000170423	*KRT78*	380.5887664	1.924890584	0.607367	3.169241	0.0015283781	0.0970487
ENSG00000188215	*DCUN1D3*	490.9316317	0.865486098	0.27282	3.172375	0.0015119764	0.0970487
ENSG00000101236	*RNF24*	802.5230879	0.95210711	0.300246	3.171085	0.0015187079	0.0970487
ENSG00000087589	*CASS4*	294.9893157	1.73106507	0.544957	3.176515	0.0014905605	0.0970487
ENSG00000147168	*IL2RG*	270.2098958	0.933031134	0.294288	3.170466	0.0015219465	0.0970487
ENSG00000125378	*BMP4*	17.60094942	-1.212353032	0.38289	-3.16632	0.0015438084	0.0976060
ENSG00000111052	*LIN7A*	40.68503686	1.801629323	0.569401	3.164079	0.0015557467	0.0979386
ENSG00000115935	*WIPF1*	622.5961766	1.143319049	0.361607	3.161768	0.0015681439	0.0982972
ENSG00000126233	*SLURP1*	62.95038101	1.64617095	0.521552	3.156293	0.0015978817	0.0997350

Table S3: Biological processes enriched at baseline between “Cold” and “No Cold” groups

ID	Description	GeneRatio	BgRatio	*P*value	*P*.adjust	qvalue	geneID	Count
GO:0042119	neutrophil activation	0.157895	0.028536908	1.06E-15	2.36E-12	2.11E-12	*PADI2/CDA/S100A12/S100A8/MNDA/FCGR3B/SELL/PTPRC/CR1/CXCR2/CXCR1/MME/IGF2R/CALML5/ALOX5/FOLR3/SLC2A3/ARHGAP9/OLFM4/ITGAX/UNC13D/PRAM1/SLC44A2/C5AR1/SIGLEC5/SIGLEC14/LILRA2/SIRPA/CD93/MMP9/PREX1/ITGB2/NFAM1*	33
GO:0002283	neutrophil activation involved in immune response	0.15311	0.027961567	4.04E-15	3.89E-12	3.48E-12	*PADI2/CDA/S100A12/S100A8/MNDA/FCGR3B/SELL/PTPRC/CR1/CXCR2/CXCR1/MME/IGF2R/CALML5/ALOX5/FOLR3/SLC2A3/ARHGAP9/OLFM4/ITGAX/UNC13D/PRAM1/SLC44A2/C5AR1/SIGLEC5/SIGLEC14/LILRA2/SIRPA/CD93/MMP9/ITGB2/NFAM1*	32
GO:0002446	neutrophil mediated immunity	0.148325	0.02870951	5.47E-14	3.16E-11	2.83E-11	*PADI2/CDA/S100A12/S100A8/MNDA/FCGR3B/SELL/PTPRC/CR1/CXCR2/CXCR1/MME/IGF2R/CALML5/ALOX5/FOLR3/SLC2A3/ARHGAP9/OLFM4/ITGAX/UNC13D/PRAM1/SLC44A2/C5AR1/SIGLEC5/SIGLEC14/SIRPA/CD93/MMP9/ITGB2/NFAM1*	31
GO:0043312	neutrophil degranulation	0.148325	0.027904033	2.54E-14	1.84E-11	1.64E-11	*PADI2/CDA/S100A12/S100A8/MNDA/FCGR3B/SELL/PTPRC/CR1/CXCR2/CXCR1/MME/IGF2R/CALML5/ALOX5/FOLR3/SLC2A3/ARHGAP9/OLFM4/ITGAX/UNC13D/PRAM1/SLC44A2/C5AR1/SIGLEC5/SIGLEC14/SIRPA/CD93/MMP9/ITGB2/NFAM1*	31
GO:0008544	epidermis development	0.138756	0.02617801	2.02E-13	9.74E-11	8.70E-11	*FLG/LCE3E/LCE3D/SPRR3/SPRR2D/SPRR2B/SPRR2E/SPRR2F/SPRR2G/EREG/SPINK5/SPINK6/CTSV/CALML5/LIPK/LIPN/CST6/KRT78/BMP4/KRT24/ZFP36/CNFN/KLK5/KLK7/KLK8/KLK12/KLK13/SNAI1/WAS*	29
GO:0050900	leukocyte migration	0.133971	0.027098556	2.94E-12	1.06E-09	9.50E-10	*PIK3CD/PADI2/CSF3R/ECM1/S100A12/S100A8/SELL/IL1A/CXCR2/CXCR1/INPP5D/CXCL2/TEK/JAML/ESAM/ITGA5/SELPLG/ITGAX/ADGRE2/TGFB1/C5AR1/SIRPA/THBD/HCK/MMP9/PREX1/ITGB2/IL17RA*	28
GO:0043588	skin development	0.119617	0.023646511	2.89E-11	7.61E-09	6.80E-09	*FLG/LCE3E/LCE3D/SPRR3/SPRR2D/SPRR2B/SPRR2E/SPRR2F/SPRR2G/ASPRV1/EREG/SPINK5/SPINK6/CTSV/LIPK/LIPN/KRT78/KRT24/ZFP36/CNFN/KLK5/KLK8/KLK12/KLK13/SNAI1*	25
GO:0009913	epidermal cell differentiation	0.114833	0.020079397	5.69E-12	1.65E-09	1.47E-09	*FLG/LCE3E/LCE3D/SPRR3/SPRR2D/SPRR2B/SPRR2E/SPRR2F/SPRR2G/EREG/SPINK5/SPINK6/CTSV/LIPK/LIPN/KRT78/BMP4/KRT24/ZFP36/CNFN/KLK5/KLK8/KLK12/KLK13*	24
GO:0030216	keratinocyte differentiation	0.110048	0.017260227	1.74E-12	7.18E-10	6.42E-10	*FLG/LCE3E/LCE3D/SPRR3/SPRR2D/SPRR2B/SPRR2E/SPRR2F/SPRR2G/EREG/SPINK5/SPINK6/CTSV/LIPK/LIPN/KRT78/KRT24/ZFP36/CNFN/KLK5/KLK8/KLK12/KLK13*	23
GO:0031424	keratinization	0.095694	0.013002704	3.83E-12	1.23E-09	1.10E-09	*FLG/LCE3E/LCE3D/SPRR3/SPRR2D/SPRR2B/SPRR2E/SPRR2F/SPRR2G/SPINK5/SPINK6/LIPK/LIPN/KRT78/KRT24/CNFN/KLK5/KLK8/KLK12/KLK13*	20

GO:0070268	cornification	0.086124	0.006501352	1.63E-15	2.36E-12	2.11E-12	*FLG/LCE3D/SPRR3/SPRR2D/SPRR2B/SPRR2E/SPRR2F/ SPRR2G/SPINK5/SPINK6/LIPK/LIPN/KRT78/KRT24/ KLK5/KLK8/KLK12/KLK13*	18
GO:0097530	granulocyte migration	0.062201	0.007134227	3.21E-09	7.75E-07	6.92E-07	*PIK3CD/CSF3R/S100A12/S100A8/IL1A/CXCR2/CXCL2/ JAML/ADGRE2/C5AR1/PREX1/ITGB2/IL17RA*	13
GO:0002521	leukocyte differentiation	0.090909	0.027558829	5.55E-06	7.65E-04	6.83E-04	*PIK3CD/PTPRC/CR1/ZFP36L2/INPP5D/EGR1/SPINK5/AGER/ PRDM1/SPI1/GAB2/BMP4/DLL4/PLCG2/EVI2B/TGFB1/ MMP9/PREX1/NFAM1*	19
GO:0002768	immune response-regulating cell surface receptor signaling pathway	0.08134	0.026350613	4.07E-05	3.37E-03	3.01E-03	*PIK3CD/THEMIS2/MNDA/PTPRC/CR1/WIPF1/INPP5D/ FYB1/GAB2/PRKCB/PLCG2/ICAM3/C5AR1/LILRA2/ HCK/NFAM1/WAS*	17
GO:0002429	immune response-activating cell surface receptor signaling pathway	0.076555	0.024509522	6.00E-05	4.34E-03	3.88E-03	*PIK3CD/THEMIS2/MNDA/PTPRC/CR1/WIPF1/INPP5D/ FYB1/PRKCB/PLCG2/ICAM3/C5AR1/LILRA2/HCK/ NFAM1/WAS*	16
GO:0042110	T cell activation	0.076555	0.02686842	1.74E-04	1.12E-02	9.99E-03	*PIK3CD/PTPRC/CR1/ZFP36L2/EGR1/SPINK5/AGER/ TREML2/PRDM1/APBB1IP/JAML/BMP4/DLL4/ TGFB1/PREX1/WAS*	16
GO:0060326	cell chemotaxis	0.07177	0.015534204	9.89E-07	1.51E-04	1.35E-04	*PIK3CD/PADI2/CSF3R/S100A12/S100A8/CXCR2/ CXCR1/CXCL2/HBEGF/JAML/ADGRE2/C5AR1/ PREX1/ITGB2/IL17RA*	15
GO:0030098	lymphocyte differentiation	0.07177	0.018871181	1.07E-05	1.23E-03	1.10E-03	*PIK3CD/PTPRC/CR1/ZFP36L2/INPP5D/EGR1/SPINK5/ PRDM1/SPI1/BMP4/DLL4/PLCG2/TGFB1/PREX1/ NFAM1*	15
GO:0031349	positive regulation of defense response	0.07177	0.025947874	3.80E-04	1.93E-02	1.72E-02	*PGLYRP4/S100A12/S100A8/NLRC4/IL1RL1/EREG/ PLCG2/ICAM3/TGFB1/KLK5/KLK7/LILRA2/HCK/ ITGB2/IL17RA*	15
GO:0040017	positive regulation of locomotion	0.07177	0.028191704	8.91E-04	3.30E-02	2.95E-02	*PIK3CD/PTPRC/IL1A/CXCL2/HBEGF/AGER/RELN/TEK/ ITGA5/BMP4/TGFB1/C5AR1/MMP9/PREX1/SNAI1*	15
GO:0030595	leukocyte chemotaxis	0.066986	0.01167942	1.70E-07	3.07E-05	2.75E-05	*PIK3CD/PADI2/CSF3R/S100A12/S100A8/CXCR2/ CXCR1/CXCL2/JAML/ADGRE2/C5AR1/PREX1/ITGB2/ IL17RA*	14
GO:1901342	regulation of vasculature development	0.066986	0.017662965	2.18E-05	2.10E-03	1.88E-03	*ECM1/IL1A/CCR3/EGR1/SPINK5/NOS3/TEK/ITGA5/ BMP4/DLL4/PRKCB/SERPINB7/C5AR1/ITGB2*	14
GO:0002697	regulation of immune effector process	0.066986	0.023128704	3.76E-04	1.93E-02	1.72E-02	*PTPRC/CR1/SPINK5/AGER/GAB2/UNC13D/PRAM1/ ADGRE2/TGFB1/C5AR1/KLK5/KLK7/ITGB2/WAS*	14
GO:0051346	negative regulation of hydrolase activity	0.066986	0.024394454	6.37E-04	2.63E-02	2.35E-02	*ECM1/RGS2/CR1/NLRC4/SPINK5/SPINK6/SPINK7/ NOS3/PI15/CST6/A2ML1/SERPINB7/CST1/MMP9*	14

GO:0052547	regulation of peptidase activity	0.066986	0.024509522	6.67E-04	2.72E-02	2.43E-02	*ECM1/S100A8/CR1/NLRC4/SPINK5/SPINK6/SPINK7/ PI15/CST6/A2ML1/NLRP1/SERPINB7/CST1/MMP9*	14
GO:0030335	positive regulation of cell migration	0.066986	0.025430067	9.52E-04	3.37E-02	3.02E-02	*PIK3CD/PTPRC/IL1A/CXCL2/HBEGF/RELN/TEK/ITGA5/ BMP4/TGFB1/C5AR1/MMP9/PREX1/SNAI1*	14
GO:1903706	regulation of hemopoiesis	0.066986	0.025775272	1.08E-03	3.71E-02	3.32E-02	*CSF3R/CR1/ZFP36L2/INPP5D/SPINK5/AGER/PRDM1/ SPI1/BMP4/PRKCB/EVI2B/ZFP36/TGFB1/NFAM1*	14
GO:2000147	positive regulation of cell motility	0.066986	0.026465681	1.39E-03	4.30E-02	3.84E-02	*PIK3CD/PTPRC/IL1A/CXCL2/HBEGF/RELN/TEK/ITGA5/ BMP4/TGFB1/C5AR1/MMP9/PREX1/SNAI1*	14
GO:0051272	positive regulation of cellular component movement	0.066986	0.027213624	1.80E-03	4.97E-02	4.44E-02	*PIK3CD/PTPRC/IL1A/CXCL2/HBEGF/RELN/TEK/ITGA5/ BMP4/TGFB1/C5AR1/MMP9/PREX1/SNAI1*	14
GO:0097529	myeloid leukocyte migration	0.062201	0.010298602	2.61E-07	4.45E-05	3.98E-05	*PIK3CD/CSF3R/S100A12/S100A8/IL1A/CXCR2/CXCL2/ JAML/ADGRE2/C5AR1/PREX1/ITGB2/IL17RA*	13
GO:0042742	defense response to bacterium	0.062201	0.016684886	5.13E-05	3.81E-03	3.40E-03	*PGLYRP4/S100A12/S100A8/NLRC4/SPINK5/DEFB103B/ DEFB103A/C10orf99/RNASE7/NLRP1/C5AR1/KLK5/KLK7*	13
GO:0045861	negative regulation of proteolysis	0.062201	0.020021863	3.13E-04	1.71E-02	1.53E-02	*ECM1/CR1/NLRC4/IL1R2/SPINK5/SPINK6/SPINK7/ PI15/CST6/A2ML1/SERPINB7/CST1/MMP9*	13
GO:0030099	myeloid cell differentiation	0.062201	0.022438295	9.09E-04	3.32E-02	2.96E-02	*PIK3CD/CSF3R/INPP5D/SPI1/GAB2/FLI1/BMP4/ PRKCB/EVI2B/RASGRP4/ZFP36/TGFB1/MMP9*	13
GO:0002683	negative regulation of immune system process	0.062201	0.023704045	1.49E-03	4.31E-02	3.85E-02	*PADI2/MNDA/PTPRC/CR1/IL1RL1/INPP5D/SPINK5/ PRDM1/BMP4/ZFP36/TGFB1/LILRA2/SAMSN1*	13
GO:0071621	granulocyte chemotaxis	0.057416	0.00632875	8.34E-09	1.86E-06	1.66E-06	*PIK3CD/CSF3R/S100A12/S100A8/CXCR2/CXCL2/ JAML/ADGRE2/C5AR1/PREX1/ITGB2/IL17RA*	12
GO:0010466	negative regulation of peptidase activity	0.057416	0.015131465	8.45E-05	5.82E-03	5.20E-03	*ECM1/CR1/NLRC4/SPINK5/SPINK6/SPINK7/PI15/ CST6/A2ML1/SERPINB7/CST1/MMP9*	12
GO:0050673	epithelial cell proliferation	0.057416	0.020769806	1.46E-03	4.30E-02	3.84E-02	*ECM1/CCR3/EREG/SLURP1/TEK/JAML/BMP4/ DLL4/ZFP36/TGFB1/C5AR1/KLK8*	12
GO:1990266	neutrophil migration	0.052632	0.005810943	3.61E-08	7.45E-06	6.66E-06	*PIK3CD/CSF3R/S100A12/S100A8/IL1A/CXCR2/ CXCL2/JAML/C5AR1/PREX1/ITGB2*	11
GO:1904018	positive regulation of vasculature development	0.052632	0.009665727	6.07E-06	7.98E-04	7.13E-04	*ECM1/IL1A/CCR3/EGR1/NOS3/TEK/ITGA5/ PRKCB/SERPINB7/C5AR1/ITGB2*	11
GO:0030217	T cell differentiation	0.052632	0.01294517	9.07E-05	6.11E-03	5.46E-03	*PIK3CD/PTPRC/CR1/ZFP36L2/EGR1/SPINK5/ PRDM1/BMP4/DLL4/TGFB1/PREX1*	11
GO:0042113	B cell activation	0.052632	0.015591738	4.54E-04	2.15E-02	1.92E-02	*PIK3CD/MNDA/PTPRC/ZFP36L2/INPP5D/ PRDM1/PRKCB/PLCG2/TGFB1/SAMSN1/NFAM1*	11
GO:0045765	regulation of angiogenesis	0.052632	0.015706806	4.83E-04	2.25E-02	2.01E-02	*ECM1/IL1A/CCR3/SPINK5/NOS3/TEK/ITGA5/ DLL4/PRKCB/C5AR1/ITGB2*	11

GO:0032103	positive regulation of response to external stimulus	0.052632	0.016167079	6.14E-04	2.57E-02	2.30E-02	*S100A12/S100A8/IL1RL1/CXCL2/AGER/TGFB1/ C5AR1/KLK5/KLK7/THBD/IL17RA*	11
GO:0050678	regulation of epithelial cell proliferation	0.052632	0.017662965	1.26E-03	4.01E-02	3.59E-02	*ECM1/CCR3/EREG/SLURP1/TEK/JAML/BMP4/ DLL4/ZFP36/TGFB1/C5AR1*	11
GO:0032496	response to lipopolysaccharide	0.052632	0.018180772	1.59E-03	4.55E-02	4.06E-02	*S100A8/CXCL2/PRDM1/NOS3/PLCG2/ZFP36/ TGFB1/C5AR1/LILRA2/THBD/HCK*	11
GO:0006959	humoral immune response	0.052632	0.018468443	1.80E-03	4.97E-02	4.44E-02	*PGLYRP4/S100A12/S100A8/CR1/SPINK5/ DEFB103B/DEFB103A/RNASE7/C5AR1/KLK5/KLK7*	11
GO:0030593	neutrophil chemotaxis	0.047847	0.005178068	1.26E-07	2.43E-05	2.18E-05	*PIK3CD/CSF3R/S100A12/S100A8/CXCR2/ CXCL2/JAML/C5AR1/PREX1/ITGB2*	10
GO:0002703	regulation of leukocyte mediated immunity	0.047847	0.009493125	3.15E-05	2.68E-03	2.40E-03	*PTPRC/CR1/AGER/GAB2/UNC13D/PRAM1/ ADGRE2/TGFB1/ITGB2/WAS*	10
GO:0051091	positive regulation of DNA binding transcription factor activity	0.047847	0.014153386	8.11E-04	3.17E-02	2.83E-02	*S100A12/S100A8/NLRC4/AGER/RELN/PRKCB/ CARD14/TGFB1/ITGB2/NFAM1*	10
GO:0010951	negative regulation of endopeptidase activity	0.047847	0.014383522	9.17E-04	3.32E-02	2.96E-02	*CR1/NLRC4/SPINK5/SPINK6/SPINK7/CST6/ A2ML1/SERPINB7/CST1/MMP9*	10
GO:1902105	regulation of leukocyte differentiation	0.047847	0.014613659	1.03E-03	3.61E-02	3.22E-02	*CR1/ZFP36L2/INPP5D/SPINK5/AGER/PRDM1/ BMP4/EVI2B/TGFB1/NFAM1*	10
GO:0050851	antigen receptor-mediated signaling pathway	0.047847	0.014786261	1.13E-03	3.80E-02	3.40E-02	*PIK3CD/THEMIS2/MNDA/PTPRC/INPP5D/ FYB1/PRKCB/PLCG2/NFAM1/WAS*	10
GO:0019730	antimicrobial humoral response	0.043062	0.006041079	4.90E-06	7.09E-04	6.34E-04	*PGLYRP4/S100A12/S100A8/SPINK5/DEFB103B/ DEFB103A/RNASE7/KLK5/KLK7*	9
GO:0045766	positive regulation of angiogenesis	0.043062	0.008457511	7.27E-05	5.13E-03	4.59E-03	*ECM1/IL1A/CCR3/NOS3/TEK/ITGA5/PRKCB/ C5AR1/ITGB2*	9
GO:0018149	peptide cross-linking	0.038278	0.003394511	5.01E-07	8.05E-05	7.19E-05	*FLG/LCE3E/LCE3D/SPRR3/SPRR2D/SPRR2B/ SPRR2E/SPRR2F*	8
GO:0051092	positive regulation of NF-kappaB transcription factor activity	0.038278	0.008054772	2.94E-04	1.64E-02	1.46E-02	*S100A12/S100A8/NLRC4/AGER/PRKCB/CARD14/ TGFB1/ITGB2*	8
GO:0050864	regulation of B cell activation	0.038278	0.008917784	5.81E-04	2.51E-02	2.24E-02	*MNDA/PTPRC/ZFP36L2/INPP5D/PRDM1/ TGFB1/SAMSN1/NFAM1*	8

GO:0045619	regulation of lymphocyte differentiation	0.038278	0.008975318	6.06E-04	2.57E-02	2.30E-02	*CR1/ZFP36L2/INPP5D/SPINK5/PRDM1/ BMP4/TGFB1/NFAM1*	8
GO:0050866	negative regulation of cell activation	0.038278	0.010010931	1.23E-03	3.99E-02	3.57E-02	*MNDA/INPP5D/PRDM1/NOS3/BMP4/TGFB1/ THBD/SAMSN1*	8
GO:0007492	endoderm development	0.033493	0.004545193	4.58E-05	3.49E-03	3.12E-03	*DUSP1/ARC/ITGA5/BMP4/TGFB1/MMP9/ ITGB2*	7
GO:0001704	formation of primary germ layer	0.033493	0.007249295	8.30E-04	3.20E-02	2.86E-02	*DUSP1/ITGA5/BMP4/KDM6B/MMP9/SNAI1/ ITGB2*	7
GO:0050777	negative regulation of immune response	0.033493	0.0075945	1.09E-03	3.71E-02	3.32E-02	*PTPRC/CR1/IL1RL1/INPP5D/SPINK5/TGFB1/ SAMSN1*	7
GO:0002819	regulation of adaptive immune response	0.033493	0.007767102	1.24E-03	3.99E-02	3.57E-02	*PTPRC/CR1/IL1RL1/AGER/TGFB1/SAMSN1/ WAS*	7
GO:0001906	cell killing	0.033493	0.007997238	1.47E-03	4.30E-02	3.84E-02	*PGLYRP4/S100A12/PTPRC/AGER/DEFB103B/ DEFB103A/UNC13D*	7
GO:0072006	nephron development	0.033493	0.007939704	1.41E-03	4.30E-02	3.84E-02	*EGR1/CALB1/TEK/ACTA2/BMP4/SERPINB7/ TGFB1*	7
GO:0050832	defense response to fungus	0.028708	0.002301364	7.68E-06	9.66E-04	8.63E-04	*S100A12/S100A8/C10orf99/RNASE7/TGFB1/ IL17RA*	6
GO:0009620	response to fungus	0.028708	0.003106841	4.49E-05	3.49E-03	3.12E-03	*S100A12/S100A8/C10orf99/RNASE7/TGFB1/ IL17RA*	6
GO:0061844	antimicrobial humoral immune response mediated by antimicrobial peptide	0.028708	0.003106841	4.49E-05	3.49E-03	3.12E-03	*PGLYRP4/S100A12/SPINK5/RNASE7/KLK5/ KLK7*	6
GO:0050830	defense response to Gram-positive bacterium	0.028708	0.005235602	8.02E-04	3.17E-02	2.83E-02	*PGLYRP4/DEFB103B/DEFB103A/C10orf99/ RNASE7/C5AR1*	6
GO:0050853	B cell receptor signaling pathway	0.028708	0.005293136	8.50E-04	3.21E-02	2.87E-02	*PIK3CD/MNDA/PTPRC/PRKCB/PLCG2/ NFAM1*	6
GO:0007613	memory	0.028708	0.006098613	1.77E-03	4.97E-02	4.44E-02	*HRH2/RELN/CALB1/ARC/ITGA5/KLK8*	6
GO:0072012	glomerulus vasculature development	0.023923	0.001438352	1.05E-05	1.23E-03	1.10E-03	*EGR1/TEK/ACTA2/BMP4/SERPINB7*	5
GO:0061437	renal system vasculature development	0.023923	0.00155342	1.56E-05	1.56E-03	1.39E-03	*EGR1/TEK/ACTA2/BMP4/SERPINB7*	5
GO:0061440	kidney vasculature development	0.023923	0.00155342	1.56E-05	1.56E-03	1.39E-03	*EGR1/TEK/ACTA2/BMP4/SERPINB7*	5

GO:0002886	regulation of myeloid leukocyte mediated immunity	0.023923	0.0025315	1.78E-04	1.12E-02	9.99E-03	*GAB2/UNC13D/PRAM1/ADGRE2/ITGB2*	5
GO:0043300	regulation of leukocyte degranulation	0.023923	0.0025315	1.78E-04	1.12E-02	9.99E-03	*GAB2/UNC13D/PRAM1/ADGRE2/ITGB2*	5
GO:0045123	cellular extravasation	0.023923	0.002876704	3.27E-04	1.74E-02	1.56E-02	*PIK3CD/IL1A/JAML/SELPLG/ITGB2*	5
GO:0031663	lipopolysaccharide-mediated signaling pathway	0.023923	0.003049307	4.30E-04	2.14E-02	1.91E-02	*PRDM1/NOS3/TGFB1/LILRA2/HCK*	5
GO:0045576	mast cell activation	0.023923	0.003221909	5.56E-04	2.48E-02	2.22E-02	*PIK3CD/S100A12/GAB2/UNC13D/ADGRE2*	5
GO:0006968	cellular defense response	0.023923	0.003452045	7.65E-04	3.07E-02	2.75E-02	*MNDA/CXCR2/CCR3/LSP1/C5AR1*	5
GO:0032835	glomerulus development	0.023923	0.003624648	9.56E-04	3.37E-02	3.02E-02	*EGR1/TEK/ACTA2/BMP4/SERPINB7*	5
GO:0032945	negative regulation of mononuclear cell proliferation	0.023923	0.003969852	1.44E-03	4.30E-02	3.84E-02	*MNDA/INPP5D/PRDM1/BMP4/TGFB1*	5
GO:0050672	negative regulation of lymphocyte proliferation	0.023923	0.003969852	1.44E-03	4.30E-02	3.84E-02	*MNDA/INPP5D/PRDM1/BMP4/TGFB1*	5
GO:1900004	negative regulation of serine-type endopeptidase activity	0.019139	0.000747943	1.33E-05	1.43E-03	1.28E-03	*CR1/SPINK5/SPINK6/SPINK7*	4
GO:1902572	negative regulation of serine-type peptidase activity	0.019139	0.000747943	1.33E-05	1.43E-03	1.28E-03	*CR1/SPINK5/SPINK6/SPINK7*	4
GO:0072109	glomerular mesangium development	0.019139	0.000863011	2.50E-05	2.19E-03	1.96E-03	*EGR1/ACTA2/BMP4/SERPINB7*	4
GO:1900003	regulation of serine-type endopeptidase activity	0.019139	0.000863011	2.50E-05	2.19E-03	1.96E-03	*CR1/SPINK5/SPINK6/SPINK7*	4
GO:1902571	regulation of serine-type peptidase activity	0.019139	0.000863011	2.50E-05	2.19E-03	1.96E-03	*CR1/SPINK5/SPINK6/SPINK7*	4
GO:0045577	regulation of B cell differentiation	0.019139	0.001495886	2.47E-04	1.49E-02	1.33E-02	*ZFP36L2/INPP5D/PRDM1/NFAM1*	4

GO:0001958	endochondral ossification	0.019139	0.00155342	2.87E-04	1.63E-02	1.45E-02	*CSGALNACT1/TEK/BMP4/PHOSPHO1*	4
GO:0036075	replacement ossification	0.019139	0.00155342	2.87E-04	1.63E-02	1.45E-02	*CSGALNACT1/TEK/BMP4/PHOSPHO1*	4
GO:0061311	cell surface receptor signaling pathway involved in heart development	0.019139	0.001610954	3.32E-04	1.74E-02	1.56E-02	*BMP4/DLL4/TGFB1/SNAI1*	4
GO:1900271	regulation of long-term synaptic potentiation	0.019139	0.001726023	4.36E-04	2.14E-02	1.91E-02	*AGER/RELN/CALB1/ARC*	4
GO:0050869	negative regulation of B cell activation	0.019139	0.001783557	4.96E-04	2.28E-02	2.03E-02	*MNDA/INPP5D/PRDM1/SAMSN1*	4
GO:0043616	keratinocyte proliferation	0.019139	0.002243829	1.20E-03	3.99E-02	3.57E-02	*EREG/SLURP1/ZFP36/KLK8*	4
GO:0090184	positive regulation of kidney development	0.019139	0.002301364	1.32E-03	4.16E-02	3.72E-02	*EGR1/BMP4/SERPINB7/TGFB1*	4
GO:0002820	negative regulation of adaptive immune response	0.019139	0.002358898	1.45E-03	4.30E-02	3.84E-02	*PTPRC/CR1/IL1RL1/SAMSN1*	4
GO:0072110	glomerular mesangial cell proliferation	0.014354	0.000575341	1.93E-04	1.19E-02	1.06E-02	*EGR1/BMP4/SERPINB7*	3
GO:0072672	neutrophil extravasation	0.014354	0.000632875	2.63E-04	1.55E-02	1.39E-02	*PIK3CD/IL1A/JAML*	3
GO:1901722	regulation of cell proliferation involved in kidney development	0.014354	0.000747943	4.48E-04	2.15E-02	1.92E-02	*EGR1/BMP4/SERPINB7*	3
GO:0090192	regulation of glomerulus development	0.014354	0.000805477	5.66E-04	2.48E-02	2.22E-02	*EGR1/BMP4/SERPINB7*	3
GO:1900424	regulation of defense response to bacterium	0.014354	0.000805477	5.66E-04	2.48E-02	2.22E-02	*SPINK5/KLK5/KLK7*	3
GO:0030889	negative regulation of B cell proliferation	0.014354	0.000920545	8.55E-04	3.21E-02	2.87E-02	*MNDA/INPP5D/PRDM1*	3
GO:0097709	connective tissue replacement	0.014354	0.001035614	1.22E-03	3.99E-02	3.57E-02	*IL1A/AGER/TGFB1*	3

GO:0072111	cell proliferation involved in kidney development	0.014354	0.001150682	1.68E-03	4.76E-02	4.26E-02	*EGR1/BMP4/SERPINB7*	3

Table S4: Molecular functions enriched at baseline between “Cold” and “No Cold” groups

ID	Description	GeneRatio	BgRatio	*P*value	*P*.adjust	qvalue	geneID	Count
GO:0017171	serine hydrolase activity	0.0591133	0.015961738	1.06E-04	7.29E-03	6.50E-03	*TMPRSS11B/TMPRSS11E/RELN/CTSV/PRSS27/KLK5/KLK6/KLK7/KLK8/KLK12/KLK13/MMP9*	12
GO:0008236	serine-type peptidase activity	0.0591133	0.01567362	8.93E-05	7.29E-03	6.50E-03	*TMPRSS11B/TMPRSS11E/RELN/CTSV/PRSS27/KLK5/KLK6/KLK7/KLK8/KLK12/KLK13/MMP9*	12
GO:0004252	serine-type endopeptidase activity	0.054187192	0.014060159	1.45E-04	8.28E-03	7.38E-03	*TMPRSS11B/TMPRSS11E/CTSV/PRSS27/KLK5/KLK6/KLK7/KLK8/KLK12/KLK13/MMP9*	11
GO:0061134	peptidase regulator activity	0.054187192	0.012561945	5.33E-05	7.29E-03	6.50E-03	*NLRC4/MAL/SPINK5/SPINK6/SPINK7/PI15/CST6/A2ML1/NLRP1/SERPINB7/CST1*	11
GO:0030414	peptidase inhibitor activity	0.044334975	0.010487496	2.97E-04	1.36E-02	1.21E-02	*NLRC4/SPINK5/SPINK6/SPINK7/PI15/CST6/A2ML1/SERPINB7/CST1*	9
GO:0019955	cytokine binding	0.039408867	0.005819984	2.43E-05	5.01E-03	4.47E-03	*CSF3R/IL1R2/IL1RL1/CXCR2/CXCR1/CCR3/ZFP36/IL2RG*	8
GO:0004896	cytokine receptor activity	0.039408867	0.005243748	1.13E-05	4.66E-03	4.15E-03	*CSF3R/IL1R2/IL1RL1/CXCR2/CXCR1/CCR3/IL17RA/IL2RG*	8
GO:0070851	growth factor receptor binding	0.034482759	0.007606316	9.29E-04	3.15E-02	2.81E-02	*ECM1/IL1A/IL36G/EREG/HBEGF/AGR2/ITGA5*	7
GO:0005154	epidermal growth factor receptor binding	0.019704433	0.001901579	5.70E-04	2.14E-02	1.90E-02	*EREG/HBEGF/AGR2/ITGA5*	4
GO:0019956	chemokine binding	0.019704433	0.001382966	1.61E-04	8.28E-03	7.38E-03	*CXCR2/CXCR1/CCR3/ZFP36*	4
GO:0001848	complement binding	0.019704433	0.001210096	9.31E-05	7.29E-03	6.50E-03	*CR1/C5AR1/CD93/ITGB2*	4
GO:0001846	opsonin binding	0.014778325	0.00080673	5.22E-04	2.14E-02	1.90E-02	*CR1/CD93/ITGB2*	3
GO:0004175	endopeptidase activity	0.068965517	0.02702547	1.28E-03	3.52E-02	3.14E-02	*CLCA4/ASPRV1/MME/TMPRSS11B/TMPRSS11E/CTSV/PRSS27/KLK5/KLK6/KLK7/KLK8/KLK12/KLK13/MMP9*	14
GO:0061135	endopeptidase regulator activity	0.039408867	0.010314625	1.24E-03	3.52E-02	3.14E-02	*NLRC4/SPINK5/SPINK6/SPINK7/CST6/A2ML1/SERPINB7/CST1*	8
GO:0004866	endopeptidase inhibitor activity	0.039408867	0.009968883	9.95E-04	3.15E-02	2.81E-02	*NLRC4/SPINK5/SPINK6/SPINK7/CST6/A2ML1/SERPINB7/CST1*	8

Table S5: Day 0 cytokine levels in infected and uninfected volunteers

Mediator (log_{10} pg/ml)	**Cold** (n=23, unless otherwise stated) Median	**No Cold** (n=25, unless otherwise stated) Median	*P*-value
IFN-α	0.046	0.046	0.176
IFN-β	1.866	0.856	0.617
IFN-γ	0	0	0.314
IL-1β	1.193	0.870	0.086
IL-6	0.991	0.659	0.103
IL-8	3.170	2.923	0.356
IL-10	0.803	0.803	0.068
IL-15	0.419	0.329	0.391
IL-17A	0.609	0.144	0.039*
CXCL10 (IP-10)	1.991	1.715	0.054
LCN-2	6.704 (n=10)	5.875 (n=9)	0.017*
MIP-1α	0.903	0.732	0.192
MPO	6.758 (n=10)	5.861 (n=9)	0.010*
CCL5 (RANTES)	0.254	0.369	0.665
TNF-α	0	0	0.692

Table S5: Day 0 cytokine levels in infected and uninfected volunteers Day 0 mediator levels in the upper respiratory tract were determined in participants who subsequently developed symptomatic RSV infection (Cold, n=23) and those that did not (No Cold, n=25). Statistical analyses used two-tailed Mann Whitney *U* tests; *$P<0.05$.

Table S6: DEGs between day 3 and day 0 in the "No Cold" group (*P*-value<0.01, LFC>0.5)

	GeneName	baseMean	log^2Fold Change	lfcSE	stat	*P*value	Padj
ENSG00000268173	*AC007192.4*	34.09618	10.71285	1.946479	5.503707	3.72E-08	0.000546
ENSG00000163734	*CXCL3*	149.3781	1.440807	0.321685	4.478942	7.50E-06	0.055023
ENSG00000081041	*CXCL2*	174.802	1.436306	0.349674	4.107556	4.00E-05	0.195535
ENSG00000177606	*JUN*	1314.332	0.725754	0.189651	3.826781	0.00013	0.274872
ENSG00000163739	*CXCL1*	1567.606	1.058814	0.272342	3.887809	0.000101	0.274872
ENSG00000159231	*CBR3*	89.53077	-0.80421	0.21029	-3.82427	0.000131	0.274872
ENSG00000140519	*RHCG*	205.5315	2.384514	0.629577	3.787487	0.000152	0.279058
ENSG00000143536	*CRNN*	332.3173	2.42925	0.700976	3.465527	0.000529	0.644422
ENSG00000137331	*IER3*	1131.598	0.773632	0.225847	3.425471	0.000614	0.644422
ENSG00000123119	*NECAB1*	17.4312	1.396028	0.40761	3.424915	0.000615	0.644422
ENSG00000196993	*NPIPB9*	90.3268	-0.60766	0.177412	-3.42512	0.000615	0.644422
ENSG00000169203	*RP11-231C14.4*	249.1964	-0.64802	0.187268	-3.46041	0.000539	0.644422
ENSG00000280893	*AC009133.23*	9.701738	-2.5609	0.758312	-3.3771	0.000733	0.691727
ENSG00000067082	*KLF6*	1426.194	0.520046	0.157306	3.305947	0.000947	0.694302
ENSG00000186474	*KLK12*	25.34081	1.839293	0.551663	3.334085	0.000856	0.694302
ENSG00000113070	*HBEGF*	259.5387	1.320102	0.402212	3.282104	0.00103	0.719647
ENSG00000091128	*LAMB4*	79.02638	1.205408	0.370164	3.256417	0.001128	0.719647
ENSG00000132932	*ATP8A2*	24.55841	0.602019	0.184236	3.267642	0.001084	0.719647
ENSG00000139318	*DUSP6*	775.636	0.686782	0.215349	3.189164	0.001427	0.807516
ENSG00000203852	*HIST2H3A*	311.1639	1.57602	0.502519	3.136242	0.001711	0.838019
ENSG00000165794	*SLC39A2*	27.49601	1.602373	0.51099	3.135821	0.001714	0.838019
ENSG00000154734	*ADAMTS1*	34.50457	1.779	0.565144	3.147873	0.001645	0.838019
ENSG00000183336	*BOLA2*	5.369005	-9.99524	3.22335	-3.10089	0.001929	0.913049
ENSG00000121742	*GJB6*	75.14953	1.351585	0.437849	3.086874	0.002023	0.923257
ENSG00000265590	*AP000275.65*	33.19193	-1.87079	0.607592	-3.07902	0.002077	0.923257
ENSG00000169509	*CRCT1*	43.10019	2.246315	0.786001	2.857904	0.004264	0.971488
ENSG00000090104	*RGS1*	260.8477	0.758897	0.261628	2.900676	0.003724	0.971488
ENSG00000263961	*C1orf186*	9.726597	1.104421	0.381009	2.898677	0.003747	0.971488
ENSG00000143878	*RHOB*	1806.952	0.509216	0.179492	2.83699	0.004554	0.971488
ENSG00000115602	*IL1RL1*	51.0304	1.606061	0.559536	2.870347	0.0041	0.971488
ENSG00000185873	*TMPRSS11B*	126.1337	2.320712	0.77744	2.98507	0.002835	0.971488
ENSG00000124875	*CXCL6*	692.2134	0.849458	0.286733	2.962539	0.003051	0.971488
ENSG00000145879	*SPINK7*	90.93384	2.305832	0.75561	3.051617	0.002276	0.971488
ENSG00000112394	*SLC16A10*	25.4085	1.106001	0.3716	2.976325	0.002917	0.971488
ENSG00000155918	*RAET1L*	74.83194	1.296183	0.451471	2.871022	0.004091	0.971488
ENSG00000197181	*PIWIL2*	16.37803	0.889869	0.298332	2.982817	0.002856	0.971488
ENSG00000104368	*PLAT*	1629.246	1.266039	0.433067	2.923424	0.003462	0.971488
ENSG00000111215	*PRR4*	92.77336	-0.82179	0.277502	-2.96137	0.003063	0.971488
ENSG00000018236	*CNTN1*	68.40497	0.892821	0.307411	2.904322	0.00368	0.971488
ENSG00000279777	*AC004813.1*	52.62626	-0.60351	0.20639	-2.92413	0.003454	0.971488
ENSG00000128965	*CHAC1*	76.63318	0.803606	0.281341	2.856341	0.004286	0.971488

ENSG00000185864	*NPIPB4*	335.7528	-0.52362	0.177264	-2.95391	0.003138	0.971488
ENSG00000171401	*KRT13*	3674.625	1.533781	0.527322	2.908621	0.00363	0.971488
ENSG00000175906	*ARL4D*	476.1744	0.578185	0.203438	2.842066	0.004482	0.971488
ENSG00000269404	*SPIB*	27.53031	0.814364	0.278475	2.924367	0.003452	0.971488
ENSG00000169035	*KLK7*	193.8601	1.85068	0.640657	2.888722	0.003868	0.971488
ENSG00000129455	*KLK8*	26.1473	2.13996	0.750293	2.852164	0.004342	0.971488
ENSG00000088882	*CPXM1*	53.04393	0.761404	0.266631	2.855645	0.004295	0.971488
ENSG00000156282	*CLDN17*	19.61386	2.754695	0.950417	2.898406	0.003751	0.971488
ENSG00000128342	*LIF*	164.0332	0.589717	0.206526	2.855406	0.004298	0.971488
ENSG00000163751	*CPA3*	103.1778	1.764197	0.637979	2.765291	0.005687	0.990244
ENSG00000188818	*ZDHHC11*	88.32456	-0.54877	0.198388	-2.76616	0.005672	0.990244
ENSG00000136943	*CTSV*	147.4117	0.920501	0.328398	2.803004	0.005063	0.990244
ENSG00000188070	*C11orf95*	136.192	0.50528	0.181364	2.785993	0.005336	0.990244
ENSG00000170426	*SDR9C7*	8.854919	2.309243	0.821713	2.81028	0.00495	0.990244
ENSG00000166211	*SPIC*	20.23969	0.594662	0.215019	2.765632	0.005681	0.990244
ENSG00000165799	*RNASE7*	49.36023	1.409505	0.504665	2.792952	0.005223	0.990244
ENSG00000197253	*TPSB2*	75.30485	1.871105	0.675495	2.769975	0.005606	0.990244
ENSG00000198156	*NPIPB6*	98.34868	-0.54924	0.198827	-2.76241	0.005738	0.990244
ENSG00000269711	*CTD-3214H19.16*	10.41424	10.46232	3.708287	2.821336	0.004782	0.990244
ENSG00000105427	*CNFN*	181.4197	1.277771	0.454088	2.813927	0.004894	0.990244
ENSG00000022556	*NLRP2*	93.76168	1.077863	0.386322	2.790064	0.00527	0.990244
ENSG00000142619	*PADI3*	97.15799	0.547472	0.20942	2.614223	0.008943	1
ENSG00000143556	*S100A7*	630.9285	1.955151	0.744234	2.627063	0.008613	1
ENSG00000196754	*S100A2*	4500.136	1.346063	0.492669	2.732187	0.006292	1
ENSG00000179914	*ITLN1*	48.25683	-1.69569	0.651444	-2.60297	0.009242	1
ENSG00000135919	*SERPINE2*	144.2735	1.144279	0.440156	2.599711	0.00933	1
ENSG00000132465	*JCHAIN*	62.01675	0.908242	0.345234	2.630798	0.008518	1
ENSG00000118785	*SPP1*	24.56759	1.089926	0.412914	2.639595	0.008301	1
ENSG00000120738	*EGR1*	360.8778	1.082594	0.406853	2.660894	0.007793	1
ENSG00000254245	*PCDHGA3*	16.88847	-0.81997	0.308613	-2.65694	0.007885	1
ENSG00000253159	*PCDHGA12*	23.25894	-0.70802	0.257928	-2.74503	0.006051	1
ENSG00000133710	*SPINK5*	1205.992	0.789563	0.296293	2.664807	0.007703	1
ENSG00000120149	*MSX2*	27.93288	0.635925	0.244592	2.599942	0.009324	1
ENSG00000276180	*HIST1H4I*	123.343	0.605086	0.230213	2.62837	0.00858	1
ENSG00000170667	*RASA4B*	32.38069	-0.65927	0.252296	-2.61307	0.008973	1
ENSG00000164604	*GPR85*	21.83782	0.745677	0.286781	2.600157	0.009318	1
ENSG00000107984	*DKK1*	176.808	0.807979	0.297051	2.720003	0.006528	1
ENSG00000117983	*MUC5B*	72.21829	-1.39958	0.515548	-2.71474	0.006633	1
ENSG00000175518	*UBQLNL*	18.33565	-0.77311	0.288423	-2.68046	0.007352	1
ENSG00000165474	*GJB2*	526.7655	0.911625	0.347925	2.620178	0.008788	1
ENSG00000134901	*KDELC1*	36.77971	0.505743	0.196205	2.577628	0.009948	1
ENSG00000249240	*AC069368.3*	5.588089	-1.7672	0.665496	-2.65546	0.00792	1
ENSG00000188508	*KRTDAP*	20.60571	2.121478	0.781522	2.714549	0.006637	1
ENSG00000102313	*ITIH6*	35.36962	-0.71756	0.263563	-2.72252	0.006479	1

ENSG00000268089	*GABRQ*	21.23443	1.933114	0.706636	2.73566	0.006226	1
ENSG00000198763	*MT-ND2*	2776.095	-0.57408	0.215711	-2.66133	0.007783	1

Table S7: DEGs between day 3 and day 0 in the "Cold" group (*P-v*alue<0.01, LFC>0.5)

	GeneName	baseMean	log^2Fold Change	lfcSE	stat	*P*value	*P*adj
ENSG00000125378	*BMP4*	22.04009	1.543324	0.297741	5.183448	2.18E-07	0.003195
ENSG00000132326	*PER2*	1311.424	-0.66742	0.14176	-4.70814	2.50E-06	0.018336
ENSG00000140006	*WDR89*	150.7693	0.632335	0.15182	4.165032	3.11E-05	0.114173
ENSG00000184313	*MROH7*	105.3837	-0.78921	0.204508	-3.85906	0.000114	0.271157
ENSG00000129757	*CDKN1C*	101.3036	0.671943	0.17645	3.80812	0.00014	0.271157
ENSG00000173451	*THAP2*	76.44963	0.624654	0.165438	3.775758	0.00016	0.271157
ENSG00000277117	*ICOSLG*	38.58432	1.309042	0.340901	3.839948	0.000123	0.271157
ENSG00000127129	*EDN2*	292.3299	2.41171	0.668713	3.606497	0.00031	0.281593
ENSG00000135045	*C9orf40*	111.4209	0.591656	0.163835	3.611298	0.000305	0.281593
ENSG00000153485	*TMEM251*	175.3835	0.621159	0.172678	3.597203	0.000322	0.281593
ENSG00000206172	*HBA1*	21.72477	-3.39372	0.944417	-3.59346	0.000326	0.281593
ENSG00000204172	*AGAP9*	156.9233	-0.68697	0.193771	-3.54528	0.000392	0.287681
ENSG00000198929	*NOS1AP*	147.7733	-0.72025	0.209007	-3.44607	0.000569	0.31136
ENSG00000118508	*RAB32*	180.2051	0.58683	0.17011	3.449702	0.000561	0.31136
ENSG00000196859	*KRT39*	38.21066	0.952273	0.274481	3.469356	0.000522	0.31136
ENSG00000152284	*TCF7L1*	33.26154	-0.7667	0.230403	-3.32767	0.000876	0.3195
ENSG00000240583	*AQP1*	61.98687	-1.05708	0.322695	-3.2758	0.001054	0.3195
ENSG00000175164	*ABO*	228.5686	-0.58983	0.178901	-3.29698	0.000977	0.3195
ENSG00000006327	*TNFRSF12A*	480.2161	0.932948	0.2811	3.318923	0.000904	0.3195
ENSG00000172000	*ZNF556*	17.04258	0.87804	0.266582	3.293689	0.000989	0.3195
ENSG00000198342	*ZNF442*	63.13852	0.754397	0.227406	3.317401	0.000909	0.3195
ENSG00000225828	*FAM229A*	41.86062	-0.5085	0.156767	-3.24367	0.00118	0.320019
ENSG00000185880	*TRIM69*	1353.204	0.629862	0.194459	3.239051	0.001199	0.320019
ENSG00000132881	*RSG1*	106.1672	0.534104	0.167607	3.186653	0.001439	0.338339
ENSG00000221886	*ZBED8*	178.3149	0.656915	0.206286	3.184482	0.00145	0.338339
ENSG00000163359	*COL6A3*	109.9409	-1.36855	0.436338	-3.13645	0.00171	0.349108
ENSG00000122641	*INHBA*	71.23154	1.845157	0.586767	3.144618	0.001663	0.349108
ENSG00000129474	*AJUBA*	371.5591	0.690348	0.222181	3.107139	0.001889	0.355797
ENSG00000188290	*HES4*	312.5322	0.669324	0.224127	2.986357	0.002823	0.360848
ENSG00000179914	*ITLN1*	71.80596	1.857605	0.620404	2.994186	0.002752	0.360848
ENSG00000164404	*GDF9*	21.44236	0.717419	0.240885	2.97826	0.002899	0.360848
ENSG00000036448	*MYOM2*	36.698	0.731788	0.245223	2.984168	0.002844	0.360848
ENSG00000123411	*IKZF4*	100.528	-0.51143	0.171315	-2.98534	0.002833	0.360848
ENSG00000132481	*TRIM47*	188.1067	0.510921	0.172017	2.970178	0.002976	0.360848
ENSG00000187187	*ZNF546*	84.94763	0.720698	0.233248	3.089832	0.002003	0.360848
ENSG00000159885	*ZNF222*	88.79954	0.594934	0.200539	2.966677	0.00301	0.360848
ENSG00000261221	*ZNF865*	88.98932	-0.55707	0.187852	-2.96546	0.003022	0.360848
ENSG00000132801	*ZSWIM3*	109.449	0.520946	0.174892	2.978677	0.002895	0.360848
ENSG00000177854	*TMEM187*	153.3936	0.525238	0.17367	3.024343	0.002492	0.360848
ENSG00000278705	*HIST1H4B*	594.7796	0.677645	0.231015	2.933342	0.003353	0.369876
ENSG00000203724	*C1orf53*	43.69044	0.605087	0.208161	2.906826	0.003651	0.374903

ENSG00000232040	*ZBED9*	37.2166	0.83489	0.285474	2.924569	0.003449	0.374903
ENSG00000104267	*CA2*	209.3763	0.919822	0.315283	2.917449	0.003529	0.374903
ENSG00000122254	*HS3ST2*	22.89722	1.033907	0.354774	2.914269	0.003565	0.374903
ENSG00000177606	*JUN*	1569.743	0.662493	0.234252	2.828126	0.004682	0.384771
ENSG00000164082	*GRM2*	20.58784	-0.7129	0.250317	-2.84799	0.0044	0.384771
ENSG00000163536	*SERPINI1*	52.52468	0.54397	0.196048	2.774681	0.005526	0.384771
ENSG00000019991	*HGF*	57.15752	0.646882	0.228819	2.827044	0.004698	0.384771
ENSG00000090266	*NDUFB2*	674.9224	0.514751	0.180961	2.844548	0.004447	0.384771
ENSG00000255823	*MTRNR2L8*	88.69851	0.80221	0.284671	2.818019	0.004832	0.384771
ENSG00000135094	*SDS*	374.6442	0.833066	0.295145	2.82257	0.004764	0.384771
ENSG00000175985	*PLEKHD1*	84.74293	-0.67052	0.240603	-2.78682	0.005323	0.384771
ENSG00000108821	*COL1A1*	144.2349	-0.83705	0.296719	-2.82103	0.004787	0.384771
ENSG00000261857	*MIA*	203.7857	0.827884	0.292163	2.833632	0.004602	0.384771
ENSG00000142530	*FAM71E1*	19.35397	0.555792	0.197434	2.815074	0.004877	0.384771
ENSG00000170775	*GPR37*	104.9986	0.566107	0.206773	2.737821	0.006185	0.389828
ENSG00000197019	*SERTAD1*	621.5665	0.515149	0.188775	2.728909	0.006354	0.391678
ENSG00000078401	*EDN1*	78.41643	1.222486	0.448687	2.724583	0.006438	0.392048
ENSG00000040608	*RTN4R*	19.66314	0.599538	0.220824	2.715001	0.006628	0.392048
ENSG00000113209	*PCDHB5*	15.93101	0.681644	0.252213	2.702646	0.006879	0.393004
ENSG00000196345	*ZKSCAN7*	91.34475	0.52829	0.195666	2.699956	0.006935	0.393055
ENSG00000165917	*RAPSN*	21.05145	-0.63449	0.236171	-2.68658	0.007219	0.400593
ENSG00000145632	*PLK2*	1570.018	0.505878	0.18918	2.67406	0.007494	0.401224
ENSG00000198939	*ZFP2*	25.53408	0.761238	0.284628	2.674505	0.007484	0.401224
ENSG00000186480	*INSIG1*	1680.1	0.590828	0.220892	2.674736	0.007479	0.401224
ENSG00000198670	*LPA*	68.50585	-0.60768	0.227745	-2.66823	0.007625	0.40529
ENSG00000214756	*METTL12*	90.15136	0.507306	0.190443	2.663816	0.007726	0.407007
ENSG00000149243	*KLHL35*	30.62397	0.540832	0.203969	2.651538	0.008013	0.407759
ENSG00000239282	*GATSL3*	163.1875	0.518584	0.195348	2.65467	0.007939	0.407759
ENSG00000088538	*DOCK3*	53.29586	-0.54609	0.207448	-2.6324	0.008478	0.414453
ENSG00000241360	*PDXP*	67.81247	0.52209	0.19822	2.633894	0.008441	0.414453
ENSG00000242866	*STRC*	49.76977	-0.67549	0.257248	-2.62583	0.008644	0.418498
ENSG00000162772	*ATF3*	603.2502	0.697791	0.268797	2.595975	0.009432	0.420723
ENSG00000187094	*CCK*	60.47584	0.800681	0.309839	2.584187	0.009761	0.420723
ENSG00000198785	*GRIN3A*	14.96359	1.201367	0.460333	2.60978	0.00906	0.420723
ENSG00000187720	*THSD4*	175.5152	-0.56348	0.218724	-2.57622	0.009989	0.420723
ENSG00000280006	*AC009060.2*	90.4094	-0.81421	0.315713	-2.57896	0.00991	0.420723

Table S8: Biological Processes Enriched in “Cold” group (d0 vs d3)

ID	Description	Gene Ratio	BgRatio	*P*value	*P*.adjust	Qvalue	geneID	Count
GO:0044057	Regulation of system process	0.148	0.0295106	6.99E-05	2.16E-02	1.75E-02	*EDN2/NOS1AP/PER2/CCK/GDF9/EDN1/AQP1/INHBA/HGF*	9
GO:0010035	Response to inorganic substance	0.131	0.0272913	2.40E-04	3.67E-02	2.97E-02	*JUN/EDN1/AQP1/HGF/GPR37/CA2/HBA1/COL1A1*	8
GO:0042326	Negative regulation of phosphorylation	0.131	0.0248321	1.26E-04	3.33E-02	2.69E-02	*JUN/ATF3/INHBA/HGF/CDKN1C/AJUBA/BMP4/RTN4R*	8
GO:0015711	Organic anion transport	0.115	0.0190139	1.52E-04	3.53E-02	2.85E-02	*PER2/CCK/GRM2/EDN1/AQP1/CA2/HBA1*	7
GO:0000302	Response to reactive oxygen species	0.115	0.0122961	9.54E-06	5.89E-03	4.76E-03	*JUN/EDN1/AQP1/HGF/GPR37/HBA1/COL1A1*	7
GO:0042542	Response to hydrogen peroxide	0.098	0.0071377	4.70E-06	4.35E-03	3.52E-03	*JUN/AQP1/HGF/GPR37/HBA1/COL1A1*	6
GO:0042476	Odontogenesis	0.098	0.0068378	3.66E-06	4.35E-03	3.52E-03	*EDN1/AQP1/INHBA/CA2/BMP4/COL1A1*	6
GO:2001236	Regulation of extrinsic signalling pathway	0.082	0.009237	2.47E-04	3.67E-02	2.97E-02	*ATF3/INHBA/HGF/BMP4/TNFRSF12A*	5
GO:0044070	Regulation of anion transport	0.066	0.0050384	2.51E-04	3.67E-02	2.97E-02	*PER2/CCK/EDN1/CA2*	4
GO:0050886	Endocrine process	0.066	0.0046785	1.89E-04	3.67E-02	2.97E-02	*EDN2/GDF9/EDN1/INHBA*	4
GO:0060395	SMAD protein signal transduction	0.066	0.0034789	5.94E-05	2.16E-02	1.75E-02	*JUN/GDF9/INHBA/BMP4*	4
GO:0015669	Gas transport	0.049	0.0011396	4.33E-05	2.01E-02	1.62E-02	*AQP1/CA2/HBA1*	3

Table S9: Biological Processes Enriched in “No Cold” group (d0 vs d3)

ID	Description	Gene Ratio	BgRatio	*P*value	*P*.adjust	Qvalue	geneID	Count
GO:0008544	Epidermis development	0.116	0.017694	2.87E-05	5.48E-03	4.73E-03	*CRCT1/S100A7/SPINK5/MSX2/CTSV/DKK1/CNFN/KLK7*	8
GO:0043588	Skin development	0.116	0.014335	6.24E-06	2.09E-03	1.80E-03	*CRCT1/S100A7/SPINK5/MSX2/CTSV/DKK1/ATP8A2/CNFN*	8
GO:0042742	Defense response to bacterium	0.101	0.015055	7.86E-05	8.76E-03	7.57E-03	*S100A7/JCHAIN/CXCL6/SPINK5/MUC5B/RNASE7/KLK7*	7
GO:0002687	Positive regulation of leukocyte migration	0.072	0.006358	7.69E-05	8.76E-03	7.57E-03	*S100A7/CXCL6/CXCL1/CXCL3/CXCL2*	5
GO:0002688	Regulation of leukocyte chemotaxis	0.072	0.005638	4.33E-05	6.77E-03	5.85E-03	*S100A7/CXCL6/CXCL1/CXCL3/CXCL2*	5
GO:0002690	Positive regulation of leukocyte chemotaxis	0.072	0.004679	1.75E-05	3.90E-03	3.37E-03	*S100A7/CXCL6/CXCL1/CXCL3/CXCL2*	5
GO:0019730	Antimicrobial humoral response	0.058	0.003239	7.27E-05	8.76E-03	7.57E-03	*JCHAIN/SPINK5/RNASE7/KLK7*	4
GO:0019731	Antibacterial humoral response	0.058	0.002879	4.56E-05	6.77E-03	5.85E-03	*JCHAIN/SPINK5/RNASE7/KLK7*	4
GO:0071622	Regulation of granulocyte chemotaxis	0.058	0.002219	1.60E-05	3.90E-03	3.37E-03	*S100A7/CXCL1/CXCL3/CXCL2*	4
GO:0001893	Maternal placenta development	0.058	0.001739	5.90E-06	2.09E-03	1.80E-03	*SPP1/CTSV/GJB2/LIF*	4
GO:0071624	Positive regulation of granulocyte chemotaxis	0.058	0.0015	3.18E-06	2.09E-03	1.80E-03	*S100A7/CXCL1/CXCL3/CXCL2*	4
GO:0046697	Decidualization	0.058	0.00114	9.94E-07	1.33E-03	1.15E-03	*SPP1/CTSV/GJB2/LIF*	4

Table S10: Molecular Functions Enriched in “No Cold” group (d0 vs d3)

ID	Description	GeneRatio	BgRatio	*P*value	*P*.adjust	qvalue	geneID	Count
GO:0030545	receptor regulator activity	0.114	0.027947	7.26E-04	1.11E-02	9.74E-03	*CXCL6/CXCL1/CXCL3/CXCL2/SPP1/HBEGF/DKK1/LIF*	8
GO:0004175	endopeptidase activity	0.114	0.027025	5.83E-04	9.80E-03	8.58E-03	*TMPRSS11B/PLAT/CTSV/TPSB2/KLK7/KLK8/KLK12/ADAMTS1*	8
GO:0048018	receptor ligand activity	0.114	0.026276	4.84E-04	9.80E-03	8.58E-03	*CXCL6/CXCL1/CXCL3/CXCL2/SPP1/HBEGF/DKK1/LIF*	8
GO:0017171	serine hydrolase activity	0.100	0.015962	1.24E-04	3.81E-03	3.34E-03	*TMPRSS11B/PLAT/CTSV/TPSB2/KLK7/KLK8/KLK12*	7
GO:0008236	serine-type peptidase activity	0.100	0.015674	1.11E-04	3.81E-03	3.34E-03	*TMPRSS11B/PLAT/CTSV/TPSB2/KLK7/KLK8/KLK12*	7
GO:0004252	serine-type endopeptidase activity	0.100	0.01406	5.62E-05	3.45E-03	3.02E-03	*TMPRSS11B/PLAT/CTSV/TPSB2/KLK7/KLK8/KLK12*	7
GO:0005125	cytokine activity	0.086	0.012677	2.59E-04	5.95E-03	5.21E-03	*CXCL6/CXCL1/CXCL3/CXCL2/SPP1/LIF*	6
GO:0005539	glycosaminoglycan binding	0.086	0.012274	2.17E-04	5.71E-03	5.00E-03	*SERPINE2/JCHAIN/CXCL6/HBEGF/RNASE7/ADAMTS1*	6
GO:0004867	serine-type endopeptidase inhibitor activity	0.057	0.005474	5.86E-04	9.80E-03	8.58E-03	*SERPINE2/SPINK5/SPINK7/ITIH6*	4
GO:0042379	chemokine receptor binding	0.057	0.003457	9.98E-05	3.81E-03	3.34E-03	*CXCL6/CXCL1/CXCL3/CXCL2*	4
GO:0008009	chemokine activity	0.057	0.002766	4.13E-05	3.45E-03	3.02E-03	*CXCL6/CXCL1/CXCL3/CXCL2*	4
GO:0045236	CXCR chemokine receptor binding	0.057	0.000922	4.26E-07	7.84E-05	6.86E-05	*CXCL6/CXCL1/CXCL3/CXCL2*	4
GO:0042834	peptidoglycan binding	0.029	0.000807	1.41E-03	2.00E-02	1.75E-02	*JCHAIN/RNASE7*	2

Table S11: KEGG Pathways Enriched in “No Cold” group (d0 vs d3)

ID	Description	GeneRatio	BgRatio	*P*value	*P*.adjust	qvalue	geneSymbol	Count
hsa04657	IL-17 signaling pathway	0.226	0.012515	7.88E-08	7.25E-06	6.14E-06	*JUN/S100A7/CXCL6/CXCL1/CXCL3/CXCL2/MUC5B*	7
hsa04060	Cytokine-cytokine receptor interaction	0.194	0.039564	1.16E-03	2.67E-02	2.26E-02	*IL1RL1/CXCL6/CXCL1/CXCL3/CXCL2/LIF*	6
hsa04668	TNF signaling pathway	0.161	0.014803	8.11E-05	3.73E-03	3.16E-03	*JUN/CXCL1/CXCL3/CXCL2/LIF*	5
hsa05132	Salmonella infection	0.129	0.011573	4.15E-04	1.27E-02	1.08E-02	*JUN/CXCL1/CXCL3/CXCL2*	4
hsa05120	Epithelial cell signaling in Helicobacter pylori infection	0.097	0.009151	2.74E-03	4.21E-02	3.56E-02	*JUN/CXCL1/HBEGF*	3
hsa05134	Legionellosis	0.097	0.007401	1.49E-03	2.74E-02	2.32E-02	*CXCL1/CXCL3/CXCL2*	3

Table S12: Molecular Functions enriched in the WGCNA "Brown" module

ID	Description	GeneRatio	BgRatio	*P*value	*P*.adjust	qvalue	geneID	Count
GO:0004175	endopeptidase activity	0.29	0.027025	4.25E-04	3.72E-03	2.80E-03	*TMPRSS11B/KLK7/KLK8/KLK12*	4
GO:0017171	serine hydrolase activity	0.29	0.015962	5.60E-05	6.54E-04	4.92E-04	*TMPRSS11B/KLK7/KLK8/KLK12*	4
GO:0008236	serine-type peptidase activity	0.29	0.015674	5.22E-05	6.54E-04	4.92E-04	*TMPRSS11B/KLK7/KLK8/KLK12*	4
GO:0004252	serine-type endopeptidase activity	0.29	0.01406	3.42E-05	6.54E-04	4.92E-04	*TMPRSS11B/KLK7/KLK8/KLK12*	4

Table S13: Molecular Functions enriched in the WGCNA "Turquoise" module

ID	Description	GeneRatio	BgRatio	*P*value	*P*.adjust	qvalue	geneID	Count
GO:1901681	sulfur compound binding	0.15	0.0133687	2.27E-03	2.36E-02	1.64E-02	*SERPINE2/HBEGF/ADAMTS1*	3
GO:0061134	peptidase regulator activity	0.15	0.0125619	1.90E-03	2.26E-02	1.57E-02	*SERPINE2/SPINK5/ITIH6*	3
GO:0005539	glycosaminoglycan binding	0.15	0.0122738	1.78E-03	2.26E-02	1.57E-02	*SERPINE2/HBEGF/ADAMTS1*	3
GO:0030414	peptidase inhibitor activity	0.15	0.0104875	1.13E-03	1.88E-02	1.31E-02	*SERPINE2/SPINK5/ITIH6*	3
GO:0061135	endopeptidase regulator activity	0.15	0.0103146	1.08E-03	1.88E-02	1.31E-02	*SERPINE2/SPINK5/ITIH6*	3
GO:0004866	endopeptidase inhibitor activity	0.15	0.0099689	9.80E-04	1.88E-02	1.31E-02	*SERPINE2/SPINK5/ITIH6*	3
GO:0008201	heparin binding	0.15	0.0092198	7.81E-04	1.88E-02	1.31E-02	*SERPINE2/HBEGF/ADAMTS1*	3
GO:0004867	serine-type endopeptidase inhibitor activity	0.15	0.0054742	1.69E-04	1.41E-02	9.80E-03	*SERPINE2/SPINK5/ITIH6*	3

Table S14: Molecular Functions enriched in the WGCNA “Blue” module

ID	Description	GeneRatio	BgRatio	*P*value	*P*.adjust	qvalue	geneID	Count
GO:0030545	receptor regulator activity	0.43	0.027947	1.15E-06	1.17E-05	4.63E-06	*CXCL6/CXCL1/CXCL3/CXCL2/SPP1/LIF*	6
GO:0048018	receptor ligand activity	0.43	0.026276	8.00E-07	9.76E-06	3.87E-06	*CXCL6/CXCL1/CXCL3/CXCL2/SPP1/LIF*	6
GO:0005125	cytokine activity	0.43	0.012677	1.07E-08	3.26E-07	1.30E-07	*CXCL6/CXCL1/CXCL3/CXCL2/SPP1/LIF*	6
GO:0005126	cytokine receptor binding	0.36	0.015443	1.51E-06	1.32E-05	5.23E-06	*CXCL6/CXCL1/CXCL3/CXCL2/LIF*	5
GO:0001228	transcriptional activator activity, RNA polymerase II transcription regulatory region	0.29	0.023683	2.57E-04	1.74E-03	6.91E-04	*JUN/EGR1/KLF6/SPIB*	4
GO:0001664	G-protein coupled receptor binding	0.29	0.015097	4.51E-05	3.44E-04	1.37E-04	*CXCL6/CXCL1/CXCL3/CXCL2*	4
GO:0042379	chemokine receptor binding	0.29	0.003457	1.26E-07	1.92E-06	7.62E-07	*CXCL6/CXCL1/CXCL3/CXCL2*	4
GO:0008009	chemokine activity	0.29	0.002766	5.05E-08	1.03E-06	4.08E-07	*CXCL6/CXCL1/CXCL3/CXCL2*	4
GO:0045236	CXCR chemokine receptor binding	0.29	0.000922	4.80E-10	2.93E-08	1.16E-08	*CXCL6/CXCL1/CXCL3/CXCL2*	4
GO:0000982	transcriptional activator activity, RNA polymerase II core promoter proximal region sequence	0.21	0.023049	3.66E-03	1.49E-02	5.91E-03	*JUN/EGR1/KLF6*	3
GO:0001158	enhancer sequence-specific DNA binding	0.14	0.005301	2.43E-03	1.23E-02	4.90E-03	*JUN/SPIB*	2
GO:0000980	RNA polymerase II distal enhancer sequence-specific DNA binding	0.14	0.004149	1.50E-03	8.29E-03	3.29E-03	*JUN/SPIB*	2
GO:0070412	R-SMAD binding	0.07	0.001325	1.84E-02	4.68E-02	1.86E-02	*JUN*	1
GO:0001965	G-protein alpha-subunit binding	0.07	0.001095	1.52E-02	4.04E-02	1.60E-02	*RGS1*	1
GO:0071837	HMG box domain binding	0.07	0.001037	1.44E-02	4.00E-02	1.59E-02	*JUN*	1
GO:0001134	transcription factor activity, transcription factor recruiting	0.07	0.000807	1.12E-02	3.26E-02	1.30E-02	*LIF*	1
GO:0033549	MAP kinase phosphatase activity	0.07	0.000807	1.12E-02	3.26E-02	1.30E-02	*DUSP6*	1
GO:0017017	MAP kinase tyrosine/serine/threonine phosphatase activity	0.07	0.000749	1.04E-02	3.26E-02	1.30E-02	*DUSP6*	1
GO:0035497	cAMP response element binding	0.07	0.000749	1.04E-02	3.26E-02	1.30E-02	*JUN*	1